

Investigations of the Mechanisms and Energetics
for Transition Metal Ion Mediated Reactions

Thesis by
Maureen Alice Hanratty

In Partial Fulfillment of the Requirements
for the Degree of
Doctor of Philosophy

California Institute of Technology
Pasadena, California
1985

(Submitted April 9, 1985)

For my family

ACKNOWLEDGMENTS

I would like to thank Jack Beauchamp for support both financial and otherwise during my stay at Caltech. The members of the Beauchamp group, past and present, who shared many cups of coffee and conversation also deserve thanks. It was a great pleasure working with Andreas Illies and Mike Bowers at UCSB and being introduced to ZAB and Son of ZAB. I would also like to acknowledge Ken Janda for the loan of the krypton ion laser. Members of the Bercaw and Goddard groups were always ready to lend chemical or theoretical reagents to help my investigations. Their help was greatly appreciated. The technical staff at Caltech, among them Tom Dunn, Tony Stark, Guy Duremberg, also deserve acknowledgment. Special thanks are due to Sharon ViGario for expert typing of this thesis.

Financial support provided by a fellowship from the Atlantic Richfield Corporation is gratefully acknowledged.

Finally, very special thanks go to Francis for making graduate school that much more enjoyable.

ABSTRACT

Multiphoton infrared activation has been used to probe the potential energy surfaces for the reactions of stable $\text{Co}(\text{C}_5\text{H}_{10})^+$ adducts, formed by ligand exchange reactions in an ion cyclotron resonance spectrometer. These investigations are discussed in Chapter II. Infrared activation effected with a cw CO_2 laser is highly selective, with dissociation occurring only by the lowest energy pathway.

Chapter III describes the use of product translational energy release distributions to investigate the potential energy surfaces for elimination of H_2 and small hydrocarbons from ionic cobalt and nickel complexes with alkanes. The measurements were made using a reverse geometry double focusing mass spectrometer. For dehydrogenation reactions, both the shape of the kinetic energy release distribution and the maximum kinetic energy release appear to be correlated with the reaction mechanism. Statistical RRKM theory is used to model the observed kinetic energy release distributions.

The kinetic energy release distributions associated with loss of H_2 and small hydrocarbons from $\text{Co}(\text{C}_5\text{H}_{10})^+$ complexes are presented in Chapter IV. The results from the ionic cobalt-alkene adducts are compared with the kinetic energy release distributions for the ionic cobalt-alkane complexes discussed in Chapter III. Collision induced dissociation is also employed to characterize the $\text{Co}(\text{C}_5\text{H}_{10})^+$ adducts.

The formation and reactions of iron and nickel clusters containing up to four metal atoms with a varying number of CO ligands are discussed in Chapter V. Ion-molecule condensation reactions result in the rapid formation of polynuclear metal carbonyl clusters which lose CO when

exposed to infrared or visible radiation. The reactivity of these ligated species is markedly different from that of the bare metal ion. The potential of this method for generating very specific unsaturated cluster compounds is demonstrated.

TABLE OF CONTENTS

	<u>Page</u>
Dedication	ii
Acknowledgments	iii
Abstract	iv
List of Figures	vii
List of Tables	xi
Chapter I. Introduction	1
References	5
Chapter II. Multiphoton Infrared Laser Activation of	8
Organometallic Species: A Novel Probe of the	
Potential Energy Surfaces for Reactions of	
Cobalt Ions with C ₅ H ₁₀ Isomers	
References	44
Chapter III. Kinetic Energy Release Distributions as a	48
Probe of Transition-Metal-Mediated H-H, C-H	
and C-C Bond Formation Processes: Reactions	
of Cobalt and Nickel Ions with Alkanes	
References	116
Chapter IV. Kinetic Energy Release Distributions as a	136
Probe of Bond Cleavage and Formation Processes	
at Transition Metal Centers: Reactions of Co ⁺	
with Isomeric Pentenes and Cyclopentane	
References	192
Chapter V. Formation and Reactions of Transition Metal	212
Clusters in the Gas Phase: A Novel Synthesis	
Using Laser-Induced Decarbonylation	
References	240

LIST OF FIGURES

Chapter II. Multiphoton IR Activation of $\text{Co}(\text{C}_5\text{H}_{10})^+$	
Figure 1. Schematic potential energy surfaces	14
Figure 2. Reaction cross sections for Co^+ with pentenes	16
Figure 3. Experimental apparatus (ICR)	21
Figure 4. Observed laser-modulated $\text{Co}(\text{2-pentene})^+$ signal intensities	24
Figure 5. Photolysis of $\text{Co}(\text{2-pentene})^+$ at various time delays	28
Figure 6. Difference spectrum for $\text{Co}(\text{1-pentene})^+$ with and without laser irradiation	31
Figure 7. Neutral C_5H_{10} isomer absorbance spectra	34
Figure 8. Potential energy diagram for $\text{Co}^+ + \text{2-pentene}$	39
Chapter III. Kinetic Energy Releases from Co^+ and Ni^+ with Alkanes	
Figure 1. Hypothetical potential energy surfaces and corresponding product kinetic energy release distributions	54
Figure 2. Loss of HD from $\text{Co}(\text{2-methylpropane})^+$ and D_2 from $\text{Ni}(\text{butane-1,1,1,4,4,4-d}_6)^+$	72
Figure 3. Loss of H_2 , HD, and D_2 from $\text{Co}(\text{butane-1,1,1,4,4,4-d}_6)^+$	74
Figure 4. H_2 loss from $\text{Co}(\text{cyclohexane})^+$ and $\text{Co}(\text{cyclopentane})^+$	77
Figure 5. CH_4 loss from $\text{Co}(\text{2-methylpropane})^+$ and $\text{Co}(\text{butane})^+$	80

Figure 6.	CH_4 loss from $\text{Co}(\text{cyclopentane})^+$ and $\text{Co}(\text{cyclohexane})^+$	82
Figure 7.	C_2H_6 loss from $\text{Co}(\text{butane-1,1,1,4,4,4-d}_6)^+$	85
Figure 8.	C_2H_4 loss from $\text{Co}(\text{cyclopentane})^+$ and $\text{Co}(\text{2-pentene})^+$, C_3H_6 loss from $\text{Co}(\text{cyclopentane})^+$ and $\text{Co}(\text{cyclohexane})^+$	87
Figure 9.	Experimental and theoretical KERD for C_2H_4 loss from $\text{Co}(\text{cyclopentane})^+$	91
Figure 10.	Experimental and theoretical KERD for H_2 loss from $\text{Co}(\text{butane})^+$, C_2H_4 from $\text{Co}(\text{butane})^+$	93
Figure 11.	Potential energy diagram for $\text{Co}^+ + \text{2-methylpropane}$	97
Figure 12.	Reaction coordinate diagram for $\text{Co}^+ + \text{butane}$	101
Figure 13.	H_2 loss from $\text{Co}(\text{2-methylpropane})^+$ and $\text{Co}(\text{2-methylpropane-2-d}_1)^+$	105
Figure 14.	C_2H_6 loss from $\text{Co}(\text{butane})^+$ and C_2D_6 loss from $\text{Co}(\text{acetone-d}_6)^+$	109
Figure 15.	CD_4 loss from $\text{Co}(\text{acetone-d}_6)^+$	114
Chapter III. Appendix:		
Figure 1A.	Schematic of ZAB-2F	126
Figure 2A.	Schematic of product ion intensity <u>vs.</u> lab energy	130
Chapter IV. Kinetic Energy Releases from Co^+ with Pentenes		
Figure 1.	Potential energy surfaces and the corresponding product kinetic energy release	142

distributions	
Figure 2. Lab energy distribution and KERD for loss of H_2 from $Co(3\text{-methyl-1-butene})^+$	155
Figure 3. Loss of H_2 from $Co(\text{cyclopentane})^+$	157
Figure 4. Loss of CH_4 from $Co(2\text{-pentene})^+$	159
Figure 5. Loss C_2H_4 from $Co(1\text{-pentene})^+$ and $Co(\text{cyclopentane})^+$ and C_3H_6 from $Co(1\text{-pentene})^+$	161
Figure 6. Experimental and theoretical KERD for loss of H_2 from $Co(2\text{-pentene})^+$	165
Figure 7. H_2 loss from $Co(2\text{-methylpropane})^+$ and $Co(2\text{-pentene})^+$	168
Figure 8. Experimental and theoretical KERD for loss of CH_4 from $Co(2\text{-pentene})^+$	171
Figure 9. CH_4 loss from $Co(2\text{-methylpropane})^+$ and $Co(2\text{-pentene})^+$	173
Figure 10. Potential energy diagram for $Co(2\text{-pentene})^+$	181
Figure 11. Potential energy diagram for $Co(1\text{-pentene})^+$	183
Figure 12. Loss of C_2H_4 from organic and organometallic species	186
Figure 13. CH_4 elimination from organic and organometallic species	188
Chapter IV. Appendix:	
Figure 1A. Calculated product intensity versus energy	202
Figure 2A. Experimental and theoretical KERD for loss of C_2H_4 from $Co(1\text{-pentene})^+$	209

Chapter V. Laser Decarbonylation of Metal Clusters

- Figure 1. Iron cluster mass spectra with IR irradiation 223
- Figure 2. Iron cluster mass spectra with visible
irradiation 227
- Figure 3. Binuclear nickel cluster mass spectra with
 C_2H_2 reaction 230

LIST OF TABLES

Chapter II. Multiphoton IR Activation of $\text{Co}(\text{C}_5\text{H}_{10})^+$		
Table I. Product yields for Co^+ and C_5H_{10}		36
Chapter III. Kinetic Energy Releases from Co^+ and Ni^+ with Alkanes		
Table I. Product intensities Co^+ and Ni^+ with alkanes		63
Table II. Reaction enthalpies for decomposition reactions		65
Table III. Product intensities Co^+ and Ni^+ with butane- d_6		69
Table IV. Product distributions Co^+ with acetone- d_6		112
Chapter III Appendix:		
Table IA. Thermochemical Estimates		134
Chapter IV. Kinetic Energy Releases from Co^+ with Pentenes		
Table I. Product distributions Co^+ with C_5H_{10} isomers		149
Table II. Reaction enthalpy, maximum and average kinetic energy release		151
Table III. Product distributions for organic and organometallic ions		189
Chapter IV Appendix:		
Table IA. Vibrational frequencies, H_2 and CH_4 elimination		199
Table IIA. Vibrational frequencies, translational energy release		205

Table IIIA. Vibrational frequencies, ethene from Co(1-pentene) ⁺	206
Table IVA. Thermochemical Estimates	211
Chapter V. Laser Decarbonylation of Metal Clusters	
Table I. Observed reactions, Fe and Ni carbonyl ions	231

CHAPTER I

INTRODUCTION

Innovations in experimental methodology have made it possible to generate and study organometallic species in the gas phase. A diversity of experimental techniques—high energy collision induced dissociation,^{1,2} laser photodissociation,³⁻⁵ supersonic molecular beams⁶⁻⁸ and metastable kinetic energy release measurements,⁹ to name a few—have found application to the study of organometallic species. Ion cyclotron resonance spectrometry¹⁰ and low energy ion beam investigations¹¹ continue to be a source of thermochemical and mechanistic information for reactions of ionic transition metal species. Laser evaporation has allowed the production of gas phase transition metal clusters.^{8,12} Exploration of the chemistry of these metal clusters have yielded some very promising results.^{8,9,12} In addition, progress in ab initio theories has provided a description of the potential energy surfaces for reactions of bare or minimally ligated metal atoms.^{13,14}

Gas phase transition metal ions are, in general, characterized by a high degree of reactivity. Typically, a bare metal ion will react with a hydrocarbon to eliminate hydrogen or a small hydrocarbon via processes postulated to involve bond formation and cleavage at the transition metal center.^{10,15} Studies using labelled hydrocarbons have proven valuable in elucidation of reaction mechanisms. The dehydration of butane-1,1,1,4,4,4-d₆ by transition metal ions, for example, demonstrates the variety in mechanisms that is possible.¹⁶ Ni⁺ reacts exclusively via a 1,4 hydrogen elimination process while Co⁺ and Fe⁺ react by both 1,4 and 1,2 processes. Collision induced dissociation^{1,2} and ligand displacement¹⁶ studies indicate that distinct product structures result from these different processes. While the mechanisms for metal ion reactions can thus be

corroborated by results from a variety of investigations, the details of the potential energy surfaces connecting reactants to products is largely unknown.

Using low power cw infrared radiation to activate gas phase molecules, it is possible to identify the lowest energy decomposition pathway.¹⁷ Infrared excitation of gas phase molecules and subsequent decomposition has been demonstrated to be very selective.¹⁸ Chapter II describes the application of multiphoton activation to the study of atomic cobalt ion reactions with isomeric pentenes and cyclopentane. The photodissociation products are found to be distinct for different isomers. On the basis of photodecomposition yield, it is possible to distinguish cobalt ion complexes with 1-pentene and cyclopentane from each other and from 2-pentene and methylbutene complexes. The lowest energy pathways for dissociation of the 1-pentene and 2-pentene complexes suggest allylic C-C bond insertion to be a facile process.

Examination of the amount of energy released to relative translation of products of a unimolecular reaction can be used to infer details of the potential energy surface. Information about the transition state can also be deduced by examining the energy distribution for molecules "in the process of falling apart."¹⁹ Chapter III describes investigations of the metastable decomposition and the accompanying kinetic energy releases for the reactions of Ni^+ and Co^+ with alkanes. The kinetic energy distributions for the 1,4 and 1,2 dehydrogenation of butane are found to be very distinctive, but both distributions suggest a large barrier and a "late" transition state for H_2 elimination. CH_4 elimination, on the other hand, appears to involve an "early" barrier. The results suggest

that there are substantial barriers for the reverse reactions, oxidative addition of H_2 and CH_4 to an ionic nickel or cobalt olefin complex.

Chapter IV details the investigations of the kinetic energy release distributions for the reactions of cobalt ions with pentene isomers and cyclopentane. The kinetic energy release distributions for hydrogen elimination are very similar to those observed with the cobalt alkane complexes. This is interpreted to indicate that the barrier for reductive elimination of H_2 is similar in both cases and primarily determines the amount of energy released into product translation. For ionic cobalt and nickel olefin compounds, it appears that addition of H_2 involves a substantial activation barrier. Comparison of the distributions obtained in the present study with those for metals which are known to add D_2 at thermal energies²⁰ will provide an interesting test of this conclusion.

The addition of ligands to a transition metal center, whether in the gas phase or in solution, can have a large influence on the reactivity of the metal center. The formation and reactions of transition metal clusters with carbonyl ligands are discussed in Chapter V. Ionic iron and nickel clusters are generated in situ in an ion cyclotron resonance spectrometer. Both infrared and visible radiation can remove carbonyl ligands from clusters containing two or more iron or nickel atoms. This provides a convenient route for generation of unsaturated and potentially reactive cluster species.

Selected References

1. a) Peake, D. A.; Gross, M. L.; Ridge, D. P. J. Am. Chem. Soc. 1984, 106, 4308.
b) Larsen, B. S.; Ridge, D. P. J. Am. Chem. Soc. 1984, 106, 1912.
2. a) Jacobson, D. B.; Freiser, B. S. J. Am. Chem. Soc. 1983, 105, 5197.
b) Jacobson, D. B.; Freiser, B. S. J. Am. Chem. Soc. 1983, 105, 736.
3. a) Miller, M. E.; Grant, E. R. J. Am. Chem. Soc. 1984, 106, 4635.
b) Whetten, R. L.; Fu, K. J.; Grant, E. R. J. Chem. Phys. 1983, 79, 4899.
4. Lewis, K. E.; Golden, D. M.; Smith, G. P. J. Am. Chem. Soc. 1984, 106, 3905.
5. Rothberg, L. J.; Gerrity, D. P.; Vaida, V. J. Chem. Phys. 1981, 74, 2218.
6. a) Whetten, R. L.; Cox, D. M.; Trevor, D. J.; Kaldor, A. J. Phys. Chem. 1985, 89, 566.
b) Trevor, D. J.; Whetten, R. L.; Cox, D. M.; Kaldor, A. J. Am. Chem. Soc. 1985, 107, 518.
7. a) Riley, S. J.; Parks, E. K.; Mao, C. F.; Pobo, L. G.; Wexler, S. J. Phys. Chem. 1982, 86, 3911.
b) Riley, S. J.; Parks, E. K.; Pobo, L. G.; Wexler, S. Ber. Bunsenges. Phys. Chem. 1984, 88, 287.
8. Geusic, M. E.; Morse, M. D.; Smalley, R. E. J. Chem. Phys. 1985, 82, 590.
9. Hanratty, M. A.; Beauchamp, J. L.; Illies, A. J.; Bowers, M. T.

- J. Am. Chem. Soc., in press.
10. Hartman, H.; Wanczek, K. P., eds.; "Lecture Notes in Chemistry"; Vol. 31; Springer-Verlag: New York, 1982.
 11. a) Armentrout, P. B.; Halle, L. F.; Beauchamp, J. L. J. Am. Chem. Soc. 1981, 103, 6624.
b) Armentrout, P. B.; Beauchamp, J. L. J. Am. Chem. Soc. 1981, 103, 6628.
 12. Wise, M. B.; Jacobson, D. B.; Freiser, B. S. J. Am. Chem. Soc. 1985, 107, in press.
 13. a) Low, J. J.; Goddard, W. A. J. Am. Chem. Soc. 1984, 106, 6928.
b) Low, J. J.; Goddard, W. A. J. Am. Chem. Soc. 1985, in press.
c) Obara, S.; Kitaura, K.; Morokuma, K. J. Am. Chem. Soc. 1984, 106, 7482.
 14. Siegbahn, P. E. M.; Blomberg, R. A.; Bauschlicher, C. W. J. Chem. Phys. 1984, 81, 1373.
 15. Houriet, R.; Halle, L. F.; Beauchamp, J. L. Organometallics 1983, 2, 1818.
 16. Halle, L. F.; Houriet, R.; Kappes, M. M.; Staley, R. H.; Beauchamp, J. L. J. Am. Chem. Soc. 1982, 104, 6293.
 17. Bomse, D. S.; Beauchamp, J. L. J. Am. Chem. Soc. 1981, 103, 3292.
 18. For a review, see: Woodin, R. L.; Bomse, D. S.; Beauchamp, J. L., in "Chemical and Biochemical Applications of Lasers"; Vol. IV, Moore, C. B., ed.; Academic Press: New York, 1979.
 19. Cooks, R. G.; Beynon, J. H.; Caprioli, R. M.; Lester, G. R. "Metastable Ions"; Elsevier: New York, 1973.
 20. a) Jacobson, D. B.; Freiser, B. S. J. Am. Chem. Soc. 1985, 107, 72.

20. b) Kappes, M. M., Ph.D. Thesis, Massachusetts Institute of Technology, 1981.

CHAPTER II

MULTIPHOTON INFRARED LASER ACTIVATION OF
ORGANOMETALLIC SPECIES:

A NOVEL PROBE OF THE POTENTIAL ENERGY SURFACES
FOR REACTIONS OF COBALT IONS WITH C_5H_{10} ISOMERS

Multiphoton Infrared Laser Activation of Organometallic Species:

A Novel Probe of the Potential Energy Surfaces

for Reactions of Cobalt Ions with C_5H_{10} Isomers

Maureen A. Hanratty, Carlotta M. Paulsen, and J. L. Beauchamp*

Contribution # 7127 from the Arthur Amos Noyes Laboratory of
Chemical Physics, California Institute of Technology, Pasadena,
California 91125.

*To whom correspondence should be addressed.

Abstract

Multiphoton infrared activation has been used to probe the potential energy surfaces for the reactions of cobalt ions with C_5H_{10} isomers. Infrared activation of stable cobalt $Co(C_5H_{10})^+$ adducts, formed by ligand-exchange processes, is highly selective, with dissociation occurring only by the lowest energy pathway. For example, infrared multiphoton activation of $Co(1\text{-pentene})^+$ and $Co(2\text{-pentene})^+$ adducts leads to the exclusive loss of C_2H_4 and CH_4 , respectively, in processes which can be interpreted as resulting from the facile insertion of the metal ion into an allylic carbon-carbon bond. This can be compared to the bimolecular association reactions of cobalt ions with these molecules, which results in the formation of a highly energetic species having sufficient energy to decompose by competitive elimination of H_2 , CH_4 , C_2H_4 , and C_3H_6 . On the basis of the observed photoproducts, 1-pentene and cyclopentane are readily distinguished from each other and from 2-pentene and the methylbutenes. Photodissociation rates are determined for all the cobalt pentene isomers. Dissociation yields are independent of IR excitation wavelength in the region accessible to the CO_2 laser. This contrasts with the single photon absorption spectra of the neutral pentenes which are highly structured in this wavelength region.

Preparation of an active transition metal catalyst often involves the creation of a coordinately unsaturated species. The ability of the metal to shuttle between a stable, saturated electron configuration and one capable of undergoing oxidative addition is an integral part of many proposed catalytic cycles.¹ Representing the extreme case of an unsaturated species, a bare transition metal atom or ion exhibits reactivity that surpasses that of the more saturated metal complexes.²⁻⁵ The extent to which the behavior of metal ions differs from the ligated metal species is apparent when their reactivity toward unactivated hydrocarbons is compared. While there are examples of ligated metals inserting into carbon hydrogen bonds of saturated hydrocarbons, it is not generally a facile process.⁶⁻⁹ Bare transition metal ions, on the other hand, react with unsaturated hydrocarbons via C-H and C-C bond cleavage.²⁻⁵ The accessibility of multiple and sequential competitive pathways leads to numerous reaction products even for relatively simple systems such as cobalt ions reacting with isomeric pentenes.³

Examination of the energetics of a general gas-phase ion-molecule reaction suggests reasons for the observed multiplicity of products.¹⁰ Consider, for example, the reaction of an ion M^+ with a neutral molecule A which has two exothermic reaction channels 1 and 2. In a bimolecular



collision between an ion and a neutral which involves a strong interaction such as bond formation, the resulting collision adduct MA^+

will contain a significant amount of internal excitation. The internal energy, E^* , available to the "chemically activated" complex may allow access to competitive reaction pathways such as 1 and 2. Three possible potential energy surfaces for this system, simplified for purposes of discussion, are presented in Figure 1. If C^+ and F^+ are both observed from the reaction of M^+ and A, all that can be inferred is that no point along the potential energy surface connecting MA^+ to products is higher in energy than the initial energy E^* . No information is obtained regarding the relative heights of the barriers to reactions, E_{a1} and E_{a2} , and hence it is not possible to distinguish between the three distinct cases depicted in Figure 1.

A more complete description of the potential energy surfaces can often be deduced from the observed changes in product ratios as the internal energy, E^* , of the collision complex is continuously varied. One method for achieving this is to use an ion beam apparatus^{11,12} in which the reactant ion, M^+ , is translationally excited prior to collision with the neutral molecule, A. In this manner, the internal excitation of MA^+ is increased beyond the initial interaction energy. The cross sections for the exothermic reactions of Co^+ with isomeric pentenes are plotted as a function of relative collision energy in Figure 2.³ Here the cobalt-pentene adduct resulting from bimolecular association is analogous to MA^+ . As is typical for exothermic reactions, the total cross sections decrease with increasing energy.¹² Note, however, that product ratios do not vary greatly with energy.¹³ Scheme I is proposed to account for all observed products via inter-

Figure 1. Three possible potential energy surfaces for the exothermic reactions of M^+ with A resulting in formation of products $C^+ + D$ and $F^+ + G$.

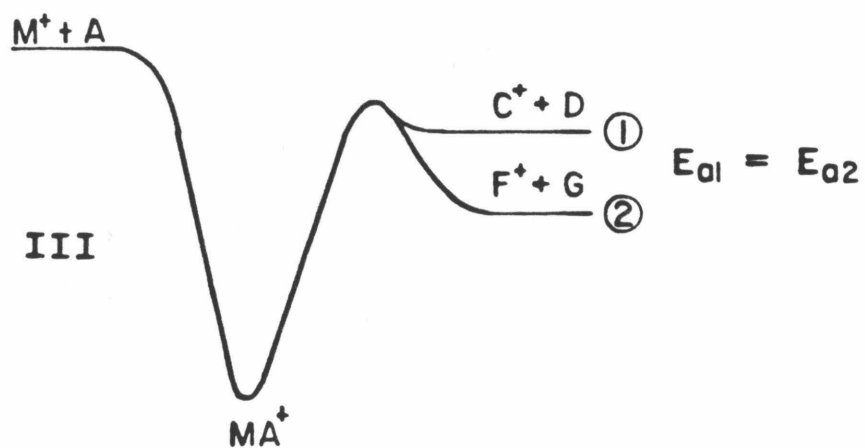
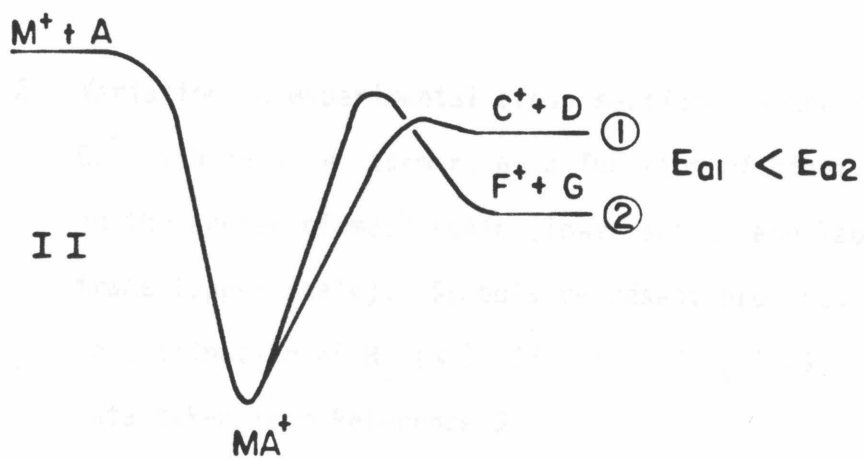
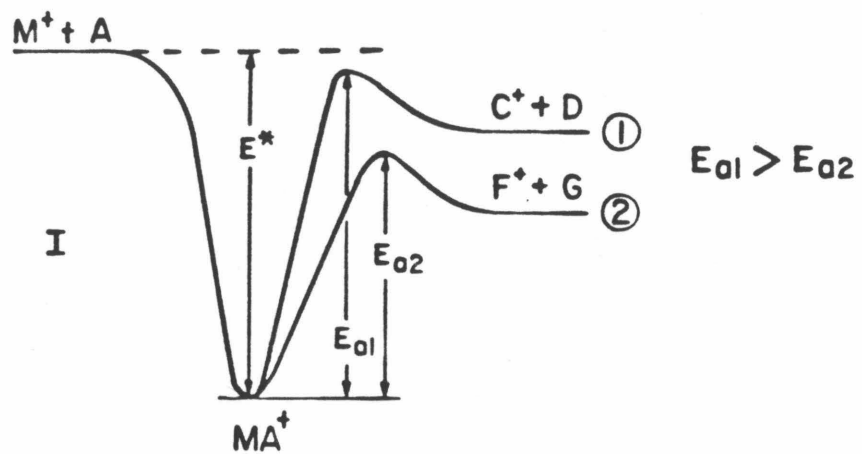
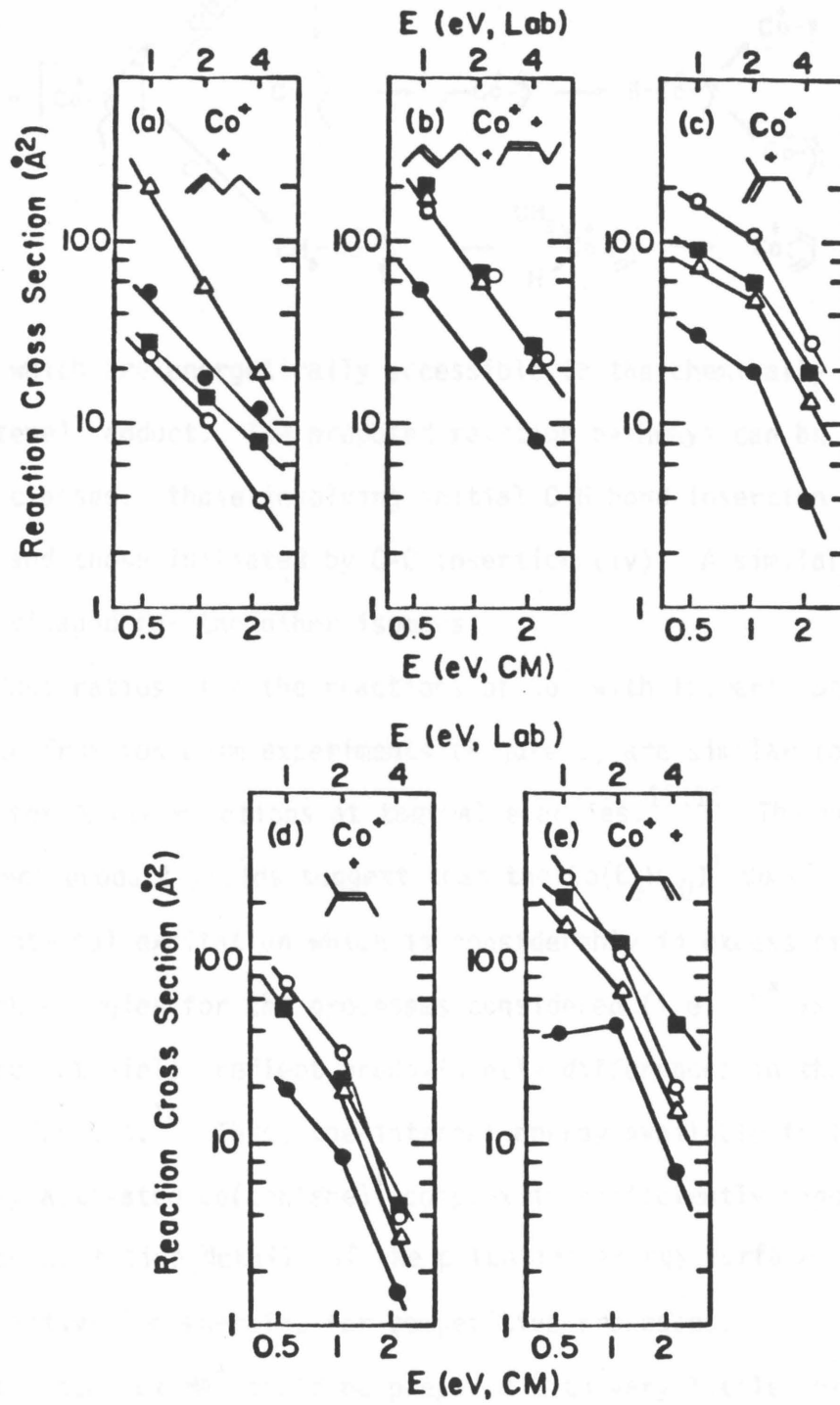
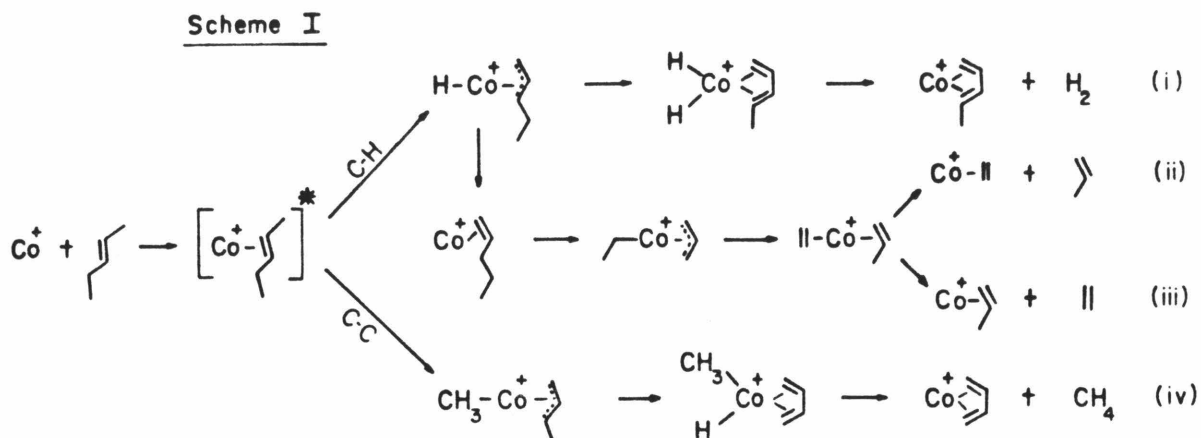


Figure 2. Variation in experimental cross-sections for the reactions of Co^+ with pentene isomers as a function of kinetic energy in the center of mass scale (lower scale) and laboratory frame (upper scale). Symbols represent products corresponding to elimination of H_2 (\circ), CH_4 (\blacksquare), C_2H_4 (\triangle), and C_3H_6 (\bullet). Data taken from Reference 3.





mediates which are energetically accessible to the chemically activated $\text{Co}(\text{2-pentene})^+$ adduct. The proposed reaction pathways can be grouped into two classes: those involving initial C-H bond insertion (i, ii, and iii) and those initiated by C-C insertion (iv). A similar scheme can be envisaged for the other isomers.

Product ratios for the reactions of Co^+ with isomeric pentenes determined from ion beam experiments (Figure 2) are similar to those obtained for these reactions at thermal energies.^{15,16} The energy-independent product yields suggest that the $\text{Co}(\text{C}_5\text{H}_{10})^+$ complexes contain internal excitation which is considerably in excess of the activation energies for the processes considered (i.e., $E^* \gg E_{a1}, E_{a2}$). Product yields reflect predominantly differences in the frequency factors.¹⁴ Thus, the internal energy available to the chemically activated $\text{Co}(\text{pentene})^+$ complex is sufficiently high to obscure quantitative details of the potential energy surfaces such as relative activation energies for competitive processes.

If the complex MA^+ could be prepared with very little internal excitation, it could then be trapped in the potential well illustrated in Figure 1. A convenient method for creating a stable adduct is through

a nearly thermoneutral ligand exchange reaction such as 3. In contrast



to the direct association adduct, the MA^+ complex formed from the ligand exchange will contain only the difference between the two metal-ligand bond energies as the maximum internal excitation. By increasing the energy available to MA^+ in small increments, it would be possible to determine which of the surfaces represented in Figure 1 is a more appropriate description of the system. If case I best represents the reaction coordinate, only the thermodynamically most stable products would be observed. In case II the higher-energy products which have the lower activation energy would be observed. Finally, if a common transition state were involved as in case III, both sets of products would be formed.¹⁷

Absorption of infrared photons provides a relatively easy method for depositing small increments (~2.5 kcal/photon) of energy into a molecule. Using low-power cw infrared laser radiation, gas-phase ions have been shown to undergo decomposition at energies near threshold.^{17,18} This facet of IR multiphoton decomposition has attracted attention due to the fact that it allows identification of the lowest energy pathway, which may be different for different isomers.^{19,20} In addition, isomeric ions may exhibit dissociation yields which vary with wavelength in a manner which allows them to be distinguished.¹⁸⁻²⁰ Thus, infrared multiphoton decomposition can yield details relating to activation parameters as well as structural information.

In this study, ion cyclotron resonance (ICR) in conjunction with

infrared multiphoton dissociation is used to probe the potential energy surfaces for the reaction of cobalt ions with isomeric pentenes and cyclopentane. Augmented by results from previous investigations, a more complete picture of the potential energy surfaces can be formulated.

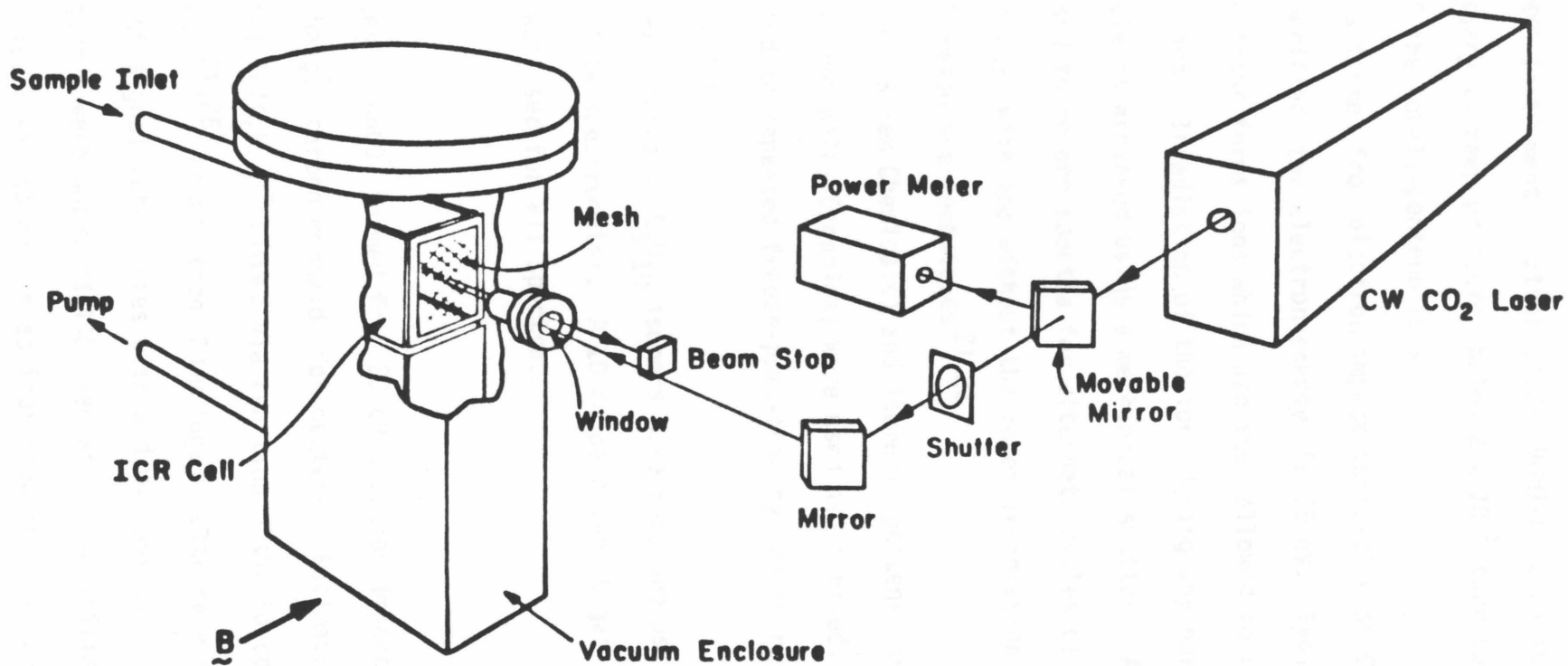
Experimental

The theory and techniques of ion cyclotron resonance spectroscopy (ICR) have been previously described.^{21,22} All experiments were performed using a conventional ion cyclotron resonance spectrometer with a marginal oscillator detector. Modifications to allow photochemical investigations include replacement of one drift plate with a 92% transmissive mesh and installation of a NaCl window as previously described.¹⁸ Light is directed into the center of the ion storage region and reflected by the back plate. Correcting for the absorption of the NaCl window and assuming the back plate is 100% reflective, the irradiance inside the cell is 1.77 times the incident irradiance.²³

Figure 3 displays a schematic of the experimental apparatus. An Apollo 550A line-tunable cw CO₂ laser provides the infrared radiation. An unfocused beam with a nearly Gaussian intensity profile (FWHM 6 mm) is used to ensure complete and uniform overlap with the ion cloud.¹⁸ Irradiances from 12 to 60 W cm⁻² are used. All laser power measurements are made using a Laser Precision RK 3440 radiometer. The reported irradiances are calculated by dividing the total beam power in the cell by the area of the beam.

Neutral pressures typically are in the 3×10^{-7} to 2×10^{-6} range. Pressure measurements are obtained using a Schulz-Phelps gauge calibrated

Figure 3. Schematic of experimental apparatus for infrared multiphoton activation studies.



against an MKS Instrument Baratron (Model 90H1-E) capacitance manometer. It was necessary to keep pressures below 2×10^{-6} torr to avoid further reaction of the cobalt-pentene ions.

CoCO^+ is formed from electron impact ionization of $\text{Co}(\text{CO})_3\text{NO}$. Unless otherwise specified, the electron energy is 20 eV. Typically, a 10 msec pulse of electrons forms ions which are then allowed to react for times up to one second. Irradiation of the ions during any portion of the trapping cycle is achieved using a mechanical shutter. A dual channel boxcar is used to record spectra for alternate cycles of laser irradiation. Reaction pathways with and without the laser irradiation are confirmed using double-resonance techniques.^{21,22}

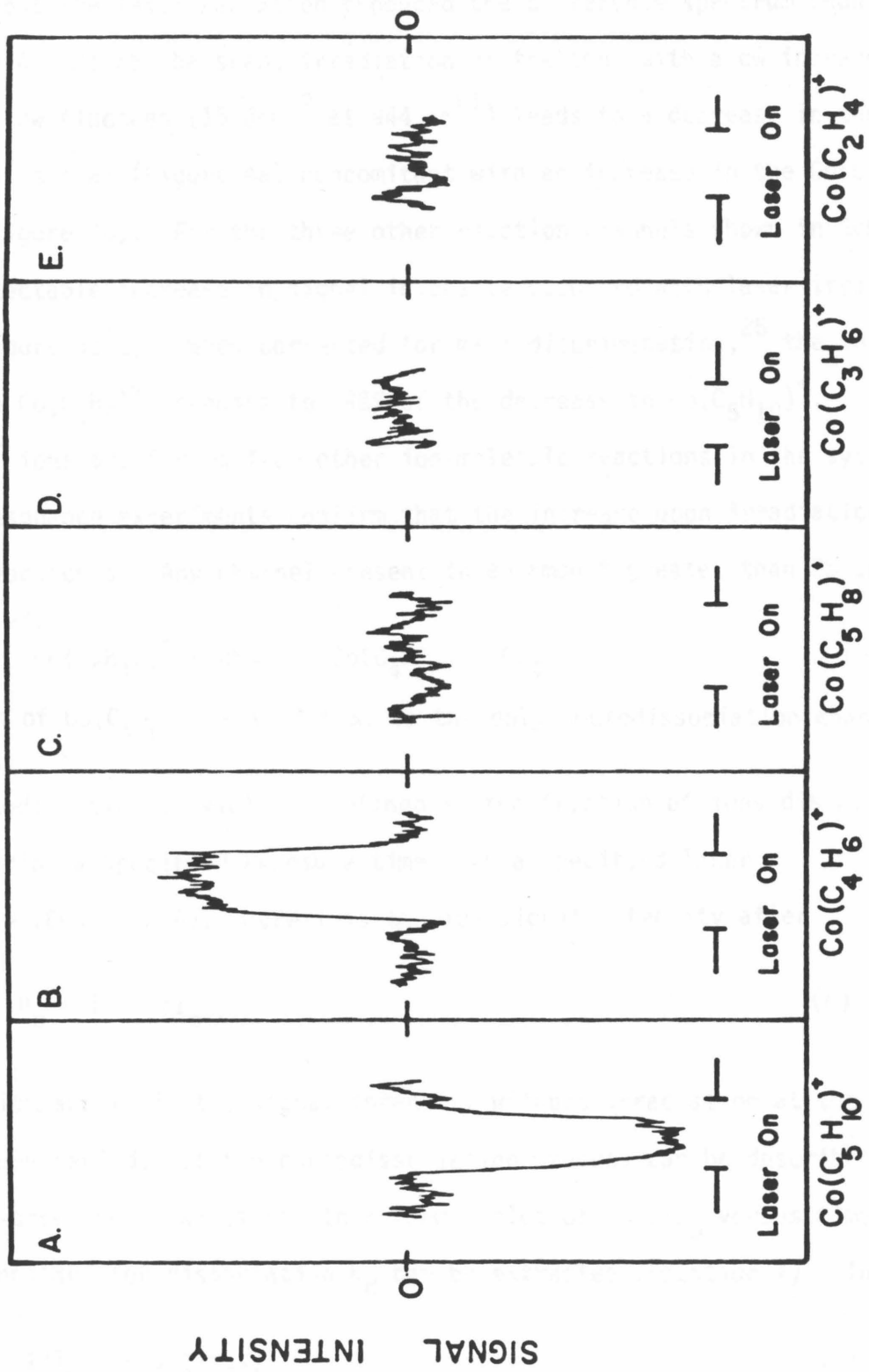
$\text{Co}(\text{CO})_3\text{NO}$ (Strem Chemicals) and isomeric pentenes and cyclopentane (>99% purity from Wiley Organics) were used as received. All samples were subjected to repeated freeze-pump-thaw cycles to remove non-condensable gases.

Infrared spectra of C_5H_{10} isomers were recorded using a Matteson Sirius 100 FT IR spectrometer. A 10 cm path length gas cell pressurized to 10 torr was used for all spectra.

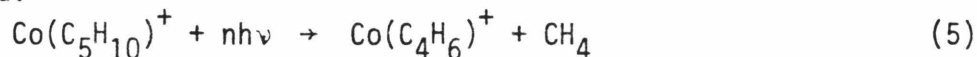
Results

2-Pentene. CoCO^+ formed from 20 eV electron impact on $\text{Co}(\text{CO})_3\text{NO}$ readily exchanges carbon monoxide for pentene. Estimated bond energies indicate that $\text{Co}(\text{C}_5\text{H}_{10})^+$ formed via reaction 3 should contain very little excess energy.^{24,25} Irradiation of the ions on alternate cycles allows the comparison of signal intensities with and without laser radiation. The data in Figure 4 were obtained 436 msec after the initial ion formation pulse. The laser was turned on as indicated for alternate cycles.

Figure 4. Variation in ICR signal intensities for five ions present in the cobalt-2-pentene system 436 msec after the initial ion-formation pulse. Ions were exposed to infrared radiation (15 J cm^{-2} at 944 cm^{-1}) on alternate cycles. The signal intensity without laser radiation was subtracted from the signal with laser radiation to produce the difference spectrum. For comparison the signal intensities of A, B, C, D, and E should be multiplied by 1.00, 1.14, 1.01, 1.28, and 1.48, respectively.²²



Subtracting the intensity for a given ion with laser irradiation from that without the laser radiation produced the difference spectrum shown in Figure 4. As can be seen, irradiation of the ions with a cw infrared laser at low fluences (15 Jcm^{-2} at 944 cm^{-1}) leads to a decrease in the $\text{Co}(\text{C}_5\text{H}_{10})^+$ signal (Figure 4a) concomitant with an increase in the $\text{Co}(\text{C}_4\text{H}_6)^+$ signal (Figure 4b). For the three other reaction channels shown in Scheme I, no detectable increase in signal intensity occurred with laser irradiation (Figure 4c-e). When corrected for mass discrimination,²⁶ the increase in $\text{Co}(\text{C}_4\text{H}_6)^+$ accounts for 98% of the decrease in $\text{Co}(\text{C}_5\text{H}_{10})^+$. Although $\text{Co}(\text{C}_4\text{H}_6)^+$ ions are formed from other ion-molecule reactions in the system, double-resonance experiments confirm that the increase upon irradiation is due to reaction 5. Any channel present in an amount greater than 2% could be detected.



Formation of $\text{Co}(\text{C}_4\text{H}_6)^+$ (Reaction 5) is the only photodissociation channel observed.

Photodissociation yield is defined as the fraction of ions dissociated during a specified exposure time with a specified laser irradiance (Equation 6). Here I is the ion signal intensity after

$$P_d = 1 - I/I_0 \quad (6)$$

irradiation, and I_0 is the signal intensity without irradiation at the end of the same period. If the photodissociation process can be described by first-order decay kinetics, then from a plot of $\ln I/I_0$ versus time a rate constant for dissociation k_d can be extracted (Equation 7). This

$$I/I_0 = \exp(-k_d t) \quad (7)$$

apparent rate constant determined at a given laser energy indicates the ease with which molecules can be photodissociated. A phenomenological cross section σ_d can also be defined for rate constants which are first order in photon flux Φ (Equation 8). The photodissociation of cobalt(2-pentene)⁺

$$k_d = \sigma_d \Phi \quad (8)$$

complexes could be characterized in this manner by a photodissociation rate of $0.034 \text{ sec}^{-1} \text{ W}^{-1} \text{ cm}^2$. Only the single product is observed at all laser powers in the wavelength region from 9.2 to 10.8 microns. At constant fluence, the photodissociation yield shows no variation with wavelength.

A small fraction (<5%) of the $\text{Co}(\text{C}_5\text{H}_{10})^+$ population is not observed to decompose with infrared radiation. Photodissociation due exclusively to a vibrationally excited population can be ruled out by the data shown in Figure 5. The ions are irradiated with 40 W cm^{-2} at 944 cm^{-1} during a "window" of 110 msec with a variable time delay. A vibrationally hot population would be expected to relax collisionally at the longer trapping times which would result in a decrease in the percent of ions decomposing.^{19,27,28} The constant fraction of ions which photodissociate indicates that vibrationally excited ions do not account for the majority of the decomposition. The photodissociation rates observed with 20 and 70 eV electron impact ionization differ by less than 5%.

1-Pentene. $\text{Co}(\text{C}_5\text{H}_{10})^+$ adducts formed from the ligand exchange reaction 3 with 1-pentene are observed to photodissociate via reaction 9.

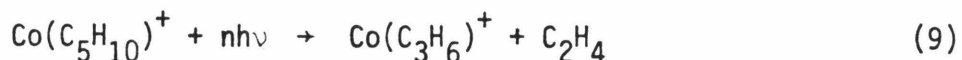


Figure 5. Normalized $\text{Co}(2\text{-pentene})^+$ ion intensity following irradiation (40 W/cm^{-2} at 944 cm^{-1}) during a 110 msec window with a variable time delay. Ions were irradiated on alternate cycles as indicated.

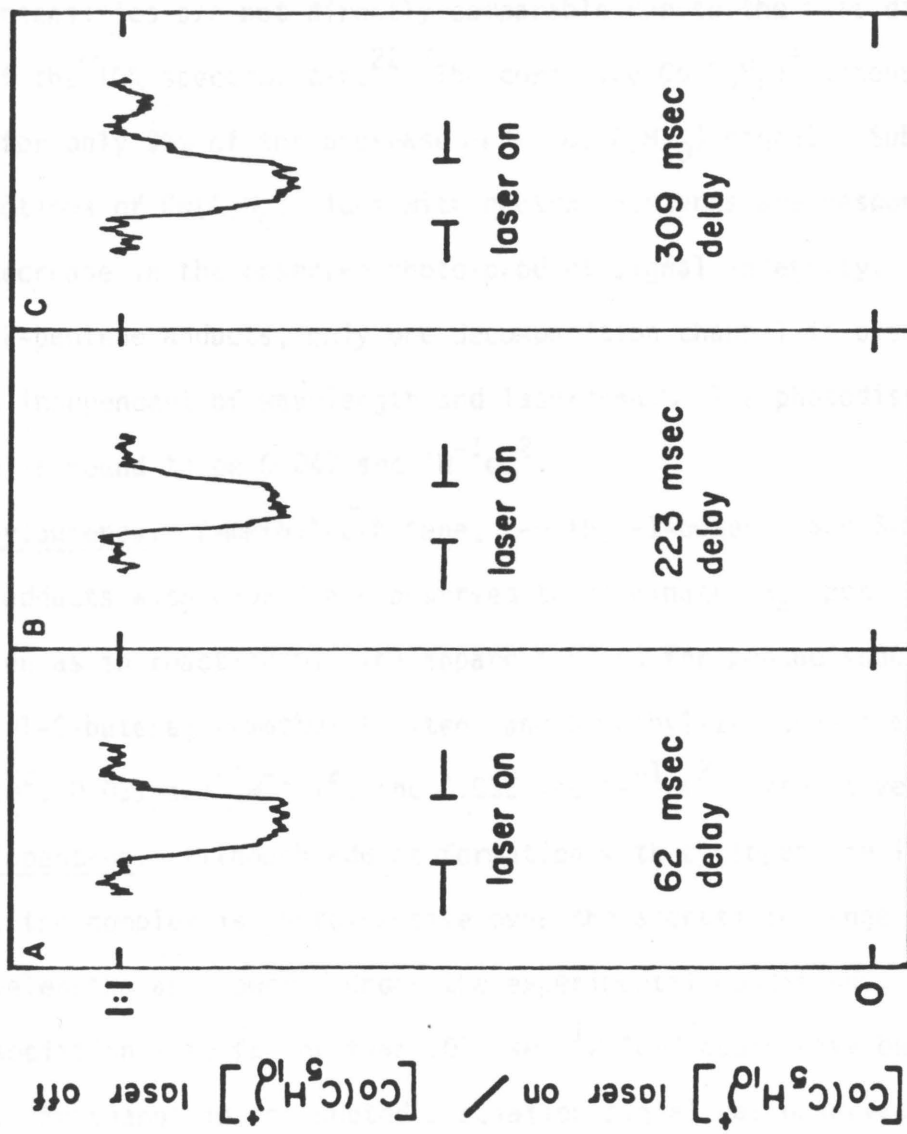
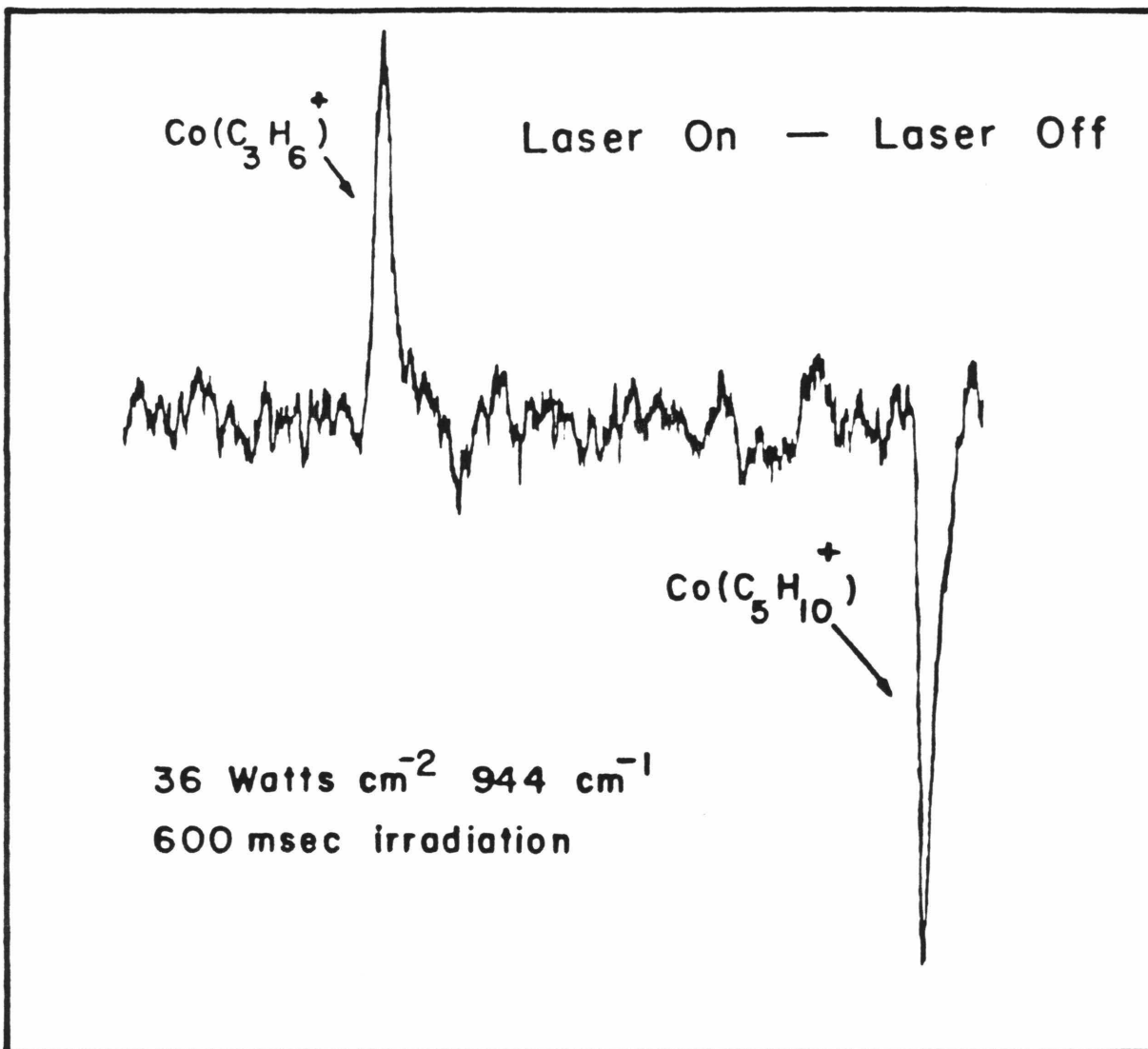


Figure 6 shows a difference mass spectrum recorded by subtracting the observed intensity without laser irradiation from the signal intensity with laser irradiation at a trapping time of 600 msec. Signals increasing upon exposure to 944 cm^{-1} radiation (36 J/cm^2) appear as positive peaks. Intensities are not directly comparable due to the mass discrimination of the ICR spectrometer.²² The corrected $\text{Co}(\text{C}_3\text{H}_6)^+$ intensity accounts for only 95% of the decrease in the $\text{Co}(\text{C}_5\text{H}_{10})$ signal. Subsequent reactions of $\text{Co}(\text{C}_3\text{H}_6)^+$ ions with neutral pentenes are responsible for the decrease in the observed photo-product signal intensity. As with the 2-pentene adducts, only one decomposition channel is observed, and it is independent of wavelength and laserpower. The photodissociation rate is found to be $0.047\text{ sec}^{-1}\text{W}^{-1}\text{cm}^2$.

Methylbutenes. 2-methyl-2-butene, 2-methyl-1-butene, and 3-methyl-1-butene adducts with cobalt are observed to eliminate CH_4 upon irradiation as in reaction 5. The apparent rates for photodissociation of 2-methyl-2-butene, 2-methyl-1-butene and 3-methyl-1-butene are $0.029\text{ sec}^{-1}\text{W}^{-1}\text{cm}^2$, $0.031\text{ sec}^{-1}\text{W}^{-1}\text{cm}^2$, and $0.035\text{ sec}^{-1}\text{W}^{-1}\text{cm}^2$, respectively.

Cyclopentane. Although adduct formation with cyclopentane is observed, the complex is photoinactive over the accessible range of laser wavelengths and power. Under the experimental conditions, a photodissociation rate faster than $.006\text{ sec}^{-1}\text{W}^{-1}\text{cm}^2$ could have been observed. No change in the photodissociation signal was observed with 70 eV electron impact ionization. $\text{Co}(\text{C}_5\text{H}_8)^+$, the dehydrogenation product from bare cobalt ions reacting with cyclopentane, is observed to lose H_2 upon irradiation.

Figure 6. Difference mass spectrum at 40 eV for 1-pentene system obtained by subtracting the observed ion intensity without laser radiation from that with laser radiation. Ions are trapped for 600 msec and exposed on alternate cycles to IR laser radiation (22 J cm^{-2} at 944 cm^{-1}).

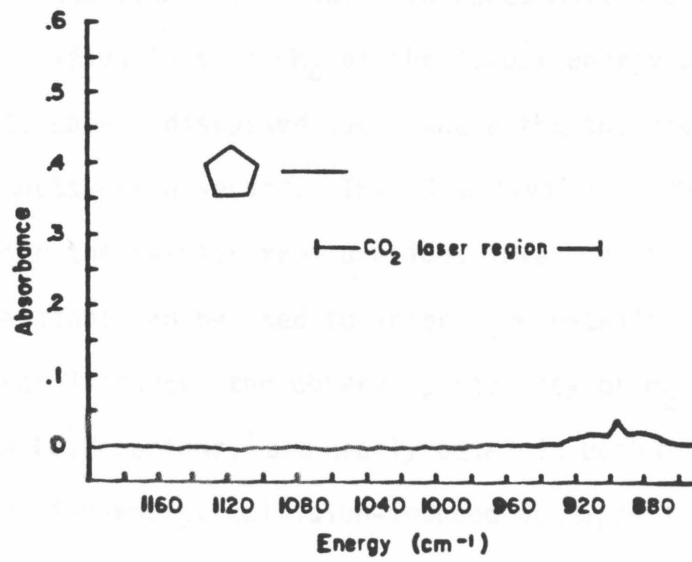
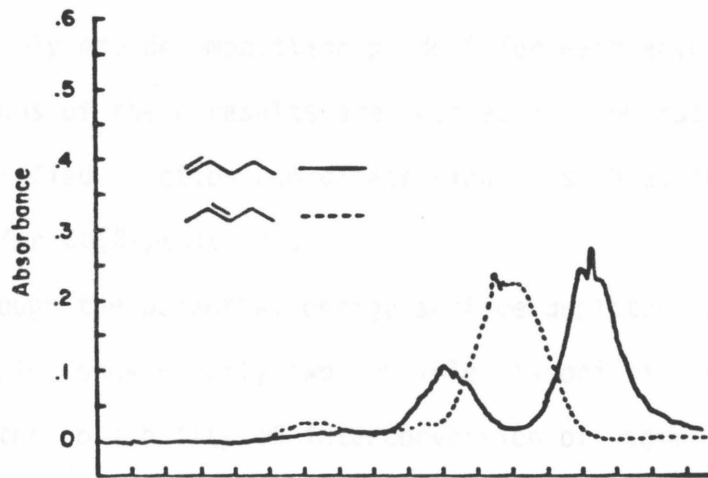
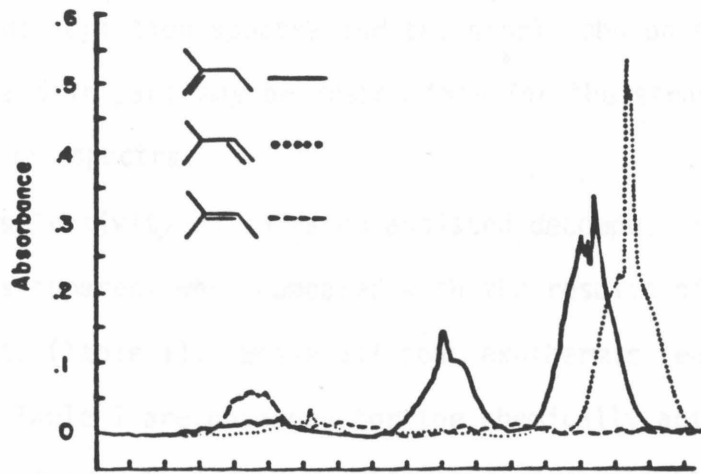


Discussion

Multiphoton dissociation represents one of the few methods for obtaining spectral information for gas-phase ions. In some instances, the photodissociation spectra of the ions are found to resemble the absorption profile for the neutral molecule.^{18,29} The photodissociation spectrum of perfluoropropene, for instance, exhibits a strong wavelength dependence.²⁹ The maximum at 1047 cm^{-1} is only slightly shifted from the neutral absorption at 1037 cm^{-1} . In contrast to this, the proton bound dimers of aliphatic alcohols exhibit no strong wavelength dependence in their photodissociation spectra.^{17a} Although there are known exceptions³⁰, it has been suggested that relatively unstructured absorption is characteristic of many molecules in the vibrational quasi-continuum.³¹

With the exception of cyclopentane and 2-methyl-2-butene, the gas-phase spectra of the neutral C_5H_{10} isomers exhibit intense absorption features in the wavelength range accessible to the CO_2 laser (Figure 7). 2-methyl-2-butene has an intense absorption at 800 cm^{-1} which is outside the range of the CO_2 laser, while cyclopentane has no strong absorptions near this region. Interestingly, the $\text{Co}(\text{C}_5\text{H}_{10})^+$ adduct formed with cyclopentane is photoinactive, while the adduct formed with 2-methyl-2-butene does photodissociate. All dissociation yields were independent of wavelength. In this respect, acyclic $\text{Co}(\text{C}_5\text{H}_{10})^+$ ions resemble the proton-bound dimers of alcohols.^{17a} Due to the strong interaction with the cobalt ion, the vibrational frequencies in the pentenes are likely to be perturbed as a result of complex formation. In addition, several conformations of the cobalt-pentene complex are

Figure 7. Infrared absorbance spectra for neutral C_5H_{10} isomers recorded at a pressure of 10 torr with a 10 cm path-length cell. The wavelength region accessible to the CO_2 laser is indicated.



possible. This may account for the lack of close correspondence between the photodissociation spectra and the single photon spectra shown in Figure 7 and in part may be responsible for the structureless photodissociation spectra.

The selectivity of infrared-assisted decomposition of $\text{Co}(\text{C}_5\text{H}_{10})^+$ adducts is apparent when compared with the results of chemical activation experiments (Table 1). While all four exothermic reaction channels listed in Table 1 are observed for the chemically activated (bimolecular association) adduct, infrared activation of the stable cobalt-pentene ion leads to only one decomposition product for each acyclic isomer. The implications of these results are most easily demonstrated with the aid of a simplified reaction coordinate diagram such as the one shown in Figure 8 for $\text{Co}(\text{2-pentene})^+$.

Although the potential energy surface depicted in Figure 8 is quite simple, showing only two possible dissociation channels and ignoring the possibility of interconversion of isomers, it is consistent with known features of the system. Infrared multiphoton dissociation clearly identifies loss of CH_4 as the lowest energy pathway. This is analogous to case I discussed above where the thermodynamically more stable products are observed. The IR activation results combined with the results from previous investigations of cobalt ion-pentene reactions can be used to infer more details regarding the surfaces. For instance, the observed intensity of H_2 and CH_4 elimination channels for $\text{Co}(\text{2-pentene})^+$ are nearly equal in both the metastable ion decomposition and high-energy collision-induced decomposition (Table 1). From the

Table I: Product Distributions for Exothermic Reactions of Co^+ with C_5H_{10} Isomers

C_5H_{10} Isomer	Neutral Lost	$\Delta\text{H}^{\text{a}}$ (kcal/mol)	Product Distributions			
			Ion ^b Beam	Meta- ^{c,d} stable	CID ^{c,d}	IR Activation
1-pentene	H_2	-46	.11	.02	.02	0
	CH_4	-55	.13	.01	.03	0
	C_2H_4	-29	.58	.95	.72	1.00
	C_3H_6	-25	.18	.01	.10	0
2-pentene	H_2	-43	.28	.47	.35	0
	CH_4	-52	.33	.43	.38	1.00
	C_2H_4	-27	.29	.09	.16	0
	C_3H_6	-23	.10	.01	.02	0
2-methyl-1-butene	H_2	-42	.46	.49	.43	0
	CH_4	-51	.26	.43	.34	1.00
	C_2H_4	-26	.20	.08	.14	0
	C_3H_6	-22	.08	.004	.02	0
3-methyl-1-butene	H_2	-44	.35	.47	.39	0
	CH_4	-53	.35	.45	.38	1.00
	C_2H_4	-28	.22	.08	.14	0
	C_3H_6	-24	.08	.004	.02	0
2-methyl-2-butene	H_2	-41	.34	.47	.42	0
	CH_4	-50	.35	.44	.35	1.00
	C_2H_4	-24	.26	.08	.14	0
	C_3H_6	-20	.10	.005	.02	0

Table I. continued.

C ₅ H ₁₀ Isomer	Neutral Lost	ΔH^a (kcal/mol)	Product Distributions			
			Ion ^b Beam	Meta- ^{c,d} stable	CID ^{c,d}	IR Activation
cyclopentane	H ₂	-32	.36	.35	.35	0
	CH ₄	-41	.03	.02	.02	0
	C ₂ H ₄	-16	.51	.58	.44	0
	C ₃ H ₆	-12	.07	.03	.05	0

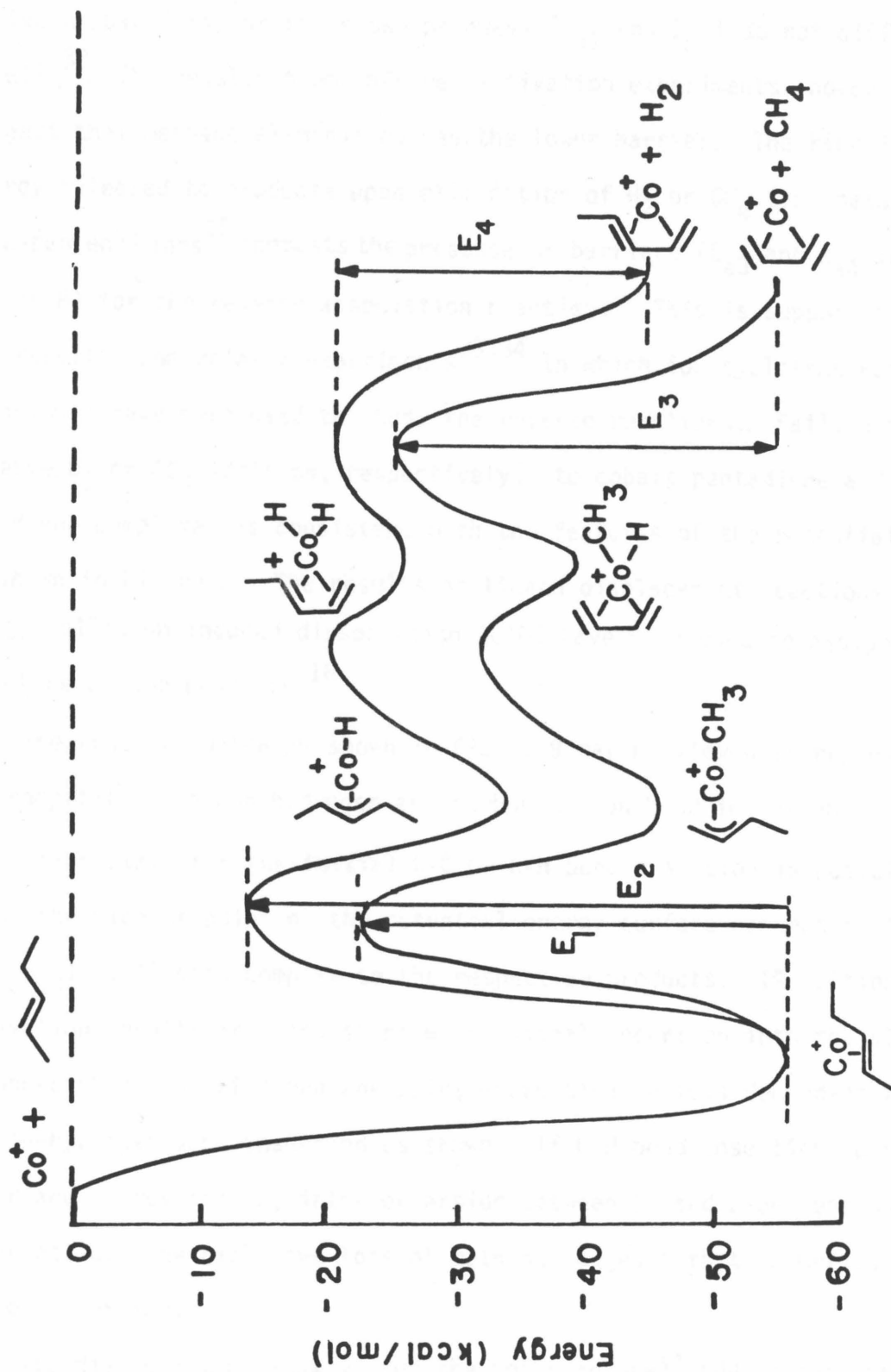
^aReaction enthalpies estimated from data given in References 15, 17, 25 and 36.

^bAll reported product distribution for ion beam studies for 0.5 ev c.m. from Reference 3.

^cAll metastable and collision-induced dissociation data are from Reference 15.

^dAll values normalized to ΣI_j . Loss of C₅H₁₀ not reported.

Figure 8. Qualitative potential-energy diagram for the reaction of Co^+ with 2-pentene, resulting in the formation of $\text{Co}(\text{C}_5\text{H}_8)^+$ and $\text{Co}(\text{C}_4\text{H}_6)^+$.



dominance of these two reaction channels, it might be expected that the activation barriers for these two pathways (E_{a1} and E_{a2}) do not differ greatly³². The results from infrared activation experiments, however, suggest that methane elimination has the lower barrier. The kinetic energy released to products upon elimination of H_2 or CH_4 from metastable $Co(2\text{-pentene})$ ions¹⁵ suggests the presence of barriers (E_{a3} and E_{a4} in Figure 8) for the reverse association reactions. This is supported by the results from related experiments^{33,34} in which ion cyclotron resonance techniques have been used to study the reverse reactions. Failure to observe D_2 or CD_4 addition, respectively, to cobalt pentadiene and cobalt butadiene complexes is consistent with the features of the potential surfaces as shown in Figure 8. The results of ligand displacement reactions and low-energy collision induced dissociation (CID) have been used to assign the structure of the products.¹⁶

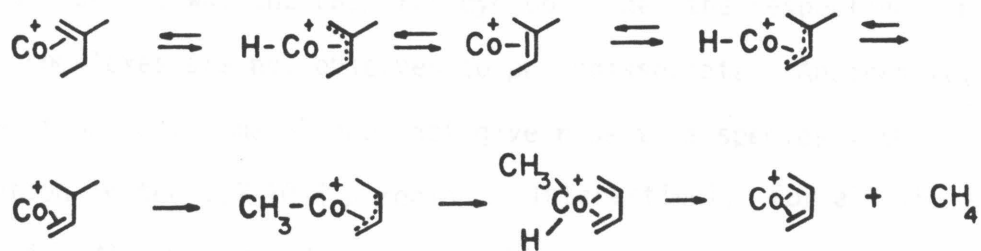
The reaction pathways shown in Figure 8 may be viewed as representing competitive carbon-hydrogen and carbon-carbon bond insertion. The transition state for the initial C-C or C-H bond insertion is postulated to be the highest point on the potential energy surface connecting the $Co(C_5H_{10})^+$ collision complex to the respective products. IR multiphoton activation results are consistent with initial insertion into the allylic carbon-carbon bond of 2-pentene being energetically less demanding than carbon-hydrogen bond insertion as shown. If C-H bond insertion does occur and is reversible, interconversion between 1- and 2-pentene would be expected. The exclusive loss of methane suggests that isomerization is not occurring.

The dissociation pathways for the $Co(1\text{-pentene})^+$ adduct can likewise be viewed as involving competitive C-C and C-H bond insertion. In this

system, loss of ethene is identified by multiphoton dissociation as the lowest energy pathway. A possible mechanism for the formation of $\text{Co}(\text{C}_3\text{H}_6)^+$ is shown in Scheme I (iii). Initially coordinated to the π bond of the olefin, the metal can insert into an allylic carbon bond and transfer a β -hydrogen to form a bis-olefin complex. This, in turn, loses ethene to yield the cobalt-propene ion. In contrast to the 2-pentene system, photoinduced decomposition of $\text{Co}(1\text{-pentene})^+$ yields the thermodynamically less stable product (case II). It is of interest to note that initial insertion into the allylic C-C bond again has the lowest activation energy.

Infrared-assisted decomposition of the cobalt-methylbutene complexes yields the same photoproducts as the $\text{Co}(2\text{-pentene})^+$ adducts. The isomerization reactions shown in Scheme II followed by decomposition

Scheme II



of the resulting Co^+ -allyl intermediate is proposed to account for the observed products. The results of metastable ion decomposition¹⁵ studies support the conclusion that isomerization to a common intermediate precedes fragmentation. There is also evidence for this in the analogous iron system where the high-energy collision-induced decomposition spectra of $\text{Fe}(\text{methylbutene})^+$ adducts are observed to be similar to

the Fe(2-pentene)⁺ spectrum.³⁵

The lack of photodissociation for the Co(cyclopentane)⁺ complex is consistent with the weak absorption for cyclopentane in the region of the CO₂ laser and suggests that the cyclopentane ring maintains its integrity. If, upon association with the metal, a linear pentene were formed, loss of CH₄ or C₂H₄ from infrared photodecomposition would be expected. High-energy CID and kinetic-energy release distributions from metastable Co(cyclopentane)⁺ ions are consistent with the ring remaining intact.^{15,36}

Related Studies with Saturated Hydrocarbons

Complexes of cobalt ions with various saturated hydrocarbons (propane, butane-1,1,1,4,4,4-d₆, pentane, cyclohexane, and methylcyclohexane) were also formed by ligand exchange (Reaction 3). The neutral hydrocarbons have fairly weak absorptions in the wavelength region of the CO₂ laser, and as was the case for cyclopentane the respective ionic cobalt complexes are not observed to photodissociate. Apparently, complexation to the metal does not give rise to a species with a strong absorption in the 9.2-10.8 μ region. Interestingly, for all the systems examined in the present study, the adducts are observed to photodissociate whenever the hydrocarbon has a strong absorption in the CO₂ laser tuning region. This is the case even though the photodissociation spectra of the complexes do not resemble the single photoabsorption spectra of the neutrals.

Conclusions

In comparison to chemical activation techniques which allow access

to multiple decomposition pathways of isomeric cobalt ion-pentene adducts, infrared multiphoton dissociation is shown to be much more selective. On the basis of the observed decomposition products, 1-pentene and cyclopentane are readily distinguished from 2-pentene and methylbutenes. In addition, IR-assisted decomposition identifies the lowest energy dissociation channel. For adducts of cobalt ions with 1- and 2-pentene, this process is postulated to involve initial insertion into the allylic carbon-carbon bond. Complexes of cobalt ions with the methylbutanes apparently isomerize prior to dissociation.

Acknowledgments

This research was supported by NSF Grant No. CHE8407857. A graduate fellowship from ARCO (MAH) and undergraduate scholarship from the Society for Applied Spectroscopy (CMP) are gratefully acknowledged. The authors would also like to thank Alan Sylvester and Burton Leland for help in obtaining the FTIR data.

References

1. For general reviews, see for example: (a) Masters, C. "Homogeneous Transition-Metal Catalysis"; Chapman and Hall: New York, 1981.
(b) Khan, M. M. T.; Martell, A. E. "Homogeneous Catalysis by Metal Complexes"; Academic Press: New York, 1974.
2. (a) Halle, L. F.; Armentrout, P. B.; Beauchamp, J. L. Organometallics 1982, 1, 963. (b) Tolbert, M. T.; Beauchamp, J. L. J. Am. Chem. Soc. 1984, 106, 8117.
3. Armentrout, P. B.; Halle, L. F.; Beauchamp, J. L. J. Am. Chem. Soc. 1981, 103, 6624.
4. (a) Byrd, G. D.; Burnier, R. C.; Freiser, B. S. J. Am. Chem. Soc. 1982, 104, 3565. (b) Burnier, R. C.; Byrd, G. D.; Freiser, B. S. ibid. 1981, 103, 4360. (c) Byrd, G. D.; Freiser, B. S. ibid. 1982, 104, 5944.
5. (a) Allison, J.; Ridge, D. P. J. Am. Chem. Soc. 1979, 101, 4998.
(b) Allison, J.; Freas, R. B.; Ridge, D. P. ibid. 1979, 101, 1332.
6. See also: Parshall, G. W. "Catalysis," Vol. 1; Chemical Society: London, 1977, p. 335.
7. (a) Crabtree, R. H.; Mellea, M. F.; Mihelcic, J. M.; Quirk, J. M. J. Am. Chem. Soc. 1982, 104, 107. (b) Crabtree, R. H.; Mihelcic, J. M.; Quirk, J. M. J. Am. Chem. Soc. 1979, 101, 7738.
8. (a) Watson, P. L. J. Am. Chem. Soc. 1983, 105, 6491. (b) Watson, P. L. J. Chem. Soc., Chem. Commun. 1983, 276.
9. (a) Janowicz, A. H.; Bergman, R. G. J. Am. Chem. Soc. 1982, 104, 352.
(b) Ibid. 1983, 105, 3929. (c) Hoyano, J. K.; Graham, W. A. G. J. Am. Chem. Soc. 1982, 104, 3723.

10. For a general discussion see: Beauchamp, J. L. in "Interactions Between Ions and Molecules"; Ausloos, P., ed.; Plenum: New York, 1975, p. 413. A more extensive treatment of the subject may be found in "Gas Phase Ion Chemistry," Vols. 1 and 2; Bowers, M. T., ed.; Academic Press: New York, 1979.
11. (a) Armentrout, P. B.; Beauchamp, J. L. J. Am. Chem. Soc. 1981, 103, 784. (b) Armentrout, P. B.; Beauchamp, J. L. J. Chem. Phys. 1981, 74, 2819.
12. Henschman, M. in "Ion-Molecule Reactions"; Franklin, J. L., ed.; Plenum Press: New York, 1972; p. 101.
13. Above ~1 eV contributions from endothermic reaction pathways which are not shown becomes significant.
14. (a) Forst, W. "Theory of Unimolecular Reactions"; Academic Press: New York, 1973. (b) Robinson, P. J.; Holbrook, K. A. "Unimolecular Reactions"; Wiley Interscience: New York, 1972.
15. Hanratty, M. A.; Illies, A. J.; Bowers, M. T.; Beauchamp, J. L. J. Am. Chem. Soc., to be submitted.
16. Jacobson, D. B.; Freiser, B. S. J. Am. Chem. Soc. 1983, 105, 5197.
17. Examples of all three cases have been demonstrated. (a) Bomse, D. S.; Beauchamp, J. L. J. Am. Chem. Soc. 1981, 103, 3292. Multiple products resulting from a photochemically prepared intermediate have also been reported. (b) Moylan, C. R.; Janiski, J. M.; Brauman, J. I. Chem. Phys. Lett. 1983, 98, 1.
18. Bomse, D. S.; Woodin, R. L.; Beauchamp, J. L. J. Am. Chem. Soc. 1979, 101, 5503.
19. (a) for a review, see: Woodin, R. L.; Bomse, D. S.; Beauchamp, J. L. in "Chemical and Biochemical Applications of Lasers" Vol.

- IV, Moore, B. C., ed.; Academic Press: New York, 1979.
20. Bomse, D. S.; Beauchamp, J. L. Chem. Phys. Lett. 1981, 77, 25.
 21. Lehman, T. A.; Bursley, M. M. "Ion Cyclotron Resonance Spectrometry"; Wiley-Interscience: New York, 1976.
 22. Beauchamp, J. L. Annu. Rev. Phys. Chem. 1971, 22, 527.
 23. This is calculated for 10.6 μ radiation where the absorption of the NaCl window is 4%.
 24. $D[\text{Ni}^+-\text{CO}]$ and $D[\text{Fe}^+-\text{CO}]$ were determined from photoionization mass spectrometry to be 48 ± 2 and 60.5 ± 2 kcal/mol, respectively.
Distefano, G. J. Res. Natl. Bur. Stand., Sect. A. 1970, 74A, 233.
The latter value appears too large and may be due to an incorrect threshold for formation of $\text{Fe}(\text{CO})^+$.^{2a} An upper limit of 43 ± 3 kcal/mol for $D[\text{Fe}-\text{CO}]^+$ has been determined from photodissociation. Cassady, C. J.; Freiser, B. S. J. Am. Chem. Soc. 1984, 106, 6176. With this in mind $D[\text{Co}^+-\text{CO}]$ is estimated to be 46 kcal/mol. Pentene is observed to displace C_3H_6 from CoC_3H_6^+ , indicating $D[\text{Co}-\text{C}_5\text{H}_{10}] > D[\text{Co}^+-\text{C}_3\text{H}_6] > 36$ kcal/mol.³ $D[\text{Co}^+-\text{C}_5\text{H}_{10}]$ is estimated to be 55 kcal/mol.
 25. Supplementary thermochemical information is from Cox, J. D.; Pilcher, G., "Thermochemistry of Organic and Organometallic Compounds"; Academic Press: New York, 1970.
 26. The decrease in $\text{Co}(\text{C}_4\text{H}_6)^+$ signal should be multiplied by 1.14 to correct for mass discrimination (Reference 22).
 27. (a) Janinski, J. M.; Rosenfeld, R. N.; Meyer, F. K.; Brauman, J. I. J. Am. Chem. Soc. 1982, 104, 652. (b) Rosenfeld, R. N.; Janinski, J. M.; Brauman, J. I. ibid. 1982, 104, 658.

28. At a pressure of 2×10^{-6} torr a $\text{Co}(\text{C}_5\text{H}_{10})^+$ ion will typically undergo 20 collisions after 0.5 sec. See Reference 10.
29. Woodin, R. L.; Bomse, D. S.; Beauchamp, J. L. Chem. Phys. Lett. 1979, 63, 630.
30. Dai, H. L.; Kung, A. H.; Moore, C. B. Phys. Rev. Lett. 1979 43, 761.
31. (a) Tsee, J. J.; Wittig, C. J. Chem. Phys. 1978, 69, 4756.
(b) Schultz, P. A.; Sudbo, A. S.; Krajnovich, D. J.; Kwok, H. S.; Shen, Y. R.; Lee, Y. T. Ann. Rev. Phys. Chem. 1979, 30, 379.
32. Cooks, R. G.; Beynon, J. H.; Caprioli, R. M.; Lester, G. R. "Metastable Ions"; Elsevier: New York, 1973.
33. Jacobson, D. B.; Freiser, B. S. J. Am. Chem. Soc. 1985, 107, 72.
34. Hanratty, M. A.; Beauchamp, J. L., unpublished results.
35. Peake, D. A.; Gross, M. L.; Ridge, D. P. J. Am. Chem. Soc. 1984, 106, 4307.
36. Armentrout, P. B.; Beauchamp, J. L. J. Am. Chem. Soc. 1981, 103, 6628.

CHAPTER III

KINETIC ENERGY RELEASE DISTRIBUTIONS
AS A PROBE OF TRANSITION-METAL-MEDIATED
H-H, C-H, AND C-C BOND FORMATION PROCESSES:
REACTIONS OF COBALT AND NICKEL IONS WITH ALKANES

Kinetic Energy Release Distributions as a Probe of
Transition-Metal-Mediated H-H, C-H, and C-C Bond Formation
Processes: Reactions of Cobalt and Nickel Ions with Alkanes

Maureen A. Hanratty and J. L. Beauchamp^{*}

Contribution No. 7157 from the Arthur Amos Noyes Laboratory
of Chemical Physics, California Institute of Technology,
Pasadena, California 91125

and

Andreas J. Illies and M. T. Bowers^{*}

Department of Chemistry, University of California, Santa
Barbara, California 93106.

^{*}To whom correspondence should be addressed.

ABSTRACT

Product translational energy release distributions are used to investigate the potential energy surfaces for elimination of H₂ and small hydrocarbons from ionic cobalt and nickel complexes with alkanes. For dehydrogenation reactions, both the shape of the distribution and the maximum kinetic energy release appear to be correlated with the reaction mechanism. For example, the amount of energy appearing in product translation is quite distinctive between reactions known to involve metal-induced 1,2- and 1,4-hydrogen elimination. The selective dehydrogenations of 2-methylpropane-2-d₁ by Co⁺ and butane-1,1,1,4,4,4-d₆ by Ni⁺ serve, respectively, as models for these processes. A comparison of these translational energy distributions with those observed for loss of H₂, HD, and D₂ from the dehydrogenation of butane-1,1,1,4,4,4-d₆ by Co⁺ suggests that 1,4-elimination is dominant for the cobalt system and that the observation of different isotopic products results from scrambling processes. All the dehydrogenation processes examined were characterized by kinetic energy release distributions which could not be described by simple statistical theories. For these reactions, the maximum kinetic energy release approaches the estimated reaction exothermicity. In contrast, the more exothermic alkane eliminations have maximum kinetic energy releases which are less than half the reaction exothermicity, and the distributions can be fit with statistical models. The amount of energy appearing as product translation can be used to infer details of the potential energy surfaces in the region of the exit channel and has implications for the ease with which the reverse reactions may occur. The potential energy surfaces for hydrogen

and alkane elimination reactions are discussed in view of the very different kinetic energy release distributions observed for these processes.

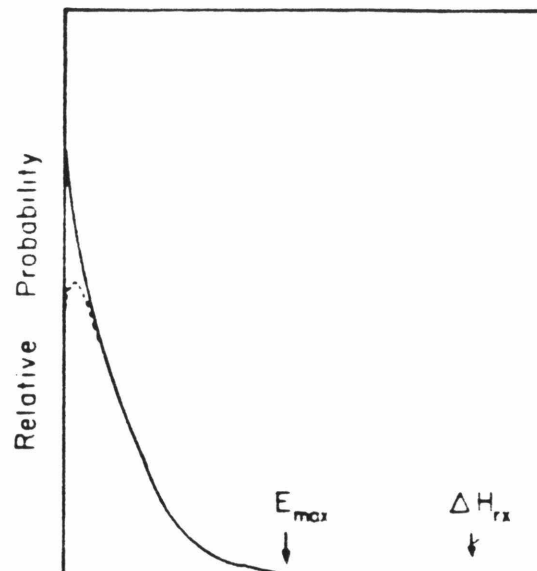
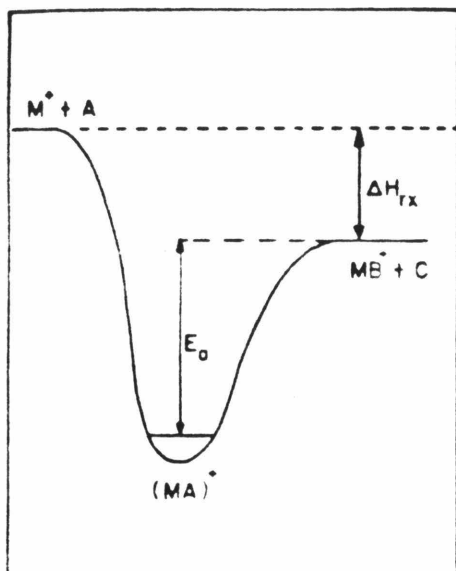
INTRODUCTION

The reactions of atomic metal ions in the gas phase, free from solvent and ligand effects, represent some of the simplest cases where the nature of the interactions of transition-metal centers with organic molecules can be probed. Gas-phase transition-metal ions typically react exothermically with saturated hydrocarbons to eliminate molecular hydrogen, alkanes, and alkenes, leaving an unsaturated and potentially more reactive species bound to the metal.¹⁻⁶ Fundamental questions still remain to be answered regarding the mechanisms and energetics for these metal-mediated processes. For instance, the final step in these elimination processes is often postulated to involve coupling of molecular fragments bound directly to the metal center. Recent results from theoretical⁷ and experimental⁸ investigations suggest alternate mechanisms which involve multicenter interactions of C-H and C-C bonds with metal-hydrogen or metal-carbon bonds. In addition, there is very little detailed information about the energetics, especially activation parameters, for these processes. Although only recently applied to the study of organometallic reactions,⁹ kinetic energy release distributions offer a unique opportunity to investigate the potential energy surfaces for gas-phase reactions. We now report the investigation of metal-mediated H-H, C-H, and C-C bond formation processes using product kinetic energy release distributions.

To illustrate how the amount of energy released to product translation for a given reaction pathway may reflect specific details of the potential energy surface, consider the two hypothetical surfaces in Figure 1. The gas-phase collision of an ion M^+ with a neutral

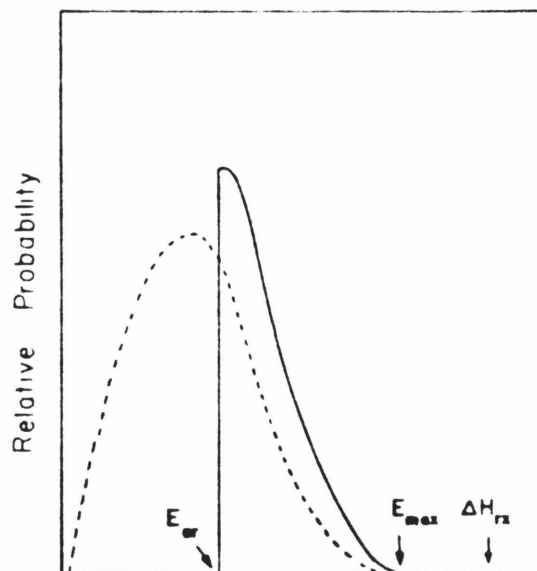
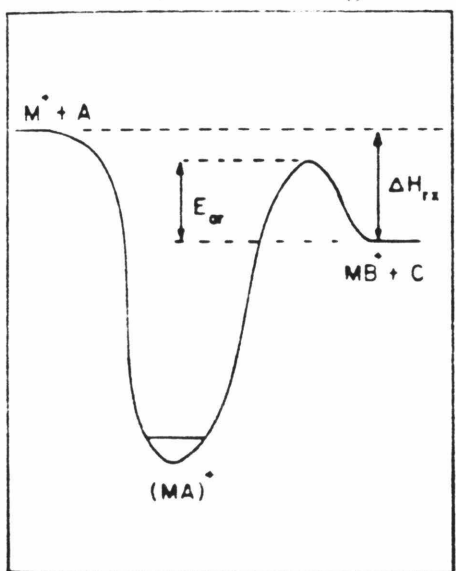
Figure 1. Two hypothetical potential energy surfaces for the reaction $M^+ + A \rightarrow MB^+ + C$ and the corresponding product kinetic energy release distributions in the center-of-mass frame.

TYPE I. No Barrier for Reverse Association Reaction



Product Kinetic Energy

TYPE II. Large Barrier for Reverse Association Reaction



Product Kinetic Energy

molecule A can result in the formation of an adduct, MA^+ , which contains internal energy, E^* . In the absence of collisions, the internal excitation may be utilized for molecular rearrangement and subsequent fragmentation. In Figure 1, the collision adduct MA^+ is depicted fragmenting to MB^+ and C along two different potential energy surfaces designated Type I and Type II.¹⁰ For a reaction occurring on a Type I surface, simple bond cleavage is involved and there is no barrier, excluding a centrifugal barrier, to the reverse association reaction. The transition state resembles very loosely associated products, and very little interaction occurs between products after the transition state has been passed. Statistical theories such as RRKM¹¹ and phase-space theory¹² have been successful in modeling translational energy release distributions for reactions occurring on this type of potential energy surface. A central assumption of these theories is that the statistical partitioning of energy between the reaction coordinate and all internal degrees of freedom at the transition state will be retained as the products separate. This predicts that the probability of a given energy's being partitioned to relative product translation will decrease rapidly with increasing energy as shown in the right-hand portion of Figure 1a. For rotating molecules ($J > 0$), angular momentum constraints may lead to a distribution such as the one indicated by the dashed line in Figure 1a.¹³ Since the energy of the system in excess of that necessary for dissociation will be statistically divided between all the modes, the average kinetic energy release, E_{av} , for a large molecule will be much less than the total reaction exothermicity ΔH . Distributions of this type are characteristic of simple bond cleavage processes.¹⁴

As shown in Figure 1b, a Type II surface involves a barrier with activation energy (E_{ar}) for the reverse association reaction. This type of surface is often associated with complex reactions which involve the simultaneous rupture and formation of several bonds in the transition state. In the absence of coupling between the reaction coordinate and other degrees of freedom after the molecule has passed through the transition state, all of the reverse activation energy would appear as translational energy of the separating fragments. Accordingly, the translational energy release would be shifted from zero by the amount E_{ar} and may again be peaked to higher kinetic energy due to angular momentum constraints (solid line, Figure 1b). The multicenter decomposition of ethyl vinyl ether to yield ethylene and acetaldehyde exhibits a release distribution indicative of a Type II surface.¹⁵ Note that with either potential energy surface, the maximum kinetic energy release, E_{max} , places a lower limit on the reaction exothermicity.

The two types of kinetic energy release distributions discussed above represent extremes. In reality, the amount of energy that appears as relative kinetic energy of products depends not only on the shape of the potential energy surface but also on dynamic effects which occur as the products separate. The amount of kinetic energy released to product translation can be greater¹⁶ or less¹⁷ than that predicted by statistical theories. Broad distributions such as the one indicated by the dashed line in Figure 1b are often attributed to "exit channel effects" that distort the translational energy distribution of the products. In such cases it is not sufficient to know the energy distribution at the maximum of the potential energy barrier. The

evolution of the system as it proceeds to products must be considered.¹⁸

Several authors have differentiated between "early" and "late" barriers. The idea of an early or late potential energy barrier is useful to indicate qualitatively whether dynamic coupling between the reaction coordinate and other degrees of freedom is expected as the products separate. If the barrier is late, the transition state lies closer to products, and not much energy redistribution is expected after the transition state. In contrast, the transition state for an early barrier resembles reactants, and energy flow occurring after the barrier has been surmounted is anticipated.¹⁹ In a reaction with an early barrier, only a fraction of the reverse activation barrier appears as relative product translation and the kinetic energy distribution is shifted to lower energies (dashed line, Figure 1b). The exact nature of the partitioning will depend on the details of the potential energy surface in the region of the exit channel and is difficult to predict. However, the shape of the product translation energy distribution can indicate the existence of a barrier to the reverse reaction, while also placing a lower limit on the height of the barrier.

Other techniques can also be used to provide additional information about the potential energy surfaces. For example, the behavior of the reaction cross sections as a function of energy can be determined using low-energy ion beams. If a reaction occurs with a large cross section at low relative kinetic energies, it can be inferred that no barrier along the reaction pathway is in excess of the energy available to the system.²⁰ On the other hand, an apparent energy threshold for a reaction which is known to be exothermic implies an activation

barrier in excess of the available energy.²¹ These same considerations apply to the reverse reactions. Notice that on a Type II surface, the association reaction of groundstate MB^+ and C to form MA^+ cannot occur. In contrast, on a Type I potential energy surface the reverse reaction can occur to give the adduct MA^+ with internal energy insufficient to yield the reactants M^+ and A. Although the reaction is nonproductive, it is possible in certain cases to determine that adduct formation did occur by use of isotopic labeling.

High-energy collision-induced dissociation has proven to be a valuable method for determining the structure of gas-phase ions.²² The structure of stable metal alkane adducts resulting from ligand displacement reactions can provide clues to the nature of the interaction of metal ions with alkanes. For instance, CID investigations of Fe^+ complexes with the isomeric butanes suggest that the adducts consist of covalently bound rearranged structures.²³ In contrast, Cr^+ complexes with isomeric butanes are found to be loosely associated metal butane adducts.²³ These results suggest very different potential energy surfaces for the interactions of iron and chromium ions with alkanes. CID can also be used to determine the structure of the products resulting from bimolecular reactions of metal ions with alkanes and thus can provide valuable information regarding reaction mechanisms.²⁴

In conjunction with the information obtained from these various techniques, metastable kinetic energy release distributions can provide more detailed information about the potential energy surfaces, particularly for the region near the exit channel. Characterizing the potential energy surfaces for the elimination of H_2 , alkanes, or alkenes from

complexes of transition metal ions with alkanes also defines the potential energy surfaces for the reverse oxidative addition reactions. Such information is central to our understanding of many fundamental processes in organometallic chemistry.

EXPERIMENTAL

All experiments were conducted using a reverse geometry double focusing mass spectrometer (VG Instruments ZAB-2F).²⁵ Cobalt and nickel ions were formed from 150 eV electron impact on $\text{Co}(\text{CO})_3\text{NO}$ and $\text{Ni}(\text{CO})_4$, respectively. Typical source operating pressures of 10^{-3} torr allowed the metal ions to undergo at most one collision with a neutral molecule. The source was operated under nearly field-free conditions to avoid imparting translational energy to the reactant species. Ions exited the source, were accelerated to 8 kV, and mass-selected. Any of the mass-selected ions which decomposed in the second field-free region between the magnetic and electric sectors were detected by scanning the energy of the electric sector.

Kinetic energy release distributions were obtained from metastable peak shapes recorded under conditions in which the energy resolution of the main beam did not contribute significantly to the observed metastable peak widths. Considerable care was taken to eliminate spurious peaks, especially those near the energy of the main beam where peaks arising from elimination of H_2 occur. Keeping the pressure in the low 10^{-3} torr region helped eliminate most of these artifacts. Despite this, some spectra did contain peaks which were not the results of the metastable ion decomposition of interest, but are thought to be due

to collisions with lenses and deflection of energetic neutralized ions into the electron multiplier.²⁶ In some cases, deuterium-labeled compounds were used to avoid interfering peaks. A more extensive discussion of the experimental method and data analysis is included in Appendix I.

In this study, the relative collision-induced dissociation (CID) intensities are reported only for the products corresponding to the metastable decomposition products. The ion population sampled in these experiments and referred to collectively as adducts may involve several possible structures, ranging from a loose association complex to the partially rearranged intermediates indicated in the reaction schemes. CID measurements were performed by admitting He into a collision cell located at the focal point between the magnetic and electric sectors until a 50% attenuation of the main beam intensity was observed.

High-resolution translational energy loss spectroscopy^{22,27} was used to identify electronically excited metal ions resulting from the electron impact ionization of the volatile metal ion precursors. A peak 1.22 eV higher in energy than the main Co^+ beam was assigned to the ^3F state of Co^+ derived from the $4s^1 3d^7$ configuration.²⁸ Similarly, peak 1.6 eV above the main Ni^+ beam energy was assigned to the ^2F excited state of Ni^+ which is derived from the $4s^1 3d^8$ configuration.²⁸ In some cases, loss of the complete alkane from the metal alkane complex occurred with a substantial release of kinetic energy. This was attributed to the metastable conversion of the electronically excited adduct to the ground state and subsequent decomposition. Although no other reactions could be attributed specifically to the excited states, it is difficult to ascertain the extent to which decomposition of

electronically excited adducts contributes to the other peaks. Complete loss of adduct was usually only a small percentage of the total product yield²⁹ and was not observed with 2-methylpropane and butane complexes. The similarity between the metastable product yields from the present study and the previously reported results from low-energy ion beam studies argues against a substantial contribution from the electronically excited adducts.^{6,30} In addition, we do not observe products of distinctly endothermic reactions such as are observed in the low-energy ion beam experiments at higher kinetic energies.⁶ We believe the contribution of electronically excited adducts to the metastable peaks is small and we make no attempt to account for such products in the data analysis.

All chemicals were obtained from commercial sources and used without further purification other than freeze-pump-thaw cycles to remove noncondensable gases. $\text{Co}(\text{CO})_3\text{NO}$ and $\text{Ni}(\text{CO})_4$ were obtained from Strem Chemical and Alpha Inorganics, respectively. 2-methylpropane- $2d_1$ and butane-1,1,1,4,4,4- d_6 (98%) were obtained from Merck, Sharp and Dohme. Acetone- d_6 (99.5 atom % D) was purchased from Stohler Isotope Chemicals.

RESULTS AND DISCUSSION

Metal alkane adducts result from the bimolecular association of a metal ion, M^+ , with a neutral hydrocarbon, RH, as exemplified by reaction 1. Under the experimental conditions employed, there is also



the possibility of a ligand exchange reaction with $\text{M}(\text{CO})^+$ ions (reaction 2). Reaction 2 has been observed with ion cyclotron resonance



spectroscopy.^{23,31} For CoCO^+ , the resulting adduct does not decompose further. Ni(CO)^+ (presumably formed in a highly excited vibrational state from electron impact ionization) can react with RH and contribute to the metastable ion population. However, the direct bimolecular association reaction 1 is believed to be responsible for formation of the majority of the energetic adducts which subsequently decompose in the second field-free region.

The relative product intensities for the exothermic reactions of cobalt and nickel ions with selected alkanes are displayed in Table I. The results of metastable ion decomposition and collision-induced dissociation (CID) obtained in the present study are compared with the results from previously reported low-energy ion beam investigations.^{5,6} To facilitate comparison, only the relative product ratios for the major reaction pathways are reported. With the exception of cyclohexane dehydrogenation, the metastable intensities correspond closely to the ion beam results. It is important to consider that in the ion beam experiments the metal alkane adduct, M(RH)^+ , is formed in the collision cell, and any reaction which occurs within the flight time to the mass spectrometer (~5 microseconds for mass 123 ions) can be detected. The situation is somewhat different for metastable decomposition studies where only reactions which occur within a time window specified by ion transit time through the second field-free region are detected.³² A metal-alkane complex with m/e 123, for example, must survive for ~15-20 microseconds.

Table I: Relative Product Intensities for the Exothermic Reactions of Co^+ and Ni^+ with Alkanes^{a,b,c}

Metal Ion	Neutral Reactant	Neutral Products Irrespective of Label														
		H_2			CH_4			C_2H_4			C_2H_6			C_3H_6		
		IB ^a	MS ^b	CID ^c	IB	MS	CID	IB	MS	CID	IB	MS	CID	IB	MS	CID
Co^+	2-methylpropane	.27	.48	.37	.73	.50	.63									
	2-methylpropane-2-d ₁	.19	.23	.27	.81	.77	.73									
	butane	.29	.35	.32	.12	.001	.14				.59	.65	.54			
	butane-1,1,1,4,4,4-d ₆	.41	.36	.28	.10	.04	.15				.49	.60	.57			
	cyclopentane	.36	.35	.35	.03	.01	.02	.51	.58	.44				.07	.03	.05
	cyclohexane	.76	.95	.26	.03	.01	.01	.03	tr ^d	.07				.18	.03	.36
Ni^+	2-methylpropane-2d ₁	.07	.08	.21	.93	.92	.67									
	butane-1,1,1,4,4,4-d ₆	.34	.49		.09	0					.58	.50				

^aIB = Ion beam results obtained at 0.5 eV center of mass kinetic energy.

MS = Metastable ion decomposition results from present work.

CID = Collision-induced decomposition product yields from present work.

^bIon beam data for cyclic alkanes taken from Reference 4.

^cIon beam data for 2-methylpropane-2-d₁ from Reference 33. All other data for acyclic alkanes are from References 5 and 6.

^dTrace amount.

For metal alkane complexes with a fixed internal energy, competitive decomposition reactions from a common intermediate will result in similar product ratios for both the metastable and low-energy ion beam experiments. If, however, decomposition occurs from distinct non-interconverting structures that decompose at different rates, differences in the product yields determined with the two methods may be expected. For example, the ratios displayed in Table I for elimination of H_2 and C_2H_6 from cobalt and nickel complexes with butane are similar and suggest that a common intermediate is involved in both elimination reactions. In contrast, the loss of CH_4 is much less abundant in the metastable experiments and is consistent with a distinct intermediate which decomposes more rapidly than the species responsible for hydrogen and ethane elimination. The reaction schemes proposed to account for these products⁵ are entirely consistent with these observations. Although the data from the present study are limited, it would be of interest to make a more extensive comparison of the low-energy ion beam and metastable product yields.

The kinetic energy release distributions were obtained from the metastable peak shapes as described previously.²⁵ The reaction enthalpies for the decomposition reactions are listed in Table II along with the maximum and the average kinetic energy releases (E_{max} and E_{av} , respectively). Thermochemical data used in calculating the reaction enthalpies are tabulated in Appendix II. The kinetic energy distributions, shown in Figures 2-8, will be discussed individually. In all cases, the maximum probability for the kinetic energy distribution is set equal to unity.

Table II. Reaction Enthalpies and Maximum Kinetic Energy Release for Exothermic Reactions of Co^+ and Ni^+ a,b,c

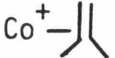
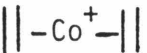
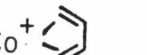
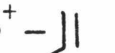
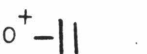
			$-\Delta H$	E_{max}	E_{av}		
Co^+		\longrightarrow	Co^+ - 	+ H_2	1.08	.94	.21
Co^+		\longrightarrow	Co^+ - 	+ H_2	1.46	} 1.4	.45
Co^+		\longrightarrow	Co^+ - 	+ H_2	1.07		
Co^+		\longrightarrow	Co^+ - 	+ H_2	1.2	} 1.2	.33
Co^+		\longrightarrow	Co^+ - 	+ H_2	1.4		
Co^+		\longrightarrow	Co^+ - 	+ H_2	1.2	1.2	.33
Co^+		\longrightarrow	Co^+ - 	+ CH_4	1.41	0.55	.13
Co^+		\longrightarrow	Co^+ - 	+ CH_4	1.5	0.60	.15
Co^+		\longrightarrow	Co^+ - 	+ CH_4	1.8	0.45	.094
Co^+		\longrightarrow	Co^+ - 	+ CH_4	1.7	0.56	.15
Co^+	$(\text{CH}_3)_2\text{CO}$	\longrightarrow	CH_2CoCO^+	+ CH_4	.61	} 0.20	.04
Co^+	$(\text{CH}_3)_2\text{CO}$	\longrightarrow	CoCH_2CO^+	+ CH_4	1.1		

Table II. Continued

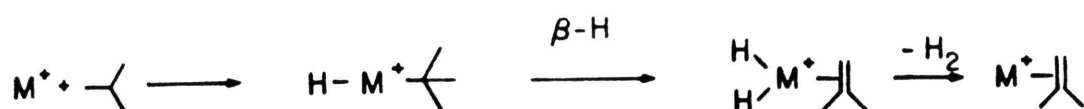
				<u>- H</u>	<u>E_{max}</u>	<u>E_{av}</u>	
Co ⁺	+ 	→	Co ⁺ -	+ C ₂ H ₆	1.09	.40	.095
Co ⁺	+ (CH ₃) ₂ CO	→	CoCO ⁺	+ C ₂ H ₆	1.8	.7	.15
Co ⁺	+ 	→	Co ⁺ -	+ C ₂ H ₄	0.70	.35	.084
Co ⁺	+ 	→	Co ⁺ -	+ C ₂ H ₄	0.65	.37	.091
Co ⁺	+ 	→	Co ⁺ -	+ C ₃ H ₆	0.53	0.32	.099
Co ⁺	+ 	→	Co ⁺ -	+ C ₃ H ₆	0.55	.35	.092
Co ⁺	+ (CD ₃) ₂ CO	→	Co(CD ₃) ₂ ⁺	+ CO	0.21	.50	.12
Ni ⁺	+ 	→	Ni ⁺	+ H ₂	1.4	1.5	.40
Ni ⁺	+ 	→	Ni ⁺ -	+ CH ₄	1.2	0.5	.13
Ni ⁺	+ 	→	Ni ⁺ -	+ C ₂ H ₆	1.1	0.4	.11

^aAll values given in eV.

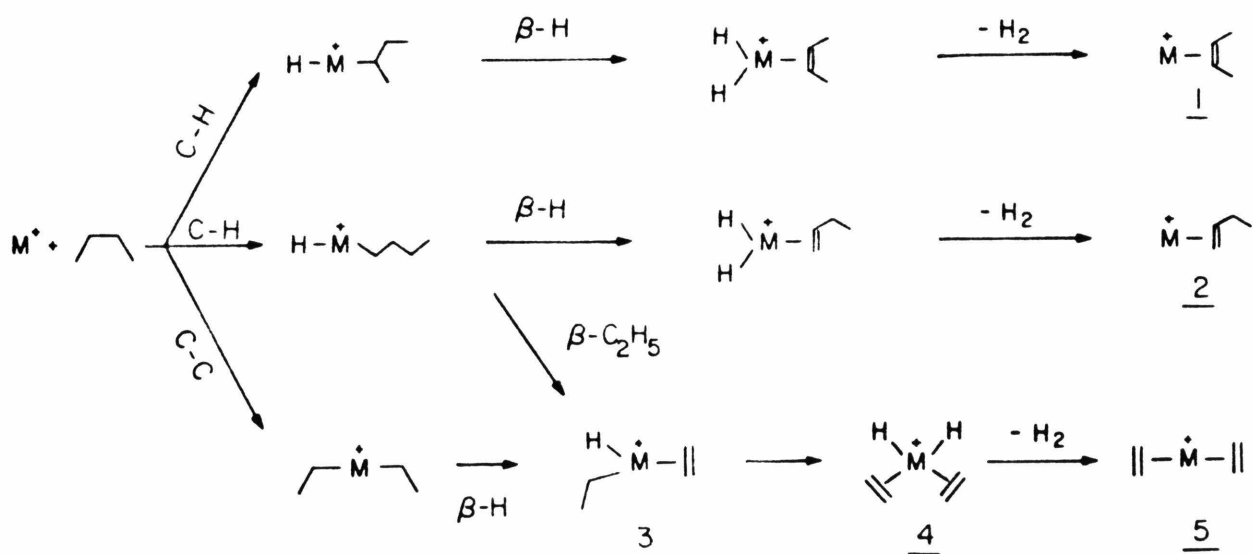
^bEstimates used to calculate enthalpies are given in Appendix I.

H-H Bond Formation Processes

C₄H₁₀ Isomers. The mechanisms for dehydrogenation of 2-methylpropane and n-butane by first-row group VIII metal ions have been extensively investigated.^{2,6,23,33-35} Exclusive loss of HD observed in the reaction of Co⁺ and Ni⁺ with 2-methylpropane-2d₁ is consistent with the 1,2-elimination represented in Scheme I.^{6,34} Loss of

Scheme I

hydrogen from n-butane could occur by a similar 1,2-elimination to form either a nickel(2-butene)⁺ complex (1) or a nickel(1-butene)⁺ complex (2). Dehydrogenation could also proceed by a 1,4-process which yields a bis-ethylene structure (5). These possibilities are delineated in Scheme II. As indicated, the 1,4-elimination may result from

Scheme II

initial C-H insertion followed by β -ethyl transfer to form intermediate 3 or, alternately, by initial C-C insertion and subsequent β -hydrogen transfer. It is estimated that both pathways for the 1,4-elimination are energetically accessible. Although it has not been possible to determine the initiating step for the 1,4-elimination, both pathways result in formation of the dihydride structure 4 from which H_2 elimination can occur. Similarly, the 1,2-elimination is postulated to involve hydrogen loss from a dihydride metal butene complex. Due primarily to the greater stability of the bis-olefin product (5), the exothermicity of the 1,2- and 1,4-processes differs by 0.4 eV (9.2 kcal/mol).

In the dehydrogenation of butane by Ni^+ , evidence from a variety of experiments supports a 1,4-elimination (Scheme II). The reaction of Ni^+ in a low-energy ion beam with butane-1,1,1,4,4,4- d_6 results in exclusive loss of D_2 as expected for a 1,4-process (Table III).^{6,33} Additional evidence for formation of the bis-olefin 5 is obtained from ion cyclotron resonance data on ligand exchange reactions³³ and from low-energy CID fragmentation patterns.³⁵

In similar ion beam experiments with cobalt ions, the dehydrogenation of $Co(\text{butane-1,1,1,4,4,4-}d_6)^+$ results in elimination of H_2 , HD, and D_2 in the respective ratios of 16:28:56 (Table III).⁶ This observation could be accounted for by postulating that either dehydrogenation occurs by the 1,2-elimination in Scheme II, leading to formation of $Co(\text{butane})^+$, or scrambling occurs before hydrogen elimination with the 1,4-process, or both.³⁶

To investigate further this question of reaction mechanisms, the kinetic energy release distributions associated with reactions known

Table III. Distribution of Labeled Products in the Reactions of Co^+ and Ni^+ with Butane-1,1,1,4,4,4- d_6

Metal Ion		Neutral Products							
		H_2	HD	D_2	CH_3D	CD_4	$\text{C}_2\text{H}_3\text{D}_3$	$\text{C}_2\text{H}_2\text{D}_4$	C_2D_6
Co^+	MS ^a	.32	.48	.20	1.0 ^d		.52	.48	
	IB ^b	.16	.28	.56	1.0		.15	.85	Tr ^e
Ni^+	MS ^a	.06 ^d	.06 ^d	.88 ^d	1.0			1.0	
	IB ^b			1.0	1.0			1.0	
Statistical ^c		.13	.54	.33	.62	.38	.47	.53	

^aMetastable product intensity.

^bIon beam product intensity measured at .5 eV relative kinetic energy. Data taken from Reference 6.

^cStatistical distribution assuming total scrambling.

^dPeak intensities were very small, and ratios are subject to large uncertainty.

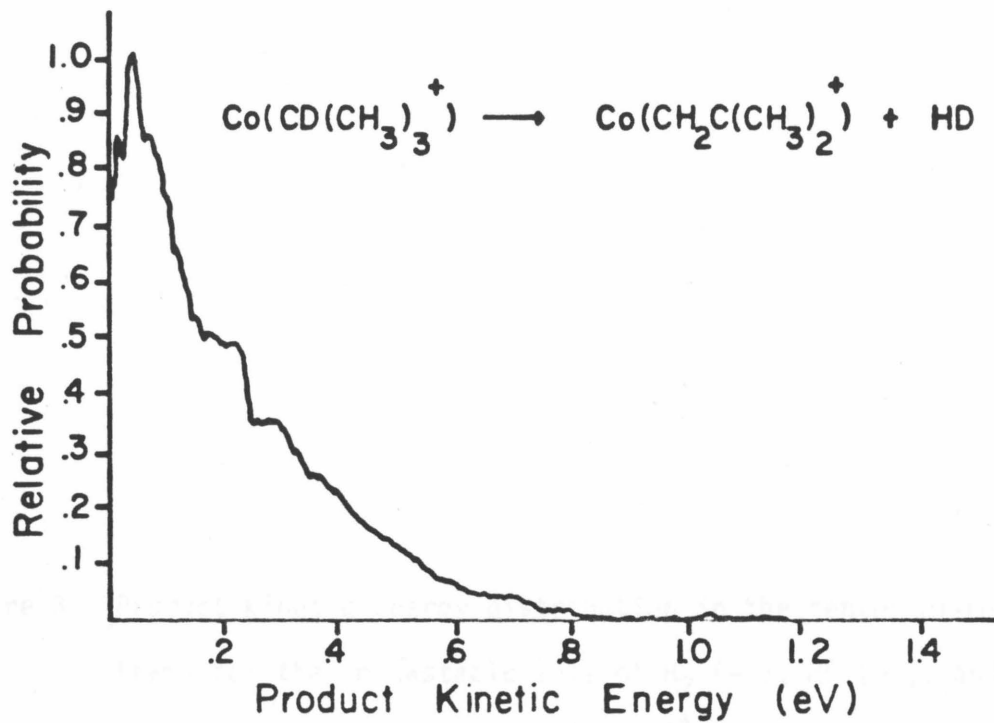
^eTrace amount.

to proceed by 1,2- and 1,4-processes were examined and compared with those resulting from the dehydrogenation of butane-1,1,1,4,4,4-d₆ by Co⁺. The elimination of HD from Co(2-methylpropane-2d₁)⁺ and the elimination of D₂ from Ni(butane-1,1,1,4,4,4-d₆)⁺ were assumed to be representative of 1,2- and 1,4-elimination processes, respectively. As shown by the data presented in Figure 2, the energy release distributions for the two processes are quite distinctive. The kinetic energy release for the 1,4-elimination (Figure 2b) is very broad with a maximum kinetic energy release of 1.4 eV. In contrast, the distribution for the 1,2-dehydrogenation of 2-methylpropane-2-d₁ (Figure 2a) is much narrower with E_{max} of only 0.8 eV. It is interesting to note that in both cases E_{max} is close to the reaction enthalpy (Table II).

The kinetic energy release distributions for loss of H₂, HD and D₂ from Co(butane-1,1,1,4,4,4-d₆)⁺ are presented in Figure 3. The similarity between all three of the kinetic energy distributions in Figure 3 and the resemblance to the distribution for 1,4-elimination of D₂ from Ni(butane-1,1,1,4,4,4-d₆)⁺ suggest that dehydrogenation of n-butane by Co⁺ proceeds predominantly by a 1,4-mechanism and that scrambling processes are responsible for the H₂ and HD eliminations. If the 1,2-process were dominant, a much narrower distribution would be expected. The respective ratio of H₂:HD:D₂ loss in the metastable study is 32:48:20³⁷ compared to 16:28:56 in the ion beam experiment.⁶ As expected, the extent of scrambling accompanying dehydrogenation and ethane loss (Table III) is increased with the longer timescale of the metastable decomposition. Interestingly, the metastable results indicate a larger than statistical ratio of products from scrambling

Figure 2. Product kinetic energy distribution in the center-of-mass frame for the metastable loss of: a) HD from Co(2-methylpropane)⁺, and b) D₂ from Ni(butane-1,1,1,4,4,4-d₆)⁺. The maximum probability is set equal to unity.

a)



b)

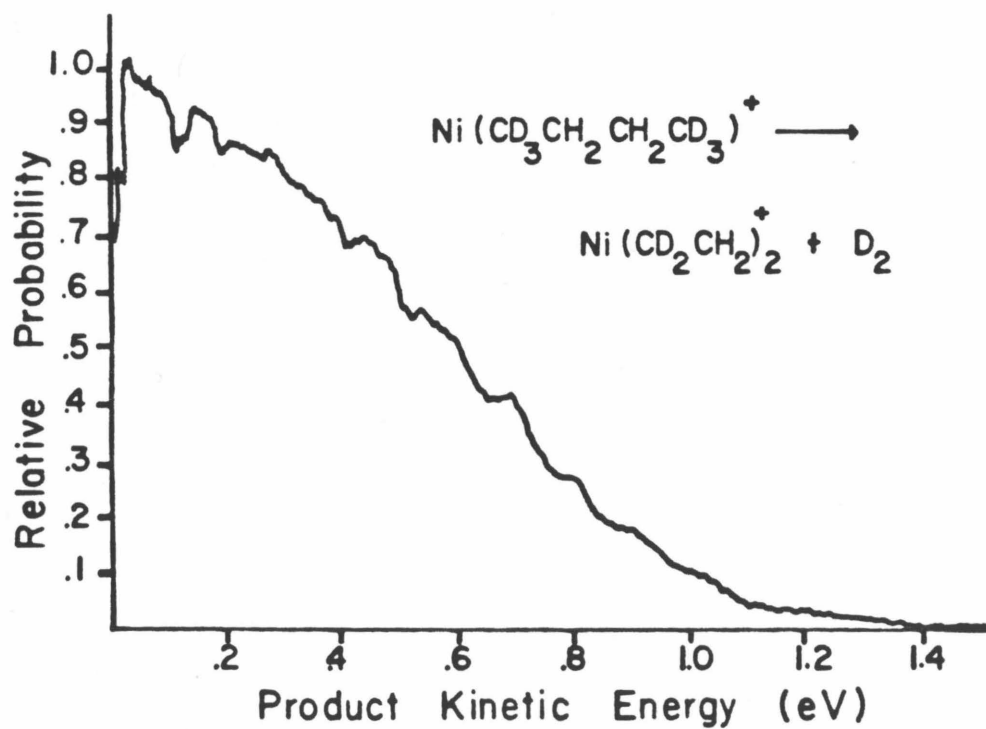
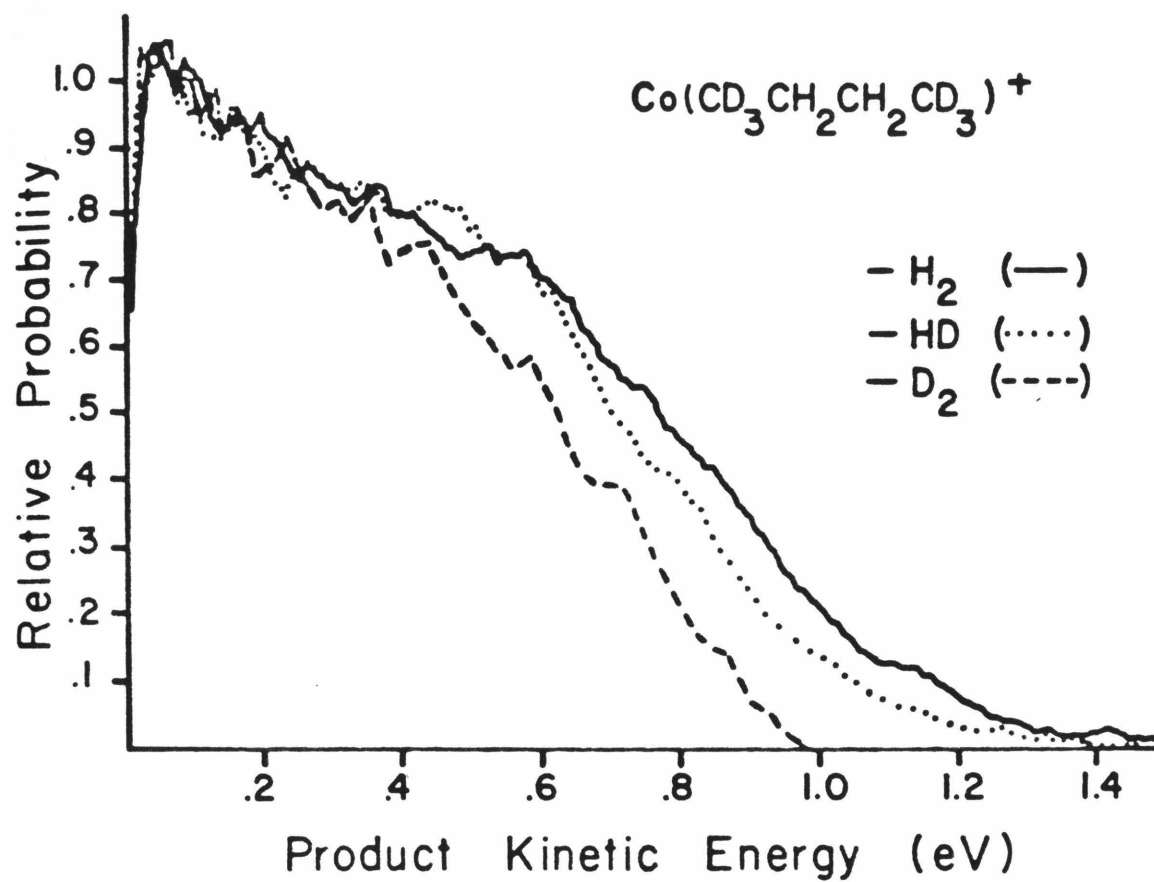


Figure 3. Product kinetic energy distribution in the center-of-mass frame for the metastable loss of H_2 (—), HD (---), and D_2 (---) from $\text{Co}(\text{butane-1,1,1,4,4,4-d}_6\text{)}^+$.



processes. This can be attributed to a kinetic isotope effect that discriminates against D_2 loss.³⁸ As can be seen from the data in Figure 3, the amount of energy released into product translation decreases in the order $H_2 > HD > D_2$. This interesting and highly reproducible isotope effect is discussed later.

Cyclopentane and Cyclohexane. Loss of H_2 from cyclopentane and cyclohexane is postulated to proceed via a 1,2-elimination as proposed in Scheme III. There is a great deal of evidence suggesting that the

Scheme III

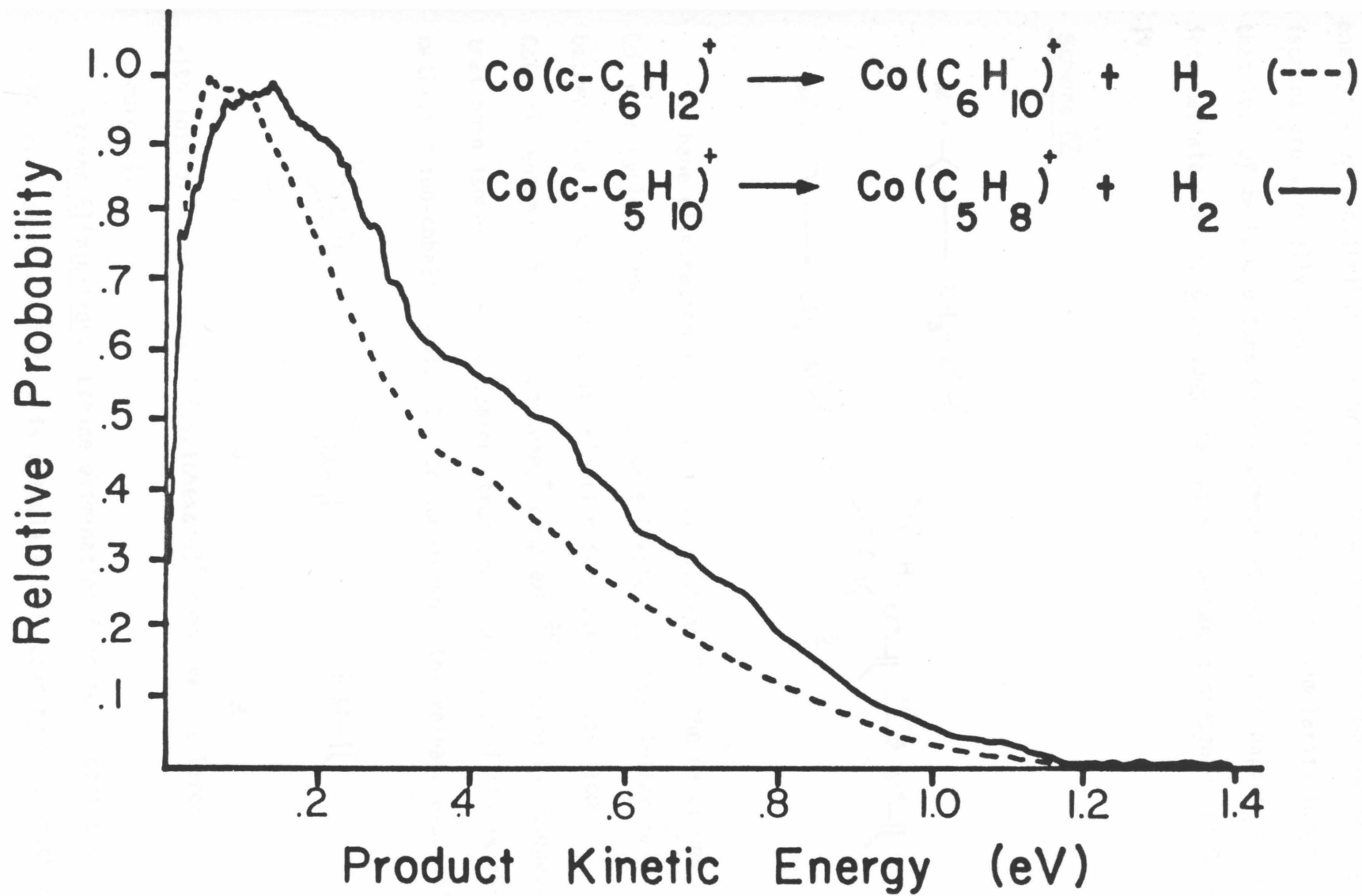


ring is maintained intact as shown.^{4,39} The kinetic energy distributions for loss of hydrogen from cobalt complexes of cyclopentane and cyclohexane are displayed in Figure 4. Although the reaction exothermicity for dehydrogenation of the cyclic alkanes is estimated to be almost twice that of 2-methylpropane (Table III), the shapes of the distributions are similar for all three.

C-H Bond Formation Processes

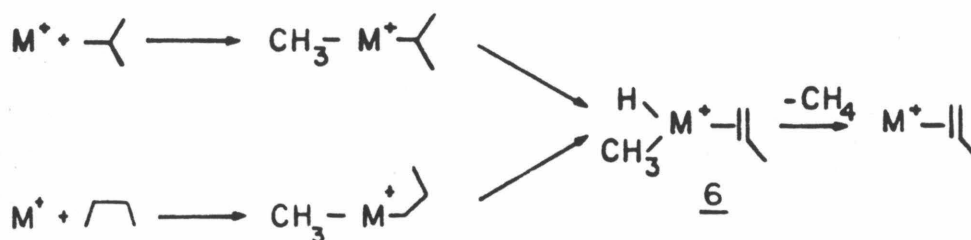
CH_4 Elimination. Product intensities listed in Table I for loss of methane from metal complexes with C_4H_{10} isomers clearly distinguish 2-methylpropane from n-butane. Methane elimination is a major pathway for decomposition of both cobalt ion and nickel ion complexes with 2-methylpropane but accounts for a much smaller percentage of the product distribution for decomposition of n-butane adducts. The kinetic

Figure 4. Translational energy distribution for elimination of H_2 from metastable $Co(cyclohexane)^+$ (\cdots) and $Co(cyclopentane)^+$ ($—$).

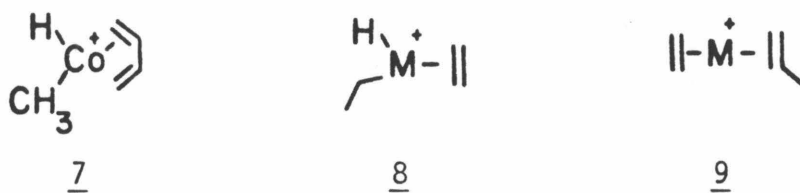


energy release distributions for methane elimination from the two C_4H_{10} isomers are virtually identical (Figure 5). This similarity suggests that loss of methane occurs from a common structure, perhaps from an intermediate such as 6 as suggested by the mechanism presented in Scheme IV.

Scheme IV



Methane elimination is a very minor pathway for the reactions of Co^+ with cyclopentane and cyclohexane (Table I). The similarity between the energy release distribution for methane loss from $Co(\text{cyclopentane})^+$ and $Co(\text{2-pentene})^+$ complexes⁴⁰ (Figure 6) suggests that both isomers access a common structure. One possibility is the methylhydrido-cobalt complex 7. In comparison, the release associated



with loss of methane from $Co(\text{cyclohexane})^+$ complexes is larger (Figure 6).

Ethane Elimination. Ethane elimination from ionic cobalt and nickel complexes with butane is postulated to occur from 8, which is

Figure 5. Kinetic energy distribution accompanying CH_4 loss from:
a) $\text{Co}(\text{2-methylpropane})^+$ and b) $\text{Co}(\text{butane})^+$.

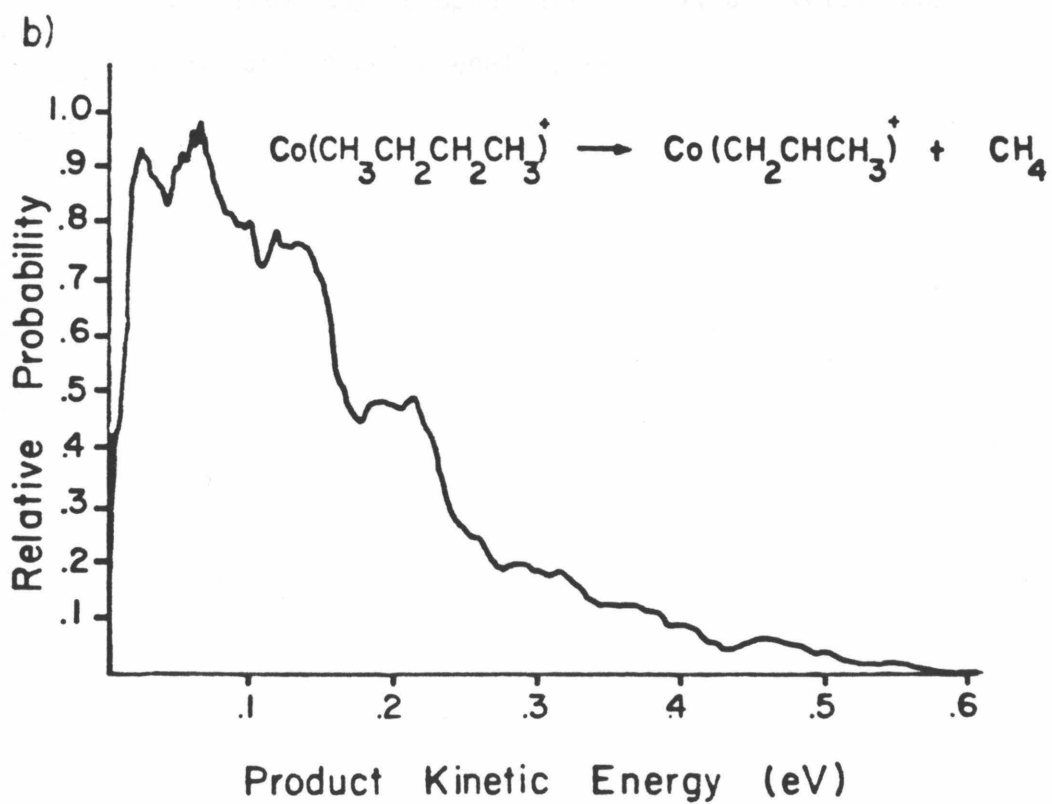
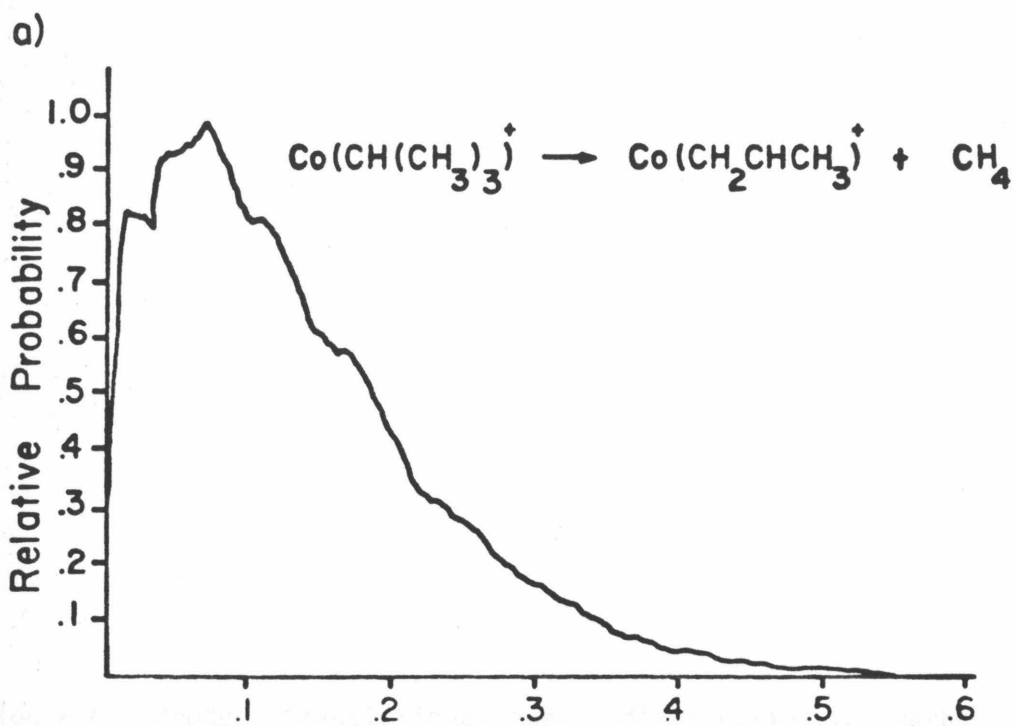
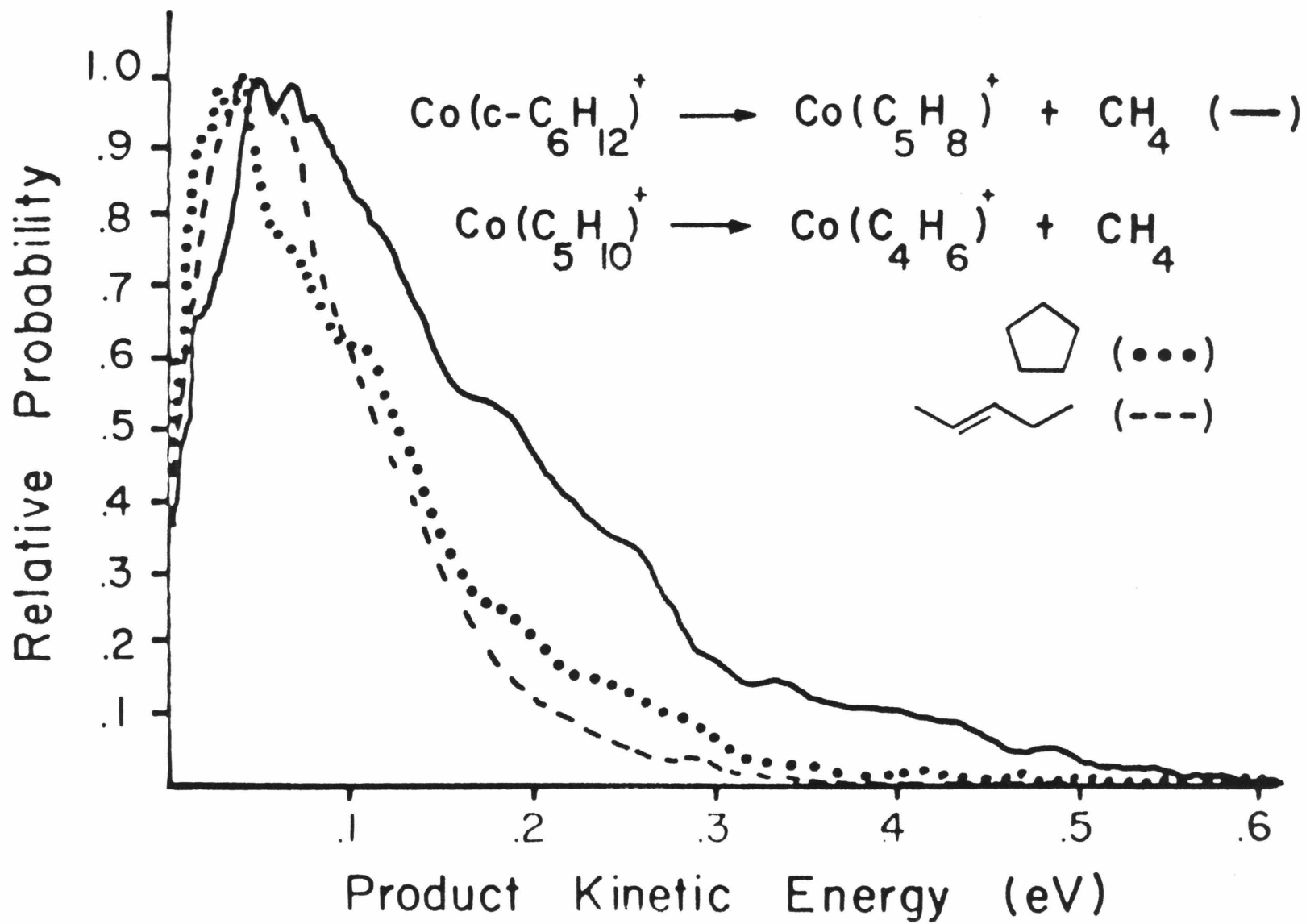


Figure 6. Product translational energy distribution for methane loss from $\text{Co}(\text{cyclopentane})^+$ (\cdots), $\text{Co}(\text{cyclohexane})^+$ (\dashrightarrow), and $\text{Co}(\text{2-pentene})^+$ ($---$).



also a proposed intermediate in the 1,4-dehydrogenation.^{5,6,33} (See Scheme II.) Apparently, ethane elimination competes effectively with transfer of a β hydrogen and subsequent loss of H_2 . The kinetic energy distribution for loss of ethane from $Co(\text{butane})^+$ complexes is shown in Figure 7. Interestingly, the distributions are the same, within experimental uncertainty, for loss of C_4H_6 from $Co(\text{butane})^+$ and loss of $C_2H_2D_4$ from $Co(\text{butane-1,1,1,4,4,4-d}_6)$. $Ni(\text{butane-1,1,1,4,4,4-d}_6)^+$ ions give essentially identical releases as the cobalt complexes. For both methane and ethane elimination processes, E_{max} is less than 50% of the reaction exothermicity. This is in sharp contrast to the dehydrogenation reactions where E_{max} was nearly equal to the reaction exothermicity.

Alkene Elimination. Elimination of ethene represents a major decomposition pathway for the $Co(\text{cyclopentane})^+$ complex. The kinetic energy distribution for C_2H_4 elimination from $Co(\text{cyclopentane})^+$ shown in Figure 8a is almost identical to that observed for loss of C_3H_6 from $Co(\text{cyclopentane})^+$ (dashed line on Figure 8b). This is consistent with alkene dissociation from a bis-olefin structure such as 9. The kinetic energy distribution accompanying C_3H_6 elimination from $Co(\text{cyclohexane})^+$ complexes (solid line in Figure 8b) is similar to that for olefin loss from $Co(\text{cyclopentane})^+$ complexes.

Interpretation of the Kinetic Energy Release Distributions

The potential energy surfaces for the reactions of cobalt and nickel ions with alkanes are more complex than the surfaces shown in Figure 1, but the same concepts and models are useful in interpreting the resulting kinetic energy release distributions. According to

Figure 7. Distribution of product kinetic energy resulting from C_2H_6 elimination from $Co(\text{butane-1,1,1,4,4,4-d}_6)^+$.

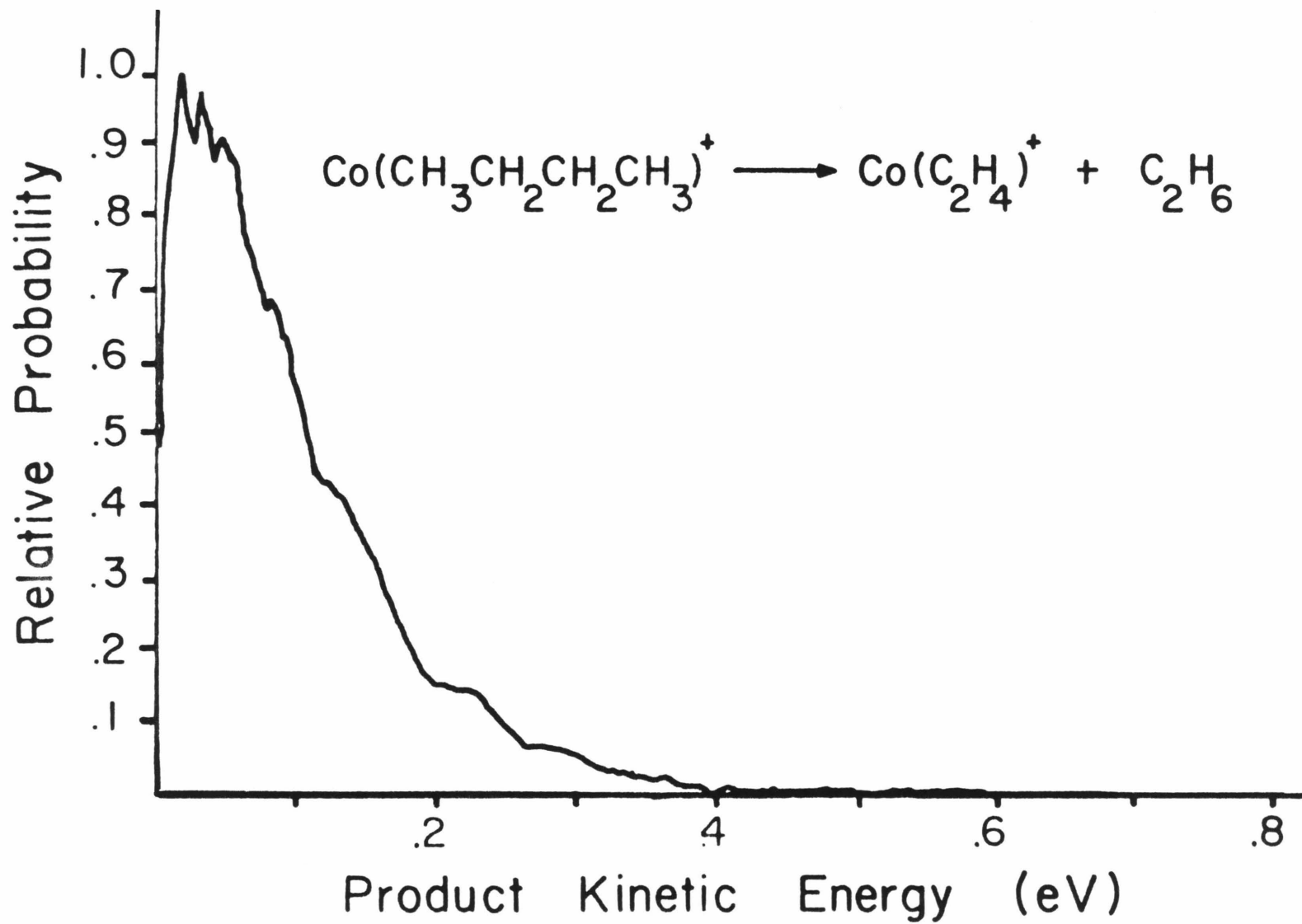
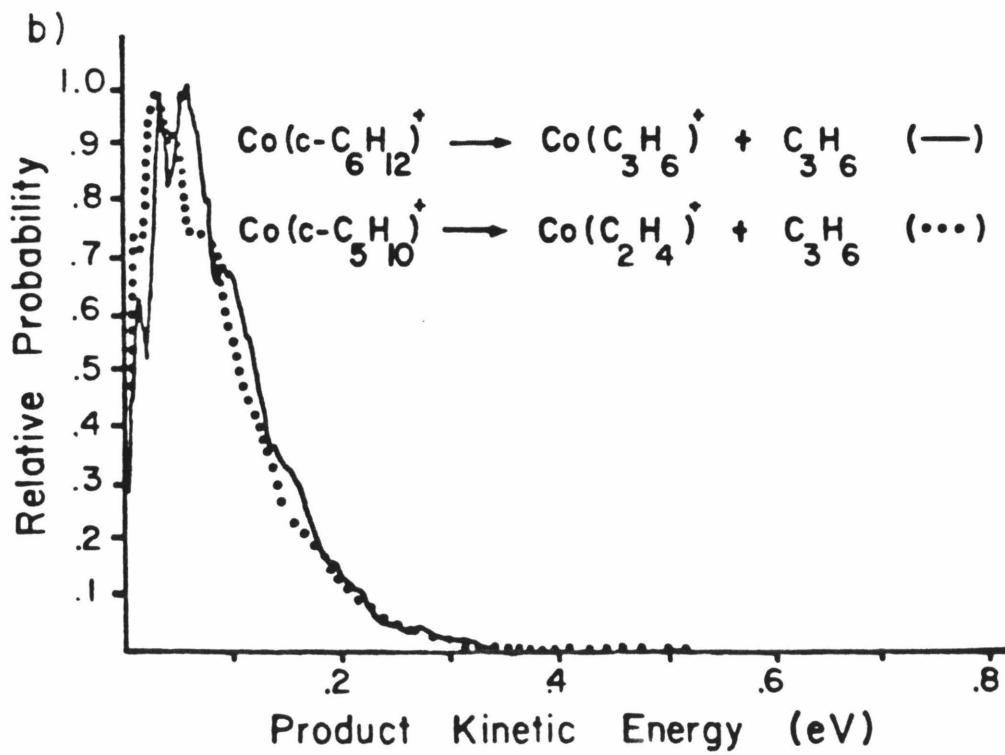
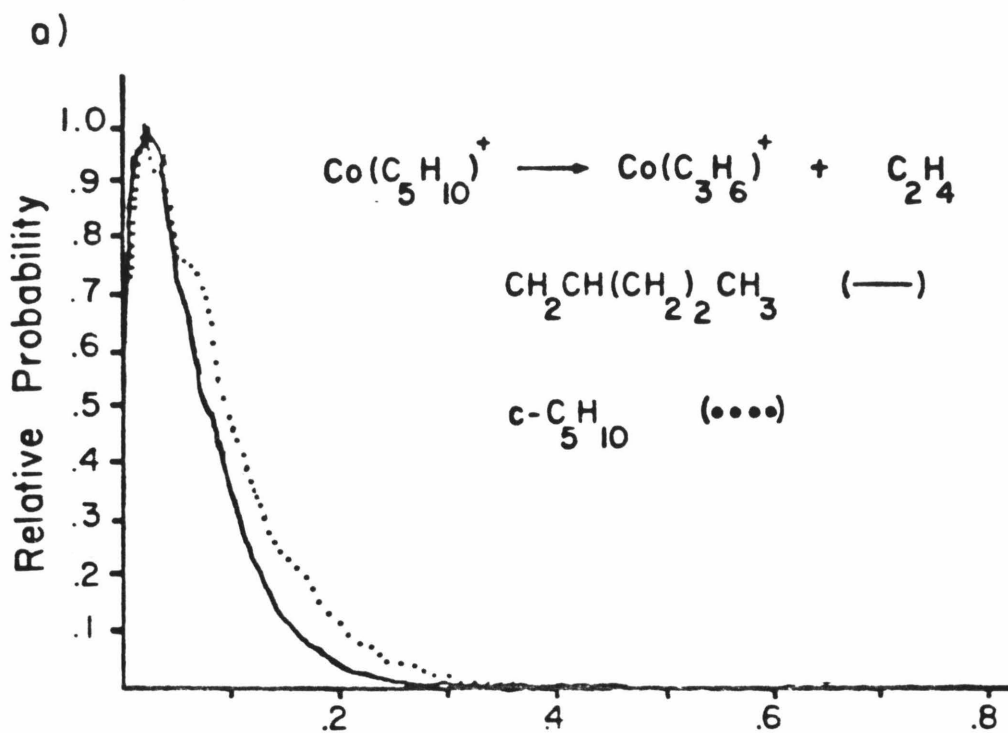


Figure 8. Product translational energy distribution for elimination of
a) C_2H_4 from $Co(cyclopentane)^+$ (\cdots) and $Co(2-pentene)^+$ (---)
and b) C_3H_6 from $Co(cyclopentane)^+$ (\cdots) and $Co(cyclohexane)^+$
(---)



statistical theories, the probability that the relative kinetic energy of the products from a unimolecular decomposition is E_t when the total available energy is $(E - E_a)$ is given by Equation 3. Here,

$$P(E_t) = \frac{N(E - E_a - E_t)}{G(E - E_a)} \cdot A_t(E_p) \quad (3)$$

$N(E - E_a - E_t)$ is the density of states for the critical configuration at an energy of $E - E_a - E_t$ and $G(E - E_a)$ is the sum of states available at the critical configuration at excess energy $E - E_a$.

$A_t(E_p)$ is the centrifugal correction term.¹³ Using the same notation, the average kinetic energy release is given by Equation 4, where E_{\max}

$$E_{\text{av}} = \frac{\int_0^{E_{\max}} E_t N(E - E_a - E_t) dE_t}{\int_0^{E_{\max}} N(E - E_a)} \quad (4)$$

is the maximum energy available for translation.

Calculation of the kinetic energy release distribution using Equation 3 is straightforward for a dissociation that involves only a centrifugal barrier (Type I surface, Figure 1a). If a Type II surface is involved, additional assumptions are necessary. It may be assumed that the energy can be divided into "fixed" and "nonfixed" portions. The energy that is used to surmount the potential energy barrier is considered fixed and must be released into relative product translation. The rest of the energy is assumed to be statistically divided among all degrees of freedom at the transition state. If no energy redistribution occurs after the transition state has been passed, the expected distribution will be shifted from zero by an amount equal to

the reverse activation barrier, E_{ar} , and will resemble the distribution indicated by the dashed line in Figure 1b.

The kinetic energy release distribution for ethene loss from $\text{Co}(\text{cyclopentane})^{\dagger}$ was modeled using RRKM theory, assuming that dissociation occurs from the bis-olefin structure 9.⁴¹ Dissociation of either C_2H_4 or C_3H_6 is expected to proceed without a barrier in excess of the bond dissociation energy (i.e., no barrier to the reverse reaction). As shown in Figure 9, the calculated distribution agrees well with the experimental results.

The kinetic energy release distributions for loss of H_2 from $\text{Co}(\text{butane})^{\dagger}$ and $\text{Co}(\text{2-methylpropane})^{\dagger}$ were modeled using Equations 3 and 4 and assuming a Type I surface. The theoretically predicted kinetic energy distribution for H_2 loss from both C_4H_{10} isomers is much narrower than the experimentally observed distribution. The calculated and experimental distributions for loss of H_2 from $\text{Co}(\text{butane})^{\dagger}$ complexes are compared in Figure 10a. While the average kinetic energy release for butane dehydrogenation is calculated to be ~ 3 kcal/mol, the experimentally determined value is 10.3 kcal/mol. The results of these calculations clearly indicate that the kinetic energy distributions for hydrogen elimination cannot be modeled by assuming a purely statistical energy release from a Type I potential energy surface.

Loss of methane from $\text{Co}(\text{2-methylpropane})^{\dagger}$ is characterized by a kinetic energy release distribution that is narrower than that for hydrogen elimination. This was unexpected since both the reaction exothermicity and the reverse activation barrier were expected to be greater for elimination of methane.⁴² Statistical models were able

Figure 9. Experimental (—) and theoretical (---) kinetic energy release distributions for loss of C_2H_4 from $Co(cyclopentane)^+$. Calculated distribution assumes no reverse activation barrier and 10 kcal/mol available for translation (E_{av}).

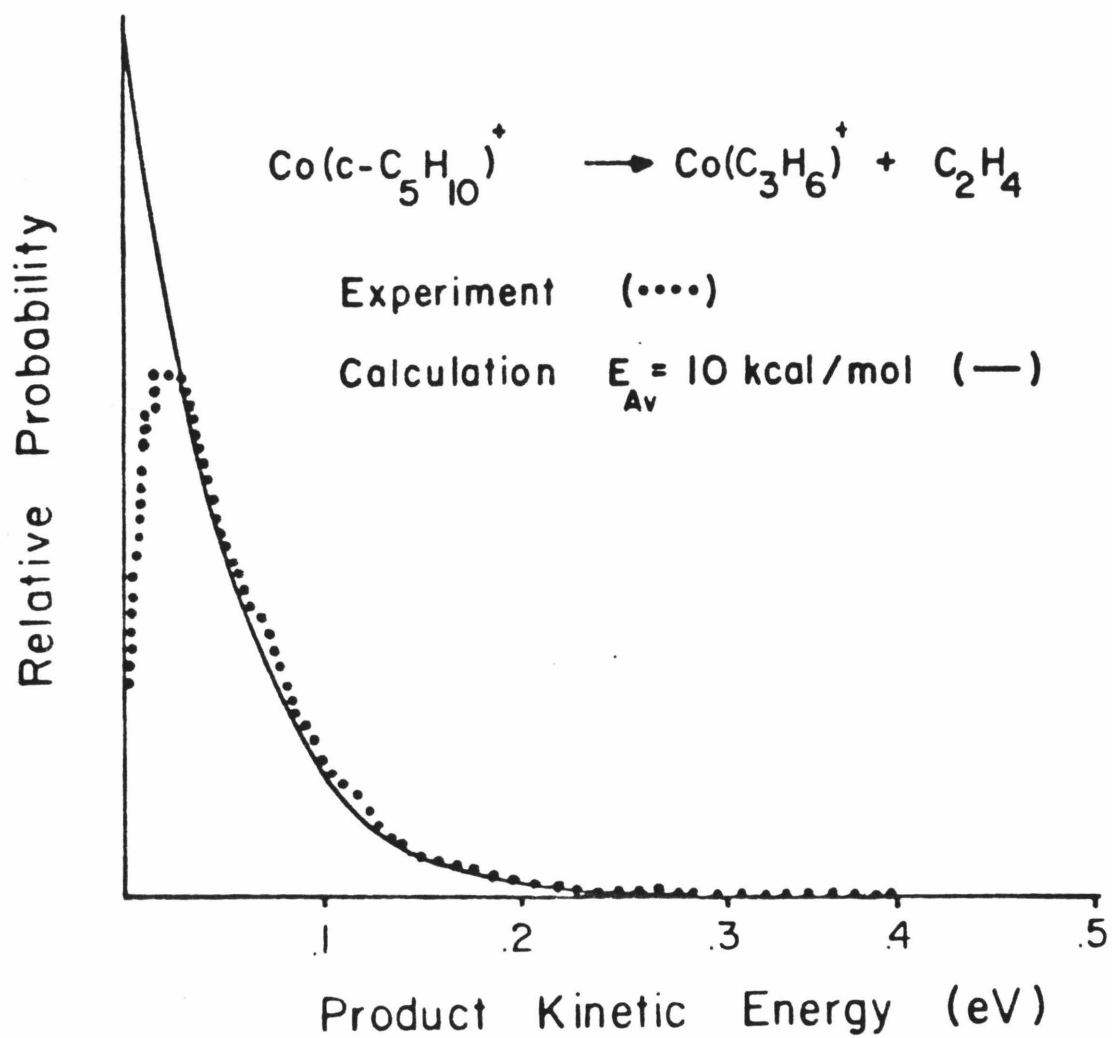
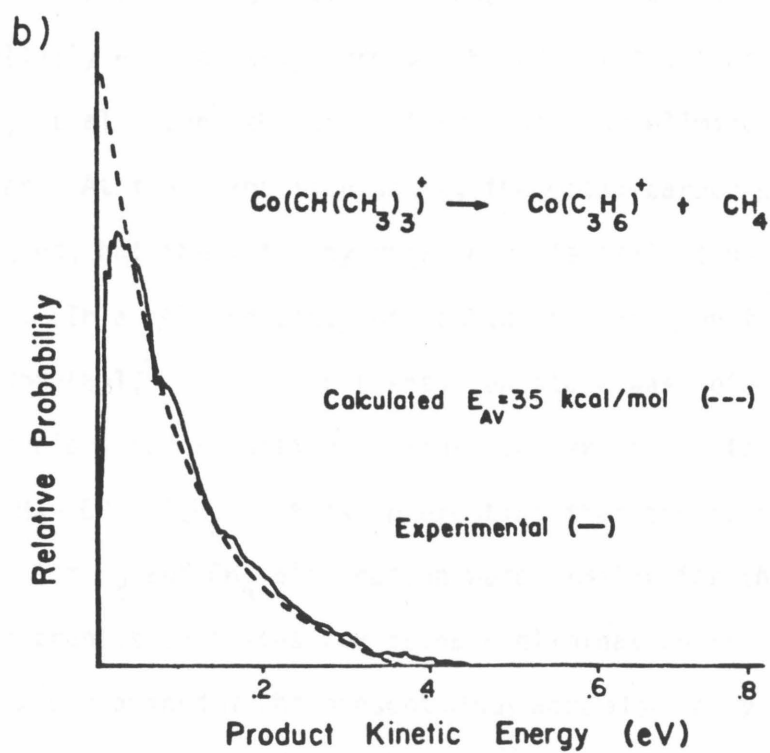
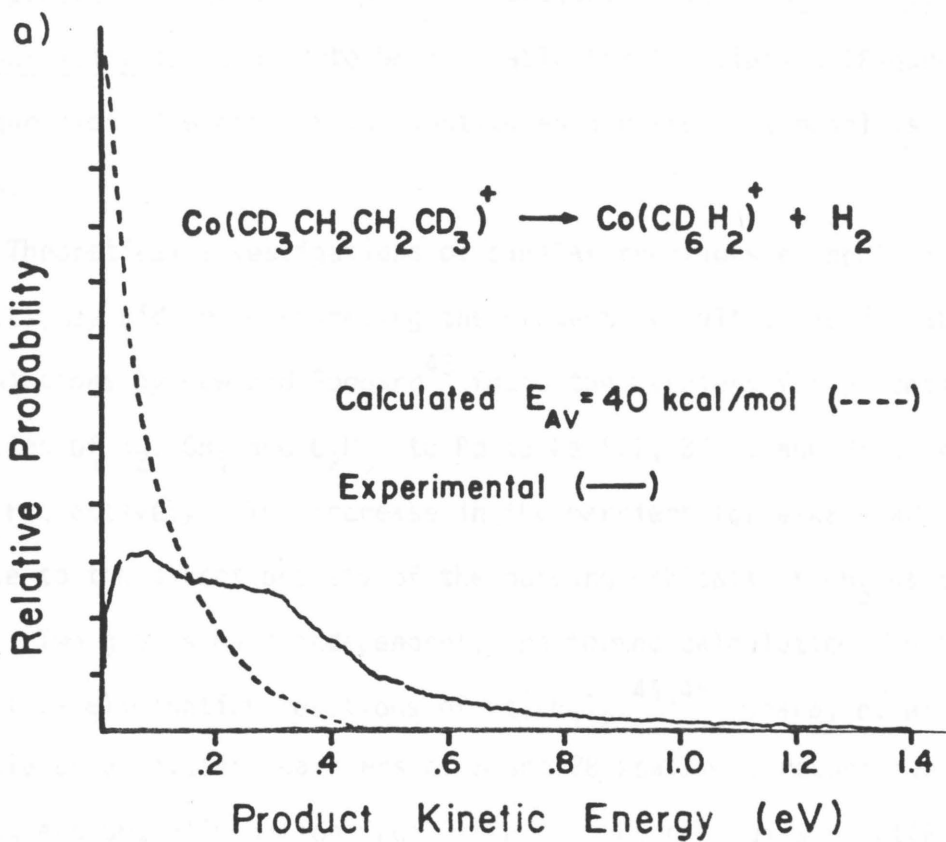


Figure 10. Experimental (—) and theoretical (···) distributions for:
a) loss of H_2 from $\text{Co}(\text{butane})^+$
b) loss of CH_4 from $\text{Co}(\text{2-methylpropane})^+$.



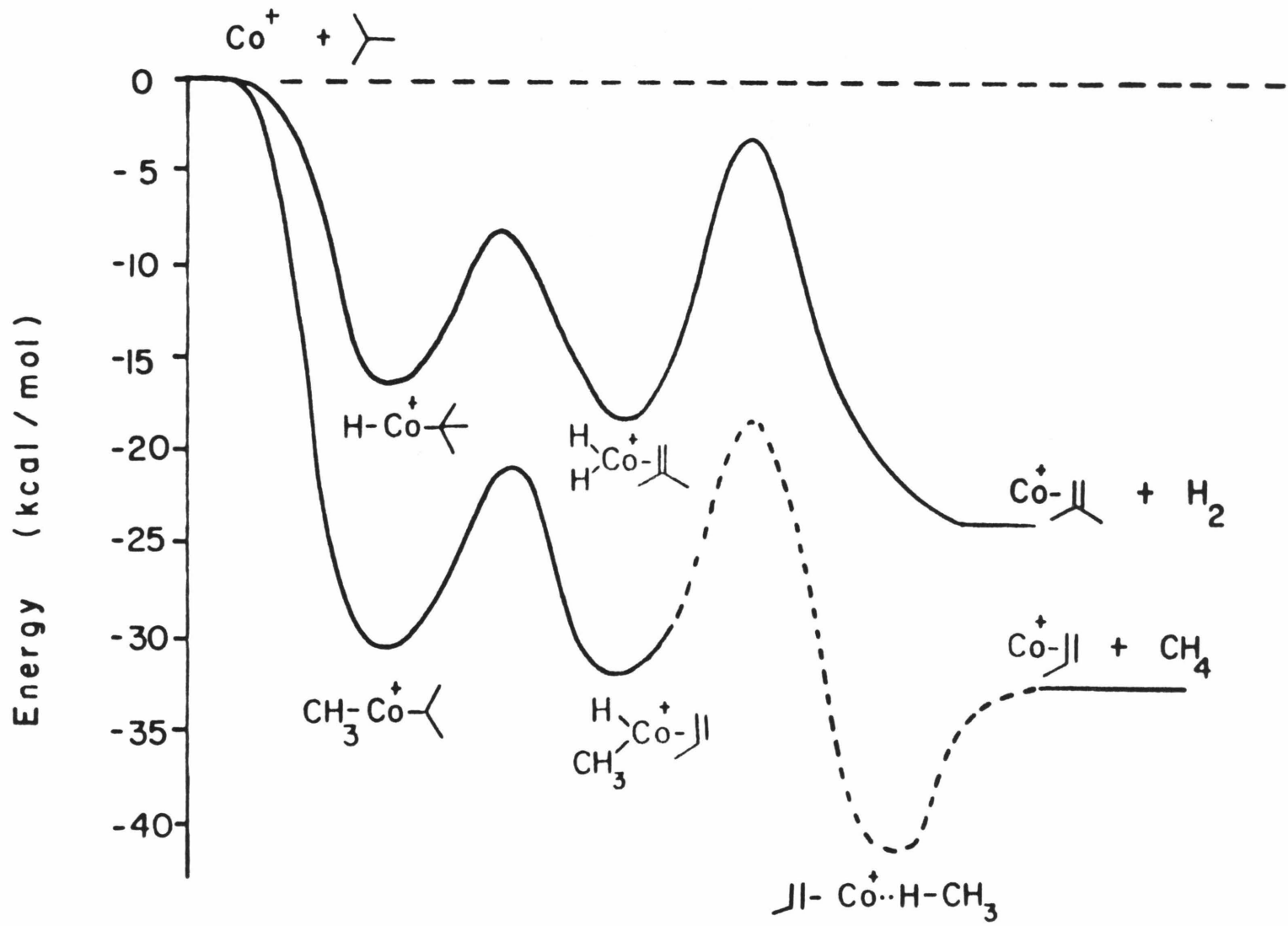
to reproduce the experimental distributions if the entire reaction exothermicity is assumed to be available for translation (Figure 10b). The question of whether this constitutes a reasonable model is discussed below.

Theoretical investigations of similar reactions at neutral metal centers may aid in interpreting the present results. Recent ab initio calculations by Low and Goddard⁴³ found the barriers for oxidative addition of H₂, CH₄ and C₂H₆ to Pd to be 5.1, 30.5, and 38.0 kcal/mol, respectively. The increase in the barriers for alkane addition is due to the directionality of the bonding orbitals in CH₃ as compared to H. Two groups have independently performed calculations on the reductive elimination reactions of Pt(PH₃)₂.^{44,45} Obara, et al.⁴⁵ calculated activation barriers of 8 and 28 kcal/mol, respectively, for H₂ and CH₄ elimination from Pt(PH₃)₂. Both studies of Pt(PH₃)₂ found that, for hydrogen elimination, the barrier is "late" with essentially a completely formed H-H bond at the transition state, while Obara, et al. found the transition state for elimination of CH₄ to be earlier. At the transition state, the metal-carbon bond is significantly elongated, but the metal-hydrogen bond is still close to the equilibrium length. In a related study of methane elimination from nickel hydridomethyl,⁴⁶ a similar transition state was determined. Again, the barriers for reductive elimination were found to increase in the order H₂ < CH₄ < C₂H₆. It is interesting that the calculated transition states for H₂ and CH₄ elimination were similar for the different metals.⁴⁷ If the transition states for methane elimination from the Ni⁺ and Co⁺ complexes examined in the present study were also early, then energy flow from the reaction coordinate into other modes after passage through the

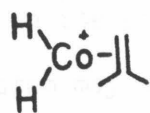
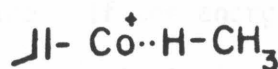
transition state is expected. In contrast, little energy redistribution is anticipated for a late transition state which is essentially a hydrogen molecule associated with a metal-olefin complex. This would then explain the observation that, for the 2-methylpropane complexes, the amount of energy converted into product translation for methane elimination is less than that for hydrogen elimination, even though the reverse activation barrier is expected to be larger for the former.

A reaction coordinate diagram is helpful in discussing the implications of the kinetic energy distributions. Qualitative potential energy surfaces for the exothermic reactions of 2-methylpropane with cobalt ion are depicted in Figure 11. Although the total reaction enthalpies are fairly well established, the energetics of the individual steps are not well known. The estimates used in constructing this diagram are listed in Appendix II. The potential surfaces are constructed in a manner which is consistent with information about the reactions known from branching ratios, labeling studies, as well as the kinetic energy release distributions determined in the present study. As mentioned in the Introduction, one might also wish to consider alternate mechanisms involving multi-centered interactions; however, there is evidence from high-energy CID studies^{23,24} for formation of strongly bound metal-alkane structures which are the proposed intermediates. Dehydrogenation reactions are presumed to occur by initial metal insertion into a C-H bond. The lack of scrambling with dehydrogenation of 2-methylpropane-2d₁ indicates that H₂ elimination must be faster than reinsertion of the olefin into the Co-H bond. This suggests that $E_1 \gg E_2$ or the frequency factors favor H₂ elimination.

Figure 11. Qualitative potential energy diagram for the exothermic reactions of Co^+ with 2-methylpropane.



The kinetic energy distributions for dehydrogenation of 2-methylpropane should be sensitive to the details of the potential energy surface connecting the dihydride 10 to the products. A significant result of

1011

this study is that the kinetic energy release distributions associated with dehydrogenation of 2-methylpropane (and all other alkanes in this study) are "nonstatistical" and have a maximum kinetic energy release approximately equal to the enthalpy of the reaction. This suggests that the maximum in the energy barrier for the final step is almost equal to the available energy. Apparently, conversion of the reverse activation energy into translational energy of the products is very efficient. For some fraction of ions, the entire reaction exothermicity appears as translational energy. Therefore, exclusive formation of excited-state products is unlikely.

As indicated in Figure 11 methane elimination from $\text{Co}(\text{2-methylpropane})^+$ is more exothermic than hydrogen elimination. The translational energy release accompanying methane loss from $\text{Co}(\text{2-methylpropane})^+$ may be distorted by energy redistribution after the reactant-like transition state has been passed. An alternate explanation for the narrow kinetic energy distribution for methane elimination is shown schematically in Figure 11. The interaction between the separating $\text{Co}(\text{olefin})^+$ ion and methane may involve the formation of a stable Lewis acid-base adduct 11. Similar adducts

between metal atoms and alkanes have been identified in low-temperature matrices.⁴⁸ In addition, weakly associated complexes of methane and ethane with Pd and Pt atoms are calculated to be bound by ~4 kcal/mol.⁴⁴ The interaction of the hydrogens with the ionic metal center may result in a deeper well on the potential surface. If the energy redistribution is rapid, the system may spend time in this potential well, and dissociation to products can indeed be described by a Type I potential energy surface. Note that even if structure 11 is a local minimum on the surface, rearrangement to the hydridomethyl species still involves an activation barrier. In either case, it appears that kinetic energy distributions for methane elimination are not very useful in determining the height of the reverse activation barrier. For this reason, the features of the exit channel in Figure 11 for CH₄ elimination are represented by dashed lines.

A qualitative potential energy diagram for loss of hydrogen and ethane from Co(butane)⁺ complexes is presented in Figure 12. The initial steps for both ethane and hydrogen elimination from Co(butane)⁺ adducts are postulated to involve C-C bond insertion followed by β -hydrogen transfer. From intermediate 9, elimination of ethane (C-H bond coupling) or transfer of a second hydrogen and subsequent H-H bond formation may occur. Scrambling of the deuterium labels occurs with ethane and hydrogen elimination from butane-1,1,1,4,4,4-d₆, suggesting that insertion of ethene into the Co-H bond is facile. This is in contrast to the Co(2-methylpropane)⁺ dehydrogenation reaction where reinsertion of 2-methylpropene into the Co-H bond does not occur. The product intensity for the ion resulting from ethane elimination from Co(butane)⁺ is larger than that corresponding to hydrogen elimination

Figure 12. Qualitative reaction coordinate diagram for the reactions of Co^+ with butane to form the products $\text{Co}(\text{C}_2\text{H}_4)^+$ and $\text{Co}(\text{C}_2\text{H}_4)_2^+$.

(Table I). This suggests that C-H bond coupling leading to ethane elimination is favored over hydrogen transfer. Both the shape of the kinetic energy distribution and the maximum energy release for loss of hydrogen from ionic cobalt or nickel complexes with butane suggest that the reverse activation barrier is a significant fraction of the reaction exothermicity. Ethane loss from $\text{Co}(\text{butane})^+$ is accompanied by a small release of kinetic energy. As was discussed for the case of methane elimination from $\text{Co}(\text{2-methylpropane})^+$, this could be due to exit channel coupling effects or dissociation from a Lewis-acid base complex.

The present results clearly indicate that addition of hydrogen to complexes of cobalt or nickel ion with certain alkenes (ethene, methylpropene, cyclopentene, and cyclohexene) involves a substantial activation barrier. In addition, the evidence is consistent with an activation barrier for oxidative addition of ethane or methane to ionic cobalt and nickel olefin complexes. These conclusions are supported by the general failure to observe any evidence of D_2 or alkane addition to a variety of cobalt and nickel olefin complexes.⁴⁹⁻⁵² This is not true for all metal olefin complexes. $\text{Rh}(\text{C}_3\text{H}_6)^+$, for example, will add D_2 and undergo H/D exchange.⁵² Similarly, Ti^+ and Nb^+ complexes with a variety of alkenes also add D_2 without an activation barrier.⁴⁹ It is of interest to note that for ethane or methane elimination, the entrance channel has no barrier, while the exit channel, which involves a similar C-H bond formation process, has a significant activation barrier. Recent theoretical studies⁵³ on the reductive elimination of nickel d^8 complexes also found the barrier to elimination to be very sensitive to coordination of the metal center. In this case,

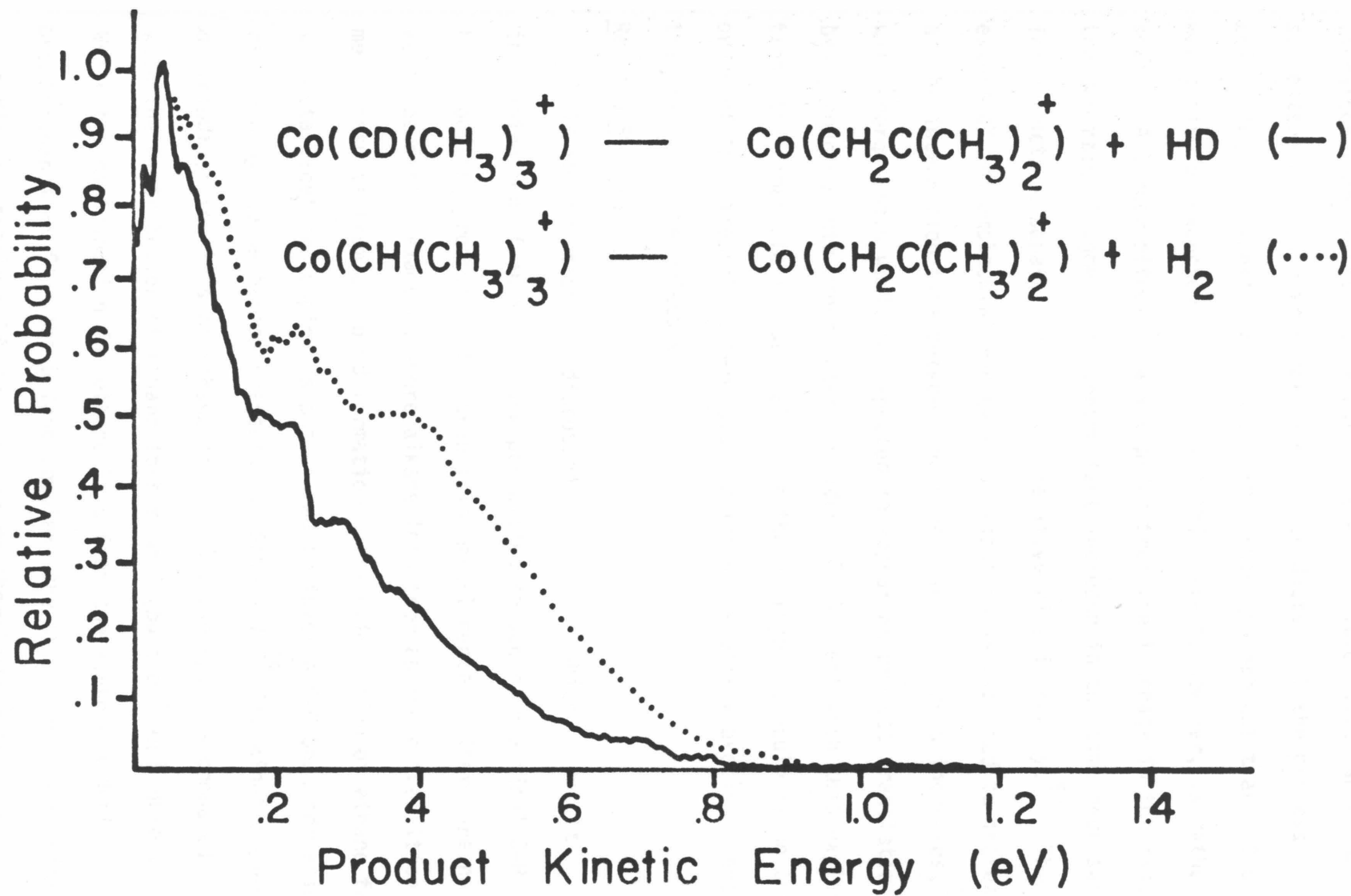
the addition of an olefin to the metal clearly alters the energetics for the elimination process.⁵⁴

Isotope Effects

In the metastable product yields for cobalt (2-methylpropane)⁺ and cobalt(2-methylpropane-2-d₁)⁺ complexes (Table I), a preference for methane elimination from the deuterated molecule is evident. There is also a striking difference in the kinetic energy distributions for loss of H₂ or HD from the respective complexes. Loss of HD from 2-methylpropane-2-d₁ results in a kinetic energy distribution that is narrower than that for H₂ loss from 2-methylpropane (Figure 13). Similarly, the kinetic energy releases become progressively narrower for loss of H₂, HD, and D₂ from Co(butane-1,1,1,4,4,4-d₆)⁺ complexes (Figure 3). This isotope effect is opposite that expected from the effect of zero-point energy differences on the activation barriers.³⁸ More generally, the amount of energy appearing in product translation for a given elimination reaction from a specific molecular complex is observed to decrease as the mass of the departing fragment increases due to isotopic substitution.⁵⁵

The effect of deuterium substitution on the reduced mass of the departing fragment is particularly significant for the dehydrogenation processes. The reduced mass of the neutral product increases by a factor of 1.33 and 2.0 for loss of HD and D₂, respectively. Exactly how this affects the kinetic energy release is not clear. For dehydrogenation reactions, the shapes of the distributions suggest that exit channel effects (some of which were considered in the Introduction) may be distorting the translational energy distribution. The isotope effect could simply reflect the decrease in the spacing of both the

Figure 13. Kinetic energy distribution for loss of: H_2 from $\text{Co}(\text{2-methylpropane})^+$ (\cdots) and HD from $\text{Co}(\text{2-methylpropane-2-d}_1)^+$ (—).

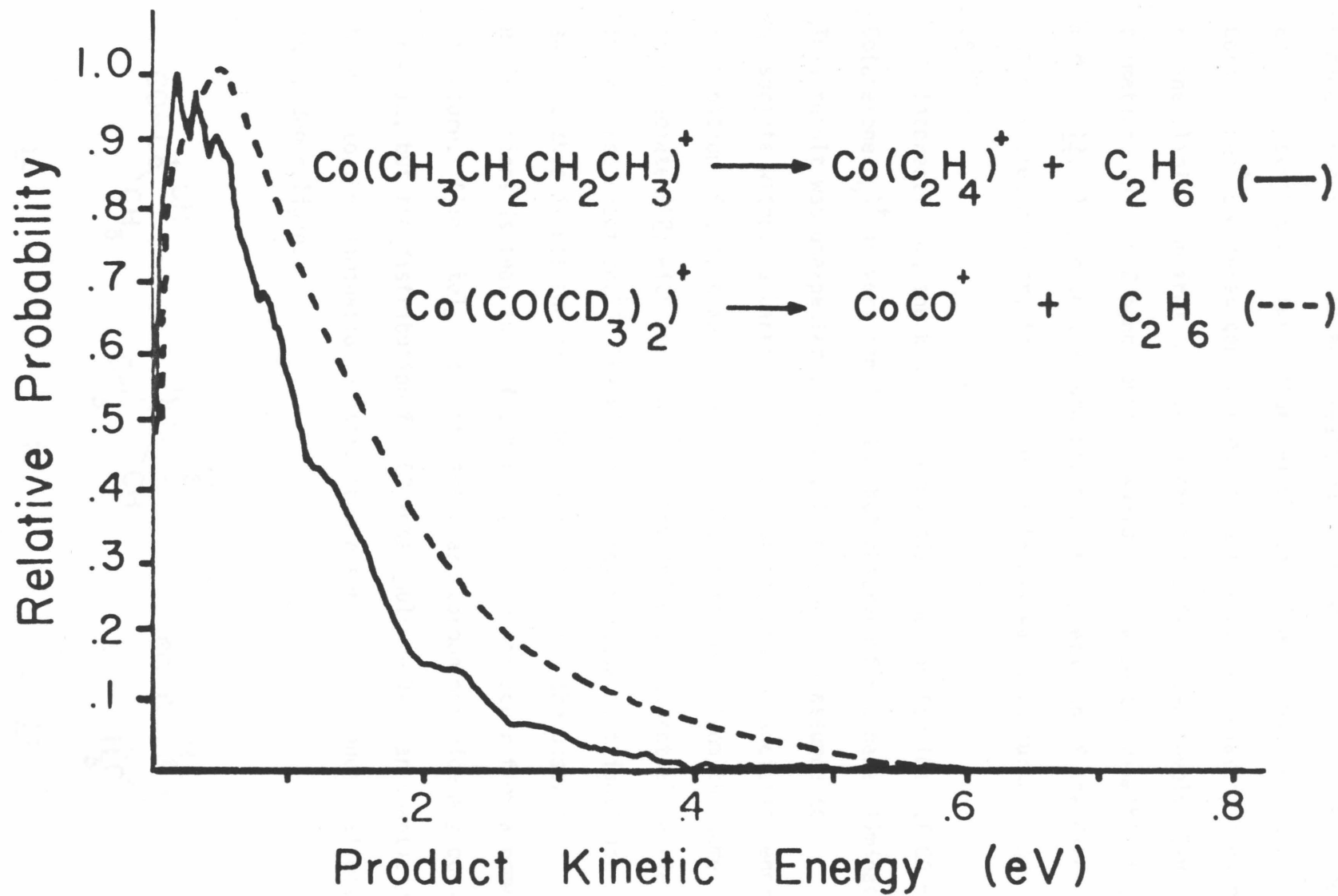


vibrational and rotational levels in the transition state which Marcus¹⁸ suggests evolve into free rotations of products. If the process is adiabatic, the excess energy that contributes to product translation would also be expected to decrease. This effect, however, is rather small. A larger effect is anticipated from the increase in the mass of the departing fragment and concomitant increase in the time necessary for products to separate at a given relative kinetic energy.⁵⁶ The extent of intramolecular energy redistribution is expected to increase as the interaction time between the separating fragments increases,⁵⁷ with energy which would be expected to appear as product translation being coupled into other internal modes. Consistent with this explanation, the timescale for separation of the hydrogen molecule is on the order of the timescale determined for intramolecular vibrational energy transfer in large molecules.⁵⁸

Related Studies

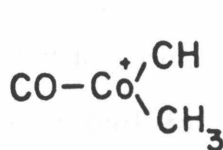
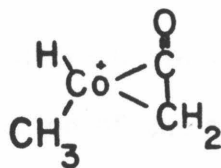
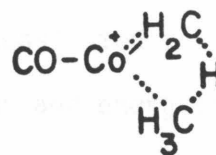
All the reactions discussed above which result in elimination of an alkane are postulated to occur by a final C-H bond coupling process at the transition metal center. There are no well-documented examples where alkane loss from an ionic transition metal results from C-C bond formation. The elimination of ethane from the metal acetone complex is postulated to involve C-C bond formation as shown by the mechanism presented in Scheme V.⁵⁹ The kinetic energy distribution for loss of ethane from $\text{Co}(\text{acetone-d}_6)^+$ is compared with the distribution of ethane loss from $\text{Co}(\text{butane})^+$ in Figure 14. While the distribution for ethane loss from the acetone adduct is broader than that from the butane complex, the shapes are quite similar. In addition, nearly half the reaction exothermicity appears as

Figure 14. Kinetic energy distribution corresponding to elimination of C_2H_6 from $Co(\text{butane})^+$ and C_2D_6 from $Co(\text{acetone-d}_6)^+$.



product translation for both reactions. The differences in the kinetic energy distributions for ethane elimination from $\text{Co}(\text{butane})^+$ and $\text{Co}(\text{acetone})^+$ complexes could be due to different dissociating structures. Ethane elimination from an hydridoethyl species would involve C-H bond formation, while C-C bond coupling would occur with the dimethyl intermediate 12. At present, an unambiguous interpretation of the data is not possible; however, the question certainly warrants further investigation.

Interestingly, the kinetic energy distribution for loss of CO from $\text{Co}(\text{acetone-d}_6)^+$ is very similar to that observed for ethane elimination. This result was unexpected since CO, like C_2H_4 , was assumed to dissociate without a barrier in excess of the bond dissociation energy. Elimination of ethane and CO was postulated to occur from the same intermediate (12) with loss of C_2H_6 involving a substantial barrier to the reverse reaction.⁵⁹ The kinetic energy release distributions suggest this is not the case. One explanation for the observed distributions is that loss of ethane and CO do not occur from a common structure. Alternately, loss of ethane and carbon monoxide may occur from 12, but the distribution for CO loss could reflect an unanticipated barrier to the elimination arising from a synergistic bonding effect of the π -donor ligand.

121314

Loss of CH_4 is also observed from $\text{Co}(\text{acetone-d}_6)^+$ complexes (Table IV) and has previously been postulated to occur from structures 12 or 13.⁶⁰ Elimination of CH_4 from 12 may involve the four-centered transition state 14, while reductive elimination of methane from 13 would be expected to involve a hydridomethyl intermediate similar to those proposed in the reactions of Co^+ with alkanes. The kinetic energy distribution for CD_4 elimination from $\text{Co}(\text{CO}(\text{CD}_3)_2)^+$ (Figure 15) is narrower than that observed from the alkane adducts despite the fact that the exothermicities of these reactions are comparable. The smaller release for CD_4 elimination for $\text{Co}(\text{CO}(\text{CD}_3)_2)^+$ may reflect changes in the reverse activation barrier. It is possible that the four-centered elimination involving 14 has a lower activation barrier than elimination of methane from the hydridomethyl metal complex. Alternatively, the presence of the ketene ligand in 13 could also influence the barrier height. Determining the structure of the product ions corresponding to the various decomposition reactions of $\text{Co}(\text{CO}(\text{CD}_3)_2)^+$ may clarify whether the differences in the kinetic energy distributions for the $\text{Co}(\text{acetone})^+$ and $\text{Co}(\text{alkane})^+$ complexes are due to distinct dissociating structures, and hence distinct bond formation processes, or the influence of the different ligands on the reverse activation barriers.

CONCLUSIONS

Product kinetic energy distributions are demonstrated to be a valuable tool for investigation of the mechanisms and energetics of gas-phase transition metal-mediated reactions. The energetics of bond coupling processes are found to be dependent on ligand

Table IV. Product Distributions for Reactions of Co^+ with Acetone- d_6

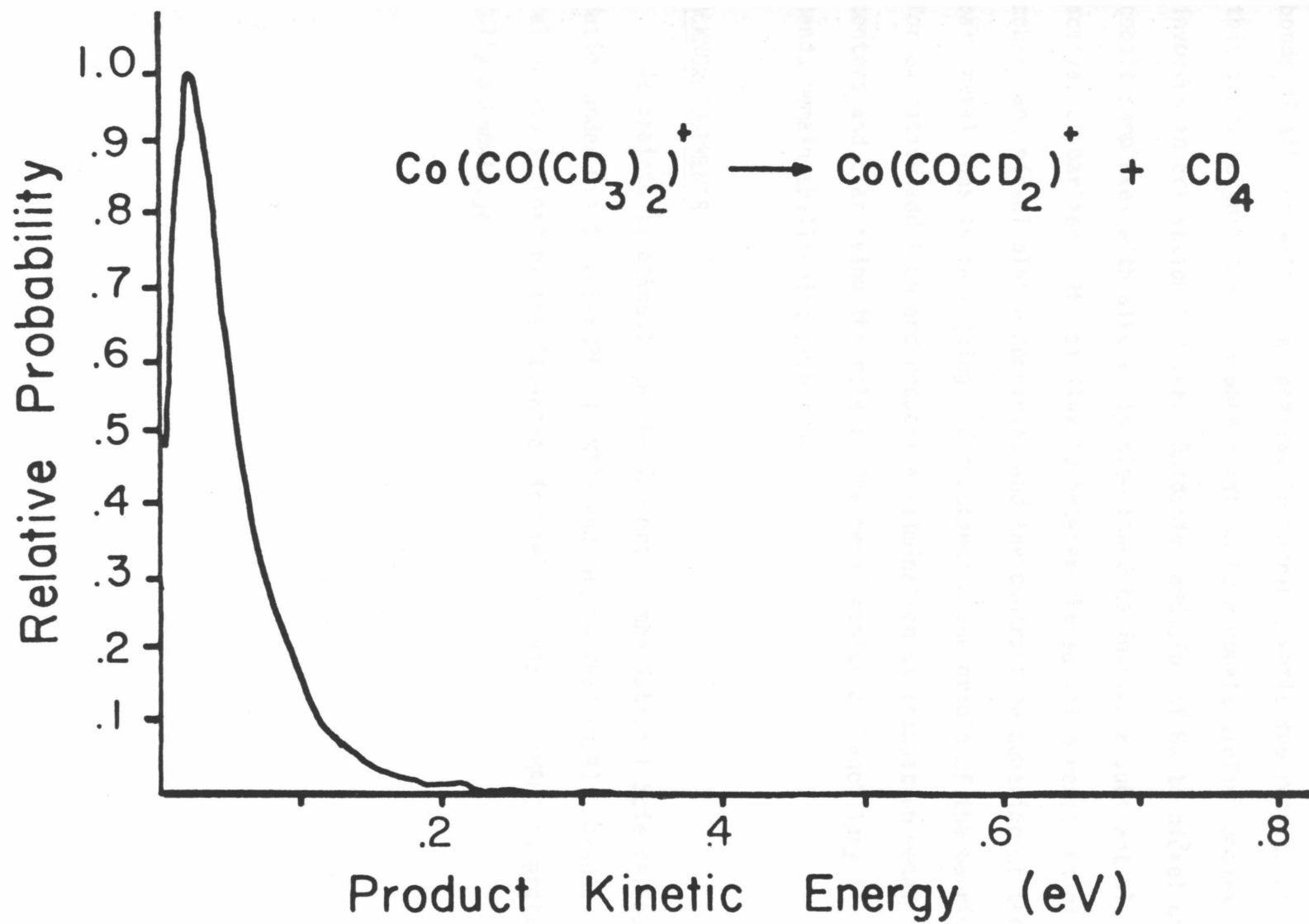
	Neutral Products			
	CD_4	CO	C_2D_6	$\text{CO}(\text{CD}_3)_2^{\text{c}}$
MS ^a	.06	.15	.60	.19
IB ^b		.10	.90	

^aMetastable product intensity normalized to ΣI_i .

^bIon beam product intensity measured at 0.5 eV relative kinetic energy as reported in Reference 53.

^cLoss of adduct could not be detected in ion beam experiment.

Figure 15. Translational energy distribution for CD_4 elimination from $\text{Co}(\text{acetone-d}_6)^+$.



coordination. For example, atomic cobalt ions apparently add to C-H bonds of alkanes without an activation barrier, while the results of this study suggest that C-H bond addition to a cobalt-olefin complex involves an activation barrier. Oxidative addition of H₂ to nickel or cobalt complexes with alkenes is also found to involve a substantial activation barrier. The similarity between the addition reactions of cobalt and nickel olefin complexes and the contrasting behavior of the bare metal ions is intriguing. Understanding the origin of the barriers for oxidative addition and reductive elimination at transition metal centers and clarifying the role of the metal center and ancillary ligands remain challenging problems.

ACKNOWLEDGEMENTS

We gratefully acknowledge the support of the National Science Foundation under Grants CHE-8020464 (MTB) and CHE-8407857 (JLB). Graduate fellowship support by the Atlantic Richfield Foundation (MAH) is gratefully acknowledged.

REFERENCES

1. Allison, J.; Freas, R. B.; Ridge, D. P. J. Am. Chem. Soc. 1979, 101, 1332.
2. a) Burnier, R. C.; Byrd, G. D.; Freiser, B. S. J. Am. Chem. Soc. 1981, 103, 4360.
b) Burnier, R. C.; Byrd, G. D.; Freiser, B. S. J. Am. Chem. Soc. 1982, 104, 3565.
3. Jacobson, D. B.; Freiser, B. S. J. Am. Chem. Soc. 1983, 105, 7492.
4. Armentrout, P. B.; Beauchamp, J. L. J. Am. Chem. Soc. 1981, 103, 6628.
5. a) Armentrout, P. B.; Beauchamp, J. L. J. Am. Chem. Soc. 1981, 103, 784.
b) Halle, L. F.; Armentrout, P. B.; Beauchamp, J. L. Organometallics 1982, 1, 963.
6. Houriet, R.; Halle, L. F.; Beauchamp, J. L. Organometallics 1983, 2, 1818.
7. There is some indication from theoretical studies that the d orbitals on the metal may facilitate concerted, multicenter reaction mechanisms. Steigerwald, M. L.; Goddard, W. A. J. Am. Chem. Soc. 1984, 106, 308.
8. Such reaction mechanisms have been postulated for the observed reactions of Sc^+ with hydrocarbons. See Tolbert, M. A.; Beauchamp, J. L. J. Am. Chem. Soc. 1984, 106, 8117.
9. A preliminary report of this work has appeared. See Hanratty, M. A.; Beauchamp, J. L.; Illies, A. J.; Bowers, M. T. J. Am. Chem. Soc., in press.

10. A more complete discussion may be found in:
 - a) Robinson, P. J.; Holbrook, K. A. "Unimolecular Reactions"; Wiley: New York, 1972.
 - b) Forst, W.; "Theory of Unimolecular Reactions"; Academic Press: New York, 1973.
 - c) Waage, E. V.; Rabinovitch, B. S. Chem. Rev. 1970, 80, 377.
11.
 - a) Marcus, R. A. J. Chem. Phys. 1952, 20, 359.
 - b) Marcus, R. A.; Rice, O. K. J. Phys. Colloid. Chem. 1951, 55, 894.
12.
 - a) Pechukas, P.; Light, J. C.; Rankin C. J. Chem. Phys. 1966, 44, 794.
 - b) Nikitin, E. Theor. Exp. Chem. (Engl. Trans.) 1965, 1, 276.
 - c) Chesnavich, W. J.; Bowers, M. T. J. Am. Chem. Soc. 1976, 98, 8301. Ibid. J. Chem. Phys. 1978, 68, 901.
13. Safron, S. A.; Weinstein, N. D.; Herschbach, D. R.; Tully, J. C.; Chem. Phys. Lett. 1982, 12, 564.
14. See, for example, Sudbø, S. Aa.; Schulz, P. A.; Grant, E. R.; Shen, Y. R.; Lee, Y. T. J. Chem. Phys. 1979, 70, 912.
15. Huisken, F.; Kranovich, D.; Zhang, Z.; Shen, Y. R.; Lee, Y. T. J. Chem. Phys. 1983, 78, 3806.
16. Farrar, J. M.; Lee, Y. T. J. Chem. Phys. 1976, 56, 1414, and discussion of the results in Reference 18b.
17. Examples of both statistical and nonstatistical energy release distributions are discussed in:
 - a) Jarrold, M. F.; Wagner-Redeker, W.; Illies, A. J.; Kirchner, N. J.; Bowers, M. T. Int. J. Ion Phys. Mass Spec. 1984, 58, 63.

- b) Butler, L. J.; Buss, R. J.; Brudzynski, R. J.; Lee, Y. T. J. Chem. Phys. 1983, 87, 5106.
18. Marcus has suggested that, in cases which involve a reverse activation barrier, the evolution of bending vibrations in the transition state into free rotations of the products should be considered. Because the spacing of vibrational levels is larger than that of the rotational levels, for an "adiabatic" process (i.e., one which conserves the original quantum number) additional energy can be released as relative translation of the products and thus produce a larger kinetic release. See:
- a) Marcus, R. A. J. Chem. Phys. 1975, 62, 1372.
- b) Worry, G.; Marcus, R. A. J. Chem. Phys. 1977, 67, 1636.
19. This is the familiar Hammond's postulate: Hammond, G. S. J. Am. Chem. Soc. 1955, 77, 334. See also Polanyi, J. C. Acc. Chem. Res. 1972, 5, 161.
20. Henschman, M. in "Ion-Molecule Reactions"; Franklin, J. L., ed.; Plenum Press: New York, 1972, p. 101.
21. Halle, L. F.; Klein, F. S.; Beauchamp, J. L. J. Am. Chem. Soc. 1984, 106, 2543.
22. Cooks, R. G., ed.; "Collision Spectroscopy"; Plenum Press: New York, 1978.
23. Freas, R. B.; Ridge, D. P. J. Am. Chem. Soc. 1980, 102, 7129.
24. See, for example:
- a) Peake, D. A.; Gross, M. L.; Ridge, D. P. J. Am. Chem. Soc. 1984, 106, 4308.
- b) Larsen, B. S.; Ridge, D. P. J. Am. Chem. Soc. 1984, 106, 1912.

25. For a description of the experimental instrumentation and methodology, see:
 - a) Illies, A. J.; Bowers, M. T. Chem. Phys. 1982, 65, 281.
 - b) Illies, A. J.; Bowers, M. T.; Jarrold, M. F.; Bass, L. M.; and Bowers, M. T. J. Am. Chem. Soc. 1983, 105, 5575.
 - c) Jarrold, M. F.; Illies, A. J.; Kerchner, N. J.; Wagner-Redeker, W.; Bowers, M. T.; Mandich, M. L.; Beauchamp, J. L. J. Phys. Chem. 1983, 87, 2313, and references therein.
26. See, for example: Ast, T.; Bozorgzaden, M. H.; Wiebers, J. L.; Beynon, J. H.; Brenton, A. G. Org. Mass. Spec. 1979, 14, 313.
27. Illies, A. J.; Bowers, M. T. Chem. Phys. 1982, 65, 281.
28. Moore, C. E. "Atomic Energy Levels"; U. S. Government Printing Office: Washington, D. C. 1971; National Standard Reference Data Series, N.B.S. 35.
29. Complete loss of adduct accounted for a small fraction (less than 3%) of the total product yield.
30. The thermionic source employed to produce metal ions for the investigation reported in References 4-6 is less likely to produce excited state ions.
31. Hanratty, M. A.; Beauchamp, J. L., unpublished results.
32. Cooks, R. G.; Beynon, J. H.; Caprioli, R. M.; Lester, G. R. "Metastable Ions"; Elsevier: New York, 1973.
33. Halle, L. F.; Houriet, R.; Kappes, M. M.; Staley, R. H.; Beauchamp, J. L. J. Am. Chem. Soc. 1982, 104, 6293.
34. Tolbert, M. A.; Beauchamp, J. L., unpublished results.
35. a) Jacobson, D. B.; Freiser, B. S. J. Am. Chem. Soc. 1983, 105, 5197.
b) Jacobson, D. B.; Freiser, B. S. J. Am. Chem. Soc. 1983, 105, 736.

36. This assumes no scrambling occurs with the 1,2-process. (No scrambling was observed for the 1,2-elimination of H₂ from 2-methylpropane.)
37. These are the integrated metastable intensities.
38. The lowest energy configuration for the molecule is with deuterium bonded to carbon and not the metal. The effect of the zero-point energy differences for the isotopically distinct dihydride ethene structures and the respective transition states is to increase the activation barrier for reductive elimination in the order H₂ < HD < D₂. The transition states for reductive elimination are assumed to have an almost completely formed H-H bond. Similar considerations predict that the activation barrier for oxidative addition will increase in the same order.
39. a) Jacobson, D. B.; Freiser, B. S. J. Am. Chem. Soc. 1983, 105 7492.
b) Jacobson, D. B.; Freiser, B. S. Organometallics 1984, 3, 513.
40. Hanratty, M. A.; Illies, A. J.; Bowers, M. T.; Beauchamp, J. L. J. Am. Chem. Soc., submitted.
41. Dissociation rates as a function of energy were calculated using the Bunker-Hase RRKM computer program with the harmonic approximation and semiclassical Whitten-Rabinovitch state counting. The calculations for ethene loss are described in detail in Reference 40. The transition states used to model H₂ and CH₄ eliminations are discussed later in the text. Frequencies were estimated from neutral hydrocarbon stretching frequencies. The calculated kinetic energy releases are fairly insensitive to the

choice of frequencies. The calculated and experimental distributions are normalized for comparison.

42. This point is discussed later in the text and in Reference 40. Addition of CH_4 to $\text{Mn}(\text{CO})_5^+$ is endothermic by 15 kcal/mol, and the activation barrier is thought to be larger than the endothermicity (Stevens, A. E.; Beauchamp, J. L. J. Am. Chem. Soc. 1979, 101, 245.
43. Low, J. J.; Goddard, W. A. J. Am. Chem. Soc. 1984, 106, 8321.
44. Low, J. J.; Goddard, W. A. J. Am. Chem. Soc. 1984, 106, 6928.
Low, J. J.; Goddard, W. A. J. Am. Chem. Soc. 1985, in press.
45. Obara, S.; Kitaura, K.; Morokuma, K. J. Am. Chem. Soc. 1984, 106, 7482.
46. Siegbahn, P. E. M.; Blomberg, R. A.; Bauschlicher, C. W. J. Chem. Phys. 1984, 81, 1373.
47. Similar complexes have been investigated for saturated organometallic species and metal surfaces. Saillard, J. Y.; Hoffman, R. J. Am. Chem. Soc. 1984, 106, 2006.
48. Turner, J. J.; Poliakoff, M. in "Inorganic Chemistry: Toward the 21st Century"; Chisholm, M. H., ed. Am. Chem. Soc. 1983, p. 35.
49. Kappes, M. M. Ph.D. Thesis, Massachusetts Institute of Technology, 1981.
50. We have searched unsuccessfully for cobalt-olefin complexes which add alkanes or hydrogen at thermal energies.
51. Jacobson, D. B.; Freiser, B. S. J. Am. Chem. Soc. 1985, 107, 72.
52. Byrd, G. D.; Fresier, B. S. J. Am. Chem. Soc. 1982, 104, 5944.
53. Tatsumi, K.; Nakamura, A.; Komiya, S.; Yamamoto, A.; Yamamoto, T. J. Am. Chem. Soc. 1984, 106, 8181.

54. Interestingly, CoCO^+ also does not react with alkanes. See Reference 23.
55. The kinetic energy distributions for loss of H_2 from $\text{Co}(\text{butane})^+$ and $\text{Co}(\text{butane-1,1,1,4,4,4-d}_6)^+$ are, within experimental error, the same. Similarly, the kinetic energy distributions for loss of CH_4 from 2-methylpropane-2-d₁ and 2-methylpropane are identical. The effect is less significant as the relative difference in the masses of the isotopically distinct neutrals diminishes. The kinetic energy distributions associated with loss of C_2H_6 from n-butane and loss of $\text{C}_2\text{D}_4\text{H}_2$ from butane-1,1,1,4,4,4-d₆ are virtually identical.
56. A hydrogen molecules with .5 eV translational energy is calculated to be traveling at a speed of $0.5 \text{ \AA}/10^{-14}$ sec while a deuterium molecule would move with a speed of $0.3 \text{ \AA}/10^{-14}$ sec.
57. See, for example,
- Kato, S.; Morokuma, K. J. Chem. Phys. 1980, 73, 3900.
 - Santamaria, J.; Benito, R. M. Chem. Phys. Lett. 1984, 109, 478.
58. Rynbrandt, J. D.; Rabinovitch, B. S. J. Chem. Phys. 1971, 54, 2275.
 Oref, I.; Rabinovitch, B. S. Acc. Chem. Res. 1979, 12, 166.
 McDonald, J. D. Ann. Rev. Phys. Chem. 1979, 30, 29.
59. Halle, L. F.; Crowe, W. E.; Beauchamp, J. L. Organometallics 1984, 3, 1694.
60. a) Szulejko, J. E.; Mendez - Amaya, A.; Morgan, R. P.; Brenton, A. G.; Beynon, J. H. Proc. R. Soc. Lond. A 1980, 373, 1.
 b) Mendez-Amaya, A.; Breton, A. G.; Szulejko, J. E.; Beynon, J. H. Proc. R. Soc. Lond. A 1980, 373, 13.

61. See, for example: Skinner, H. A. Adv. Organometal. Chem. 1964, 2, 49. Simões, J. A. Martinho; Beauchamp, J. L. Chem. Rev., in press.
62. Thermochemical data for hydrocarbons taken from Cox, J. D.; Plicher, G. "Thermochemistry of Organic and Organometallic Compounds"; Academic Press: New York, 1970. Heats of formation of radical species taken from: McMillen, D. F.; Golden, D. M. Ann. Rev. Phys. Chem. 1982, 53, 493. Schultz, J. C. ; Houle, F. A.; Beauchamp, J. L. J. Am. Chem. Soc. 1984, 106, 3917.
63. DiStefano, G. J. Res. Natl. Bur. Stand., Sect. A 1970, 74A, 233.
64. Cassady, C. J.; Freiser, B. S. J. Am. Chem. Soc. 1984, 106, 6176.
65. Jones, R. W.: Staley, R. H. J. Phys. Chem. 1982, 86, 1387.
66. Kappes, M. M.; Staely, R. H. J. Am. Chem. Soc. 1982, 104, 1819.
67. Jacobson, D. B.; Fresier, B. S. J. Am. Chem. Soc. 1984, 106, 3891.

APPENDIX I. Experimental Method and Data Analysis

A schematic of the experimental apparatus is presented in Figure A-1. Metal ions are created in a variable temperature source by electron impact ionization. The source has adjustable slits which allow low-pressure electron impact studies or high-pressure chemical ionization studies to be performed.²⁵ There is an extraction plate located immediately after the exit slit, but this is typically operated only a few volts above ground. This should minimize the fringing fields which could cause translational excitation of the reactant ions. Under the experimental conditions employed, residence times for the ions in the source are ~5 microseconds. Ions exit the source, are accelerated to 8 kV, and mass-selected in the magnetic analyzer.

During the flight time through the second field-free region, unimolecule decomposition may occur (Reaction A-1). Ions which decompose



in the second field-free region will enter the electric section with a velocity and energy different from that of the parent ions. The energy of the fragment ions is given by Equation A-2.³² Here, M_1 and M_2 are

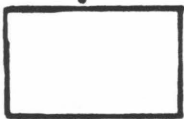
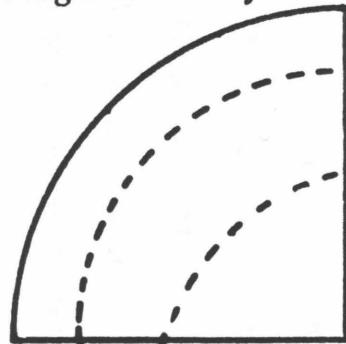
$$eV_2 = (M_2/M_1)eV \quad (\text{A-2})$$

the masses of the parent and fragment ions, respectively, eV is the accelerating voltage of the parent ions, and eV_2 is the new voltage of the electric sector corresponding to the energy of the fragment ions. The relationship between the energy release in the center-of-mass frame, T , and the laboratory energy, E , can be derived from conservation

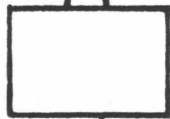
Figure 1A. Schematic of ZAB-2F.

Magnetic Analyzer

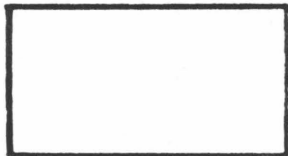
Electrostatic Analyzer



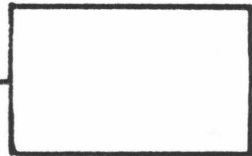
Ion Source



Electron Multiplier



Computer



Pulse Counting
Equipment



of momentum and energy considerations. Using the same definitions as above and defining M_3 as the mass of the neutral fragment, this relationship is given by Equation A-3. As can be seen,

$$T = \left(\frac{M_1^2}{4M_2M_3 \text{ eV}} \right) E^2 \quad (\text{A-3})$$

there is an amplification of the center-of-mass release in the laboratory frame which can be quite substantial at high translational energies. From Equation A-3 it can be shown that the energy resolution in the center-of-mass frame ΔT is related to the energy spread of the initial beam in the laboratory frame ΔE by Equation A-4. The experiments reported in

$$\Delta T = \left(\frac{M_1^2}{M_2M_3 \text{ eV}} \right)^{\frac{1}{2}} T^{\frac{1}{2}} \Delta E \quad (\text{A-4})$$

the present study were conducted at an energy resolution such that the energy spread of the main beam did not contribute significantly to the widths of the metastable peaks.

The kinetic energy release distributions were derived from the product ion peak shape using Equation A-5. Here $P(T)$ is the probability

$$P(T) = dI/dE \quad (\text{A-5})$$

of a given energy T being released into translation in the center-of-mass frame, I is the peak intensity, and E is the laboratory energy. A detailed derivation of this equation can be found elsewhere and will be described only briefly.^{25c,60} For ions that fragment with an isotropic angular distribution with a single value of the relative kinetic energy, the peak measured by scanning the electric sector will be rectangular with the area proportional to the number of product ions.

Consider the peak shown in Figure A-2. The probability of kinetic energy released in the range T to $T + dT$ is proportional to the area of the rectangle dA . Thus, the probability of a given kinetic energy release can be written as shown in Equation A-6. The measured energy

$$P(T) = dA/dT = 2E (dI/dT) \quad (\text{A-6})$$

E is related to the center-of-mass relative kinetic energy T by Equation A-3. Differentiating Equation A-3 yields Equation A-7, where

$$dT = 2c (EdE) \quad (\text{A-7})$$

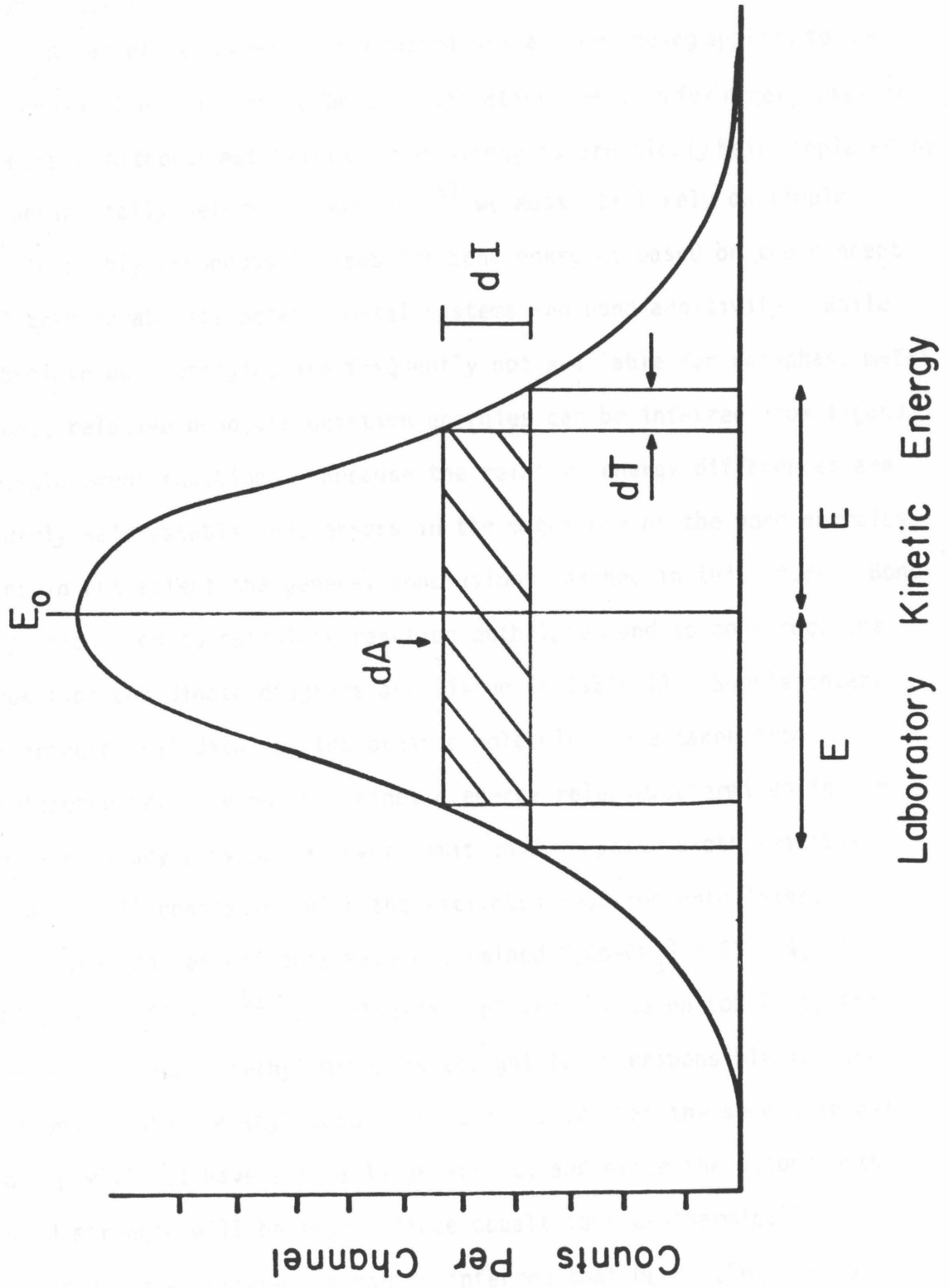
$c = \frac{M_1^2}{4M_2M_3}$ eV. Substitution into Equation A-6 results in the following

expression (Equation A-8). The kinetic energy release distribution

$$P(T) = c^{-1} dI/dT = \text{constant} (dI/dE) \quad (\text{A-8})$$

is obtained simply by differentiating the measured peak which can readily be achieved by numerical differentiation. Finally, the energy axis must be changed to the center-of-mass scale by use of Equation A-3.

Figure 2A. Schematic showing intensity vs. laboratory energy, E , for a metastable peak.



Appendix II.

A variety of experimental techniques are now being applied to the determination of gas-phase bond dissociation energies for organometallic species. Although estimates of bond strengths are slowly being replaced by experimentally determined numbers,⁶¹ we must still rely on simple and possibly erroneous guesses for bond energies based on the concept of transferability between metal systems and bond additivity. While absolute bond energies are frequently not available for gas-phase metal ions, relative bond dissociation energies can be inferred from ligand displacement reactions. Because the relative energy differences are fairly well-established, errors in the magnitude of the bond energies should not affect the general conclusions reached in this study. Bond energies used to calculate reaction enthalpies and to construct the reaction coordinate diagrams are listed in Table IA. Supplementary thermochemical data for the organic molecules were taken from Reference 62. The maximum kinetic energy releases determined in the present study provide a lower limit on the reaction exothermicities and are all consistent with the estimated reaction enthalpies.

Ion beam experiments have determined $D[\text{Co-CH}_3] = 61 \pm 4$, $C[\text{Co-H}^+] = 52 \pm 4$.⁵¹ Stabilization of the charge on cobalt by the more polarizable methyl group is thought to be responsible for the stronger cobalt methyl bond. It is expected that the second methyl group will not have such a large effect, and hence the second methyl bond strength will be less. Since cobalt ions exothermically decarbonylate acetone, it can be inferred that $D[\text{Co-2(CH}_3)] > 96$. A previous estimate of 101 kcal/mol for the sum of the two cobalt

methyl bonds implies that the decarbonylation reaction is exothermic by only 5 kcal/mol. The maximum kinetic energy release determined in the present study suggests that this reaction is exothermic by at least 14 kcal/mol and thus $D[\text{Co}-2\text{CH}_3^+] \geq 110$ kcal/mol. This latter value is used to calculate the reaction enthalpies listed in Table II. Larger alkyl groups are assumed to have bond energies equal to that of methyl.

The binding energy of carbon monoxide to cobalt ions has not been measured but can be estimated from known bond dissociation energies of other metal carbonyl ions. Photoionization threshold measurements have determined $D[\text{Ni}^+-\text{CO}] = 48 \pm 2$ kcal/mol and $D[\text{Fe}^+-\text{CO}] = 60 \pm 2$.⁶³ It has been suggested that the latter value is too high.⁵⁹ In support of this, an upper limit of 43 kcal/mol has been determined by Cassady and Freiser from photodecomposition threshold for FeCO^+ .⁶⁴ A value of 46 kcal/mol is estimated for $D[\text{CoCO}^+]$. The bond energy for carbon monoxide is expected to decrease as more ligands are added to the metal.

Ethene is known to displace CO in CoCO^+ and NiCO^+ . Therefore, the binding energy of C_2H_4 to cobalt and nickel is assumed to be greater than 46 and 48 kcal/mol, respectively. This is consistent with the lower limit of 36 kcal/mol for $D[\text{Co}^+-\text{C}_2\text{H}_4]$ determined from ion-beam experiments.⁵ Relative two-ligand binding energies to cobalt⁶⁵ and nickel⁶⁶ ions have also been measured. For linear olefins, ethene through butene, it is found that, as the number of carbon atoms in the olefin increases, the two-ligand binding energy increases by ~2-3 kcal/mol. For instance, the difference between $D[\text{Co}^+(\text{1-butene})_2]$ and $D[\text{Co}^+(\text{propene})_2]$ is 3 kcal/mol, while for nickel ions, the difference is 1.7 kcal/mol. The binding energy of dienes to cobalt ions is less

certain. Based on failure to observe displacement of the hydride ligand in Co-H^+ by butadiene, Jacobson and Freiser concluded that $D[\text{CoC}_4\text{H}_6] < 52 \text{ kcal/mol}$.⁶⁷ We feel that this could be due to kinetic and not thermodynamic factors and have assigned a value of 68 kcal/mol to the cobalt butadiene bond energy. The bond strength is expected to increase slightly as the diene becomes more substituted. The metal-olefin interaction is assumed to weaken as more σ bonding substituents are added to the metal.

Table IA. Thermochemical Estimates Used in Constructing Potential Energy Diagrams and Estimating Reaction Enthalpies.

<u>Bond</u>	<u>Binding Energy (kcal/mol)</u>
Co^+-H	$52 \pm 4^{\text{a}}$
Co^+-CH_3	$61 \pm 4^{\text{a}}$
$\text{Co}^+=\text{CH}_2$	$85 \pm 7^{\text{a}}$
Co^+-CO	46
$\text{Co}^+- $	48
$\text{Co}^+- $	52
$\text{Co}^+- $	53
$\text{Co}^+- $	54
$\text{Co}^+- $	55
Co^+-	56
Co^+-	57
$\text{Co}^+ \leq$	68
$\text{Co}^+ \leftarrow$	70
$\text{Co}^+(\text{CH}_2\text{CO})$	48^{b}
RCo^+-CO	42
$\text{Co}^+-2\text{C}_2\text{H}_4$	88

<u>Bond</u>	<u>Binding Energy (kcal/mol)</u>
$\text{OCCo}^+=\text{CH}_2^+$	80
RCo^+-H	51
$\text{Co}^+-2(\text{CH}_3)$	110
RCo^+-CH_3	50
HCo^+-R	57
$\text{ }-\text{Co}^+-2(\text{H})$	90
$(\text{H})_2\text{Co}^+-2(\text{C}_2\text{H}_4)$	80
$\text{Ni}^+-\text{ }$	50
$\text{Ni}^+-\text{ }$	55
$\text{Ni}^+-\text{ }$	57
$\text{Ni}^+-\text{ }$	57
$\text{Ni}^+-2(\text{C}_2\text{H}_4)$	90

^aDetermined in Reference 5a.

^bValue taken from Reference 59.

CHAPTER IV

KINETIC ENERGY RELEASE DISTRIBUTIONS AS A PROBE OF
BOND CLEAVAGE AND FORMATION PROCESSES AT TRANSITION METAL CENTERS:
REACTIONS OF Co^+ WITH ISOMERIC PENTENES AND CYCLOPENTANE

Kinetic Energy Release Distributions as a Probe of Bond Cleavage
and Formation Processes at Transition Metal Centers:
Reactions of Co^+ with Isomeric Pentenes and Cyclopentane

Maureen A. Hanratty and J. L. Beauchamp*

Contribution #7163 from the Arthur Amos Noyes Laboratory of Chemical
Physics, California Institute of Technology, Pasadena, California 91125

Andreas J. Illies and M. T. Bowers*

Department of Chemistry, University of California, Santa Barbara,
California 93106.

*To whom correspondence should be addressed.

ABSTRACT

Product kinetic energy release distributions and collision-induced dissociation are used to probe the potential energy surfaces for the reactions of cobalt ions with pentene isomers and cyclopentane. The results of this study complement the findings from previous investigations of these reactions and corroborate many of the conclusions. For instance, both the kinetic energy-release distributions and the collision induced dissociation spectra suggest that interconversion occurs for isomeric $\text{Co}(\text{pentene})^+$ adducts formed at thermal energies and that dissociation occurs from common intermediates. The results are also consistent with the proposal of a unique structure for the product of dehydrogenation of $\text{Co}(\text{cyclopentane})^+$. In addition, the kinetic energy distributions indicate the loss of C_3H_6 from $\text{Co}(\text{pentene})^+$ isomers occurs from two distinct structures. Kinetic energy-release distributions allow a unique opportunity to characterize the potential energy surfaces in the region of the exit channel. Dehydrogenation of $\text{Co}(\text{pentene})^+$ complexes results in a substantial release of kinetic energy which suggests that the reverse process involves an activation barrier. These nonstatistical distributions are very similar to those previously observed for dehydrogenation of $\text{Co}(\text{alkane})^+$ complexes and suggest similar potential energy surfaces for the two processes. The kinetic energy releases accompanying methane elimination also resemble those observed with the cobalt alkane complexes. The implications of these results for the potential energy surfaces of $\text{Co}(\text{alkene})^+$ reactions is discussed.

INTRODUCTION

An intriguing aspect of metal-ion chemistry is the facility with which gas-phase atomic metal ions induce skeletal rearrangements of hydrocarbons.¹⁻⁶ For example, atomic cobalt ions react exothermically with hydrocarbons to eliminate hydrogen, alkanes, or alkenes by processes which involve both bond cleavage and formation. In a recent investigation,⁷ it was demonstrated that kinetic energy release distributions resulting from decomposition of metastable cobalt alkane complexes can provide additional insight into the energetics and mechanisms of metal-mediated bond formation processes. In the present study, product kinetic energy-release distributions in conjunction with collision-induced dissociation (CID) are used to probe the potential energy surfaces for the reactions of cobalt ions with isomeric pentenes and cyclopentane.

In a gas-phase bimolecular association reaction between an ion (M^+) and a neutral (A) which involves a strong interaction such as bond formation, the association adduct $M(A)^+$ may contain a large amount of internal excitation. In the absence of collision, the "chemically activated" complex MA^+ may utilize the excess internal energy for molecular rearrangement and subsequent fragmentation to yield one or more products (e.g., Reaction 1).⁸ For the specific reactions being



considered in the present study, M^+ would correspond to an atomic cobalt ion, and A represents one of the C_5H_{10} isomers. It is possible to measure the relative translational energies of the products MB^+ and

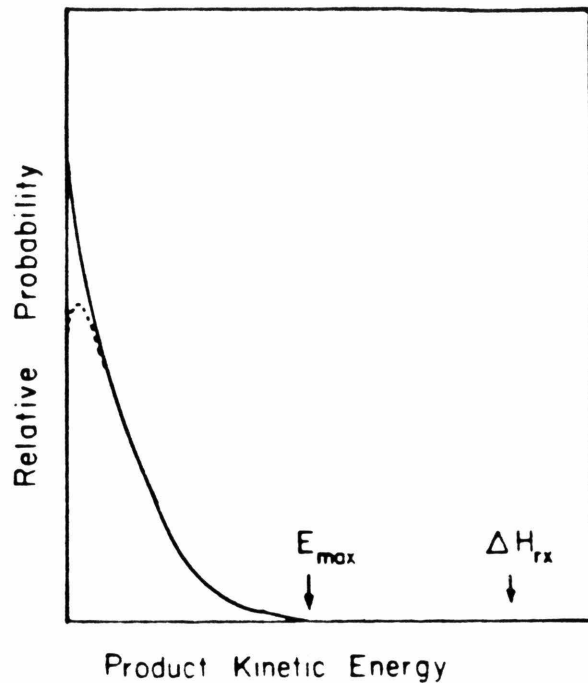
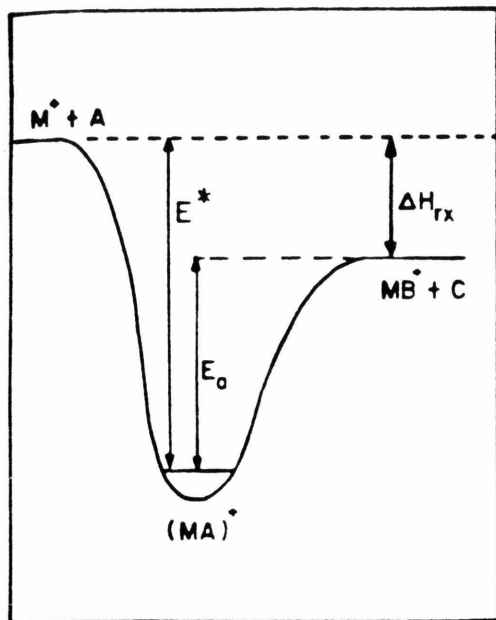
C as they separate using a reverse geometry double-focusing mass spectrometer. Any internal energy that is converted into translational energy during the dissociation will cause a spread in the energy of the product ions which is easily detected.⁹ Deconvolution of the peak shape yields a translational energy-release distribution in the center-of-mass frame which can reveal details about the potential energy surface over which the dissociation occurs.¹⁰

Simplified reaction coordinate diagrams such as those presented in Figure 1 illustrate how the amount of energy appearing in product translation for a given dissociation reaction can reflect specific details of the potential energy surface. In Figure 1, the collision adduct MA^+ containing internal energy E^* is depicted fragmenting to MB^+ and C along two hypothetical potential energy surfaces.¹¹ For a reaction occurring on a Type I surface, simple bond cleavage is involved and there is no barrier, excluding a centrifugal barrier,¹² to the reverse association reaction (Figure 1a). Statistical theories such as RRKM¹¹ and phase-space theory¹³ have been successful in modeling translational energy-release distributions for simple bond fission reactions. These theories predict a product translational energy distribution such as the one shown in the right-hand portion of Figure 1a. For rotating molecules, angular momentum constraints may lead to a distribution that peaks at higher energies as shown by the dashed line.¹⁴ Distributions of this type have been observed, for example, in radical elimination reactions.¹⁵

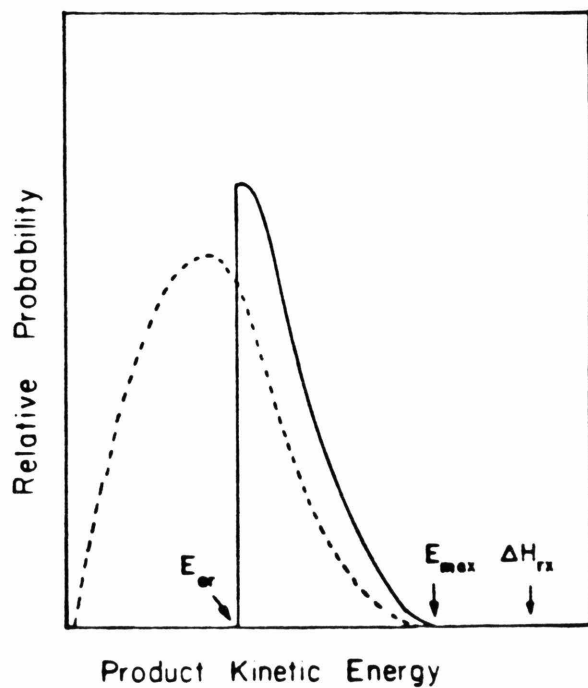
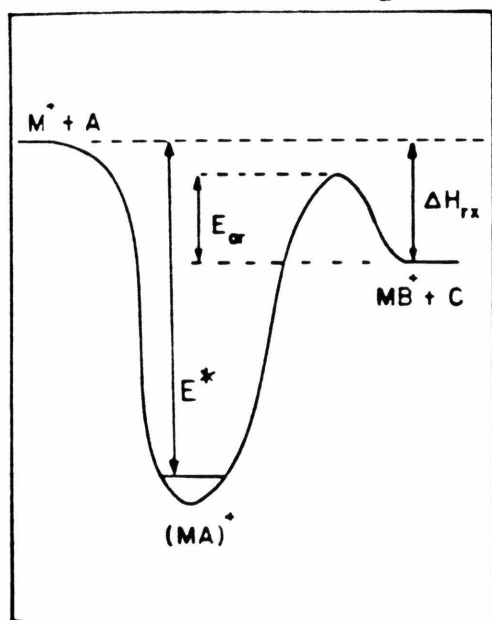
As shown in Figure 1b, a Type II surface involves a barrier with activation energy (E_{ar}) for the reverse association reaction. In the

Figure 1. Two hypothetical potential energy surfaces for the reaction $M^+ + A \rightarrow MB^+ + C$ and the corresponding product kinetic energy-release distributions in the center-of-mass frame.

TYPE I. No Barrier for Reverse Association Reaction



TYPE II. Large Barrier for Reverse Association Reaction



absence of coupling between the reaction coordinate and the other degrees of freedom after the transition state has been passed, all of the reverse activation energy will appear as translational energy of the separating fragments. The resulting translational energy release is shifted from zero by the amount E_{ar} and may be peaked to higher kinetic energy due to angular momentum constraints.¹⁴

Even without a detailed knowledge of transition state structures and activation parameters, qualitative features of the potential energy surface can be deduced from the shape of the kinetic energy release distribution. For instance, the maximum energy release, E_{max} , places a lower limit on the reaction exothermicity regardless of the type of potential energy surface. Although the two cases discussed above represent extremes, they are useful as models with which to interpret observed kinetic energy distributions. Frequently, exit channel effects¹⁶ distort the translational energy of the products as they separate and shift the energy distribution to lower energies.¹⁷ The amount of energy appearing as relative translation of the products will depend on the details of the potential energy surface and the dynamic effects which occur as the products separate. Nevertheless, the shape of the kinetic energy distribution and the maximum kinetic energy release often suggest which type of potential energy surface is the more appropriate description for the system.

The potential energy surfaces for the bimolecular reactions of metal ions with hydrocarbons are in general more complex than the above examples since they often involve a variety of products which result from multiple and perhaps interconnecting pathways. For example, the

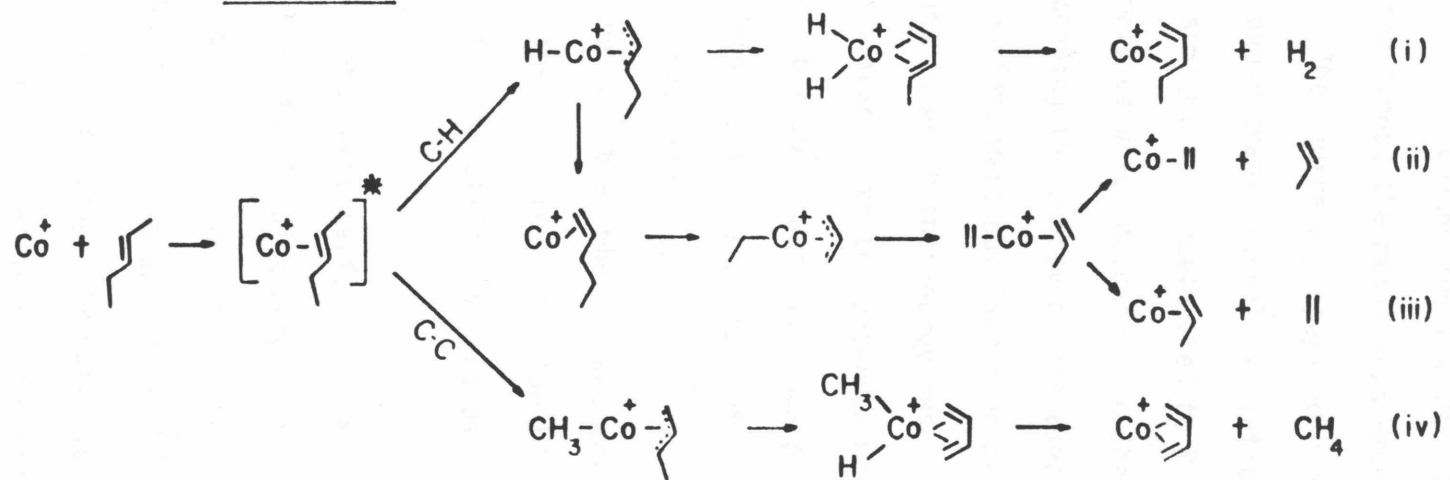
exothermic reactions of cobalt ions with C_5H_{10} isomers result in the elimination of H_2 , CH_4 , C_2H_4 or C_3H_6 as important reaction pathways.⁶ The mechanisms depicted in Scheme I have been proposed to account for the observed reaction products of Co^+ with 2-pentene through intermediates accessible to the chemically activated $Co(2-pentene)^+$ complexes.⁶ Similar mechanisms can be envisioned for the other pentene isomers.

Information about the energetics for competitive processes can often be deduced from behavior of product-branching ratios as the internal energy of the molecule is varied.⁸ An advantage of studying the reactions of Co^+ with C_5H_{10} isomers is that they have been investigated previously using a variety of techniques which encompass different energy regimes. Low-energy (~ 0.5 to 2 eV) ion beam studies have established the product ratios as a function of translational energy imparted to the cobalt ion.⁶ The branching ratios as well as product structure for these reactions at thermal energies have been characterized using Fourier-transform ion cyclotron resonance spectroscopy and low-energy CID.¹⁸ In addition, multiphoton excitation and dissociation of stable $Co(pentene)^+$ adducts with an infrared laser have recently been used to identify the lowest energy pathway for decomposition.¹⁹ We now report an extension of these investigations to include high-energy collision-induced dissociation and kinetic energy-release distributions from metastable decomposition of cobalt ion complexes with C_5H_{10} isomers.

EXPERIMENTAL

All experiments were conducted using a reverse geometry double-focusing mass spectrometer (VG Instruments ZAB-2F) which has been

Scheme I



previously described.²⁰ Cobalt ions were obtained from 150 eV electron impact ionization of $\text{Co}(\text{CO})_3\text{NO}$. Typical source pressures were 8×10^{-4} torr $\text{Co}(\text{CO})_3\text{NO}$ and 1×10^{-3} torr of the C_5H_{10} isomer. Under these conditions, the metal ions undergo a single collision while in the source. The source was operated under nearly field-free conditions to avoid translational excitation of the reactant ions. Ions exit the source, are accelerated to 8 kV and mass-selected. $\text{Co}(\text{C}_5\text{H}_{10})^+$ complexes which decompose in the second field-free region are detected by scanning the energy of the electric sector. Kinetic energy-release distributions were obtained from metastable peak shapes recorded under conditions in which the energy resolution of the main beam did not contribute significantly to the observed metastable peak widths.²¹ At pressures above $\sim 6 \times 10^{-3}$ torr, spurious peaks which did not correspond to metastable decomposition reactions of the $\text{Co}(\text{C}_5\text{H}_{10})^+$ ion were prevalent in the metastable spectra.²² This was a special problem near the energy of the main beam where peaks arising from elimination of H_2 occur. Keeping the pressure in the low 10^{-3} torr region helped eliminate most of these artifacts. Despite this, some spectra did contain spurious peaks.

CID measurements were performed by admitting He into a collision cell located at the focal point between the magnetic and electric sectors until a 50% reduction in the main beam intensity was observed. Although there are exceptions,²³ the product kinetic energy-release distributions arising from collision-induced dissociation processes usually are broader than those resulting from metastable decomposition reactions. The contribution from collision-induced

dissociation processes (arising from collisions with the lenses and background gases) to the metastable peaks are negligible except when the metastable decomposition reaction is a minor channel. To assess the possible CID contribution for the weak metastable dissociation channels, the shapes of the kinetic energy-release distributions resulting from metastable and collision-induced dissociations were compared.

The available instrumentation made it possible to use high-resolution translational energy loss spectroscopy^{24,25} to assess the presence of any electronically excited Co^+ ions formed in the source. A super-elastic peak 1.2 eV from the main beam was assigned to the ^3F excited state of Co^+ which is derived from the $3\text{d}^74\text{s}^1$ configuration.²⁶ It was possible to quench the excited state with Ar (10^{-2} torr), but the appearance of spurious peaks with excess Ar present precluded any measurement of peak shapes resulting from metastable decomposition of the $\text{Co}(\text{C}_5\text{H}_{10})^+$ ions under these conditions.²²

All chemicals were obtained from commercial sources and used without further purification other than freeze-pump-thaw cycles to remove noncondensable gases. Isomeric pentenes (>99.9% purity) were obtained from Wiley Organics. $\text{Co}(\text{CO})_3\text{NO}$ was purchased from Strem Chemicals.

RESULTS

$\text{Co}(\text{C}_5\text{H}_{10})^+$ adducts are formed in the source from bimolecular association reactions exemplified by Reaction 2. In addition, ligand



displacement by pentene isomers (Reaction 3) can also yield $\text{Co}(\text{C}_5\text{H}_{10})^+$



complexes with sufficient energy to decompose further.²⁷ The adduct resulting from ligand displacement should contain very little excess energy unless the Co(CO)^+ ion is internally excited.²⁸ This is confirmed by the observation that only a small fraction of the $\text{Co(C}_5\text{H}_{10})^+$ ions formed in an ion cyclotron resonance spectrometer by Reaction 3 have sufficient energy to decompose. The decomposition reactions as well as the structures of the reaction products are expected to be the same for metastable $\text{Co(C}_5\text{H}_{10})^+$ adducts formed by either reaction.²⁹ Although the differences in the exothermicities of Reactions 2 and 3 may lead to formation of $\text{Co(C}_5\text{H}_{10})^+$ adducts with a broad range of internal energies, only those ions with lifetimes defined by the arrival and departure times in the second field-free region will be detected in the metastable decomposition spectrum. Thus, the actual range of internal energies sampled may be quite small.⁹

H₂ Elimination. The observed product intensities for metastable-ion decomposition and collision-induced decomposition of isomeric $\text{Co(C}_5\text{H}_{10})^+$ complexes are presented in Table I along with the results from low-energy ion beam⁶ and infrared multiphoton dissociation¹⁹ studies. The average and maximum kinetic energy releases (E_{av} and E_{max} , respectively) for each channel are given in Table II along with the estimated exothermicity for the reaction. The reaction enthalpies are calculated assuming Reaction 2 is the exclusive reaction channel.³¹ As noted in the previous section, Reaction 3 can contribute to the population of ions which dissociate in the second field-free region in the case of the pentene isomers. For these ions, the estimated reaction exothermicity may represent an upper limit. Although the average kinetic

Table I. Product Distributions for Exothermic Reactions of Co^+ with C_5H_{10} Isomers

C_5H_{10} Isomer	Neutral ^a Lost	Product Distributions		
		Meta- stable ^b	CID ^b	Ion Beam ^c
1-pentene	H_2	.02	.02	.11
	CH_4	.01	.03	.13
	C_2H_4^*	.95	.72	.58
	C_3H_6	.01	.10	.18
2-pentene	H_2	.47	.35	.28
	CH_4^*	.43	.38	.33
	C_2H_4	.09	.16	.29
	C_3H_6	.01	.02	.10
2-methyl-1-butene	H_2	.49	.43	.46
	CH_4^*	.43	.34	.26
	C_2H_4	.08	.14	.20
	C_3H_6	.004	.02	.08
3-methyl-1-butene	H_2	.47	.39	.35
	CH_4^*	.45	.38	.35
	C_2H_4	.08	.14	.22
	C_3H_6	.004	.02	.08
2-methyl-2-butene	H_2	.47	.42	.34
	CH_4^*	.44	.35	.35
	C_2H_4	.08	.14	.26
	C_3H_6	.005	.02	.10

C ₅ H ₁₀ Isomer	Neutral ^a Lost	Product Distributions		
		Meta- stable ^b	CID ^b	Ion Beam ^c
cyclopentane	H ₂	.35	.35	.36
	CH ₄	.02	.02	.03
	C ₂ H ₄	.58	.44	.51
	C ₃ H ₆	.03	.05	.07

^aAsterisk identifies lowest energy decomposition pathway as identified by IR multiphoton absorption and dissociation in Reference 19. Cyclopentane adduct was not observed to dissociate.

^bAll values normalized to ΣI_i . Loss of C₅H₁₀ not reported.

^cAll reported product distribution for ion beam studies for 0.5 eV c.m. from Reference 6.

Table II. Reaction Enthalpy, Maximum and Average Kinetic Energy Release for Exothermic Reactions of Co^+ with C_5H_{10} Isomers^{a,b,c}

C_5H_{10} Isomer		Neutral Product			
		H_2	CH_4	C_2H_4	C_3H_6
1-pentene	$-\Delta\text{H}$	2.0	2.4	1.3	1.1
	E_{max}	.8	.40	.25	.60
	E_{av}	.22	.10	.07	.23
2-pentene	$-\Delta\text{H}$	1.9	2.3	1.2	1.0
	E_{max}	.8	.40	.25	.60
	E_{av}	.22	.10	.06	.25
2-methyl-1-butene	$-\Delta\text{H}$	1.8	2.2	1.1	.95
	E_{max}	.8	.38	.58	.60
	E_{av}	.24	.11	.13	.24
3-methyl-1-butene	$-\Delta\text{H}$	1.9	2.3	1.2	1.0
	E_{max}	.8	.35	.52	.60
	E_{av}	.23	.09	.11	.20
2-methyl-2-butene	$-\Delta\text{H}$	1.8	2.2	1.0	.87
	E_{max}	.8	.35	.60	.60
	E_{av}	.23	.09	.12	.21
cyclopentane	$-\Delta\text{H}$	1.4	1.8	.69	.52
	E_{max}	1.1	.32	.32	.25
	E_{av}	.33	.09	.08	.10

^aAll values in eV.

^bReaction enthalpy calculated for reaction products shown in Scheme I.

See Reference 28.

^cAverage kinetic energy calculated directly from kinetic energy distribution.

energy release gives some indication of the amount of energy appearing in product translation, it is more informative to examine the shape of the entire distribution. Kinetic energy distributions were obtained from a numerical differentiation of the metastable peak shape and subsequent transformation from the laboratory energy scale to a center-of-mass scale.^{9,10} The average kinetic energy release was obtained directly from the distribution. As an example, the metastable peak resulting from the elimination of H_2 from $Co(3\text{-methyl-1-butene})^+$ is plotted in the laboratory energy scale in Figure 2a along with the resulting kinetic energy distributions in center-of-mass energy Figure 2b. The distribution is peaked close to zero, with a maximum release of 0.7 eV. Within experimental error, the distributions for H_2 loss from all aliphatic $Co(C_5H_{10})^+$ isomers were the same. A broader distribution peaked at higher energy (0.15 eV) is observed for the dehydrogenation of $Co(C_5H_{10})^+$ derived from cyclopentane (Figure 3).

CH_4 Elimination. Methane elimination occurs with varying intensity from all the cobalt pentene adducts (Table I). The kinetic energy distribution for CH_4 loss from $Co(2\text{-pentene})^+$ is presented in Figure 4. All isomers yielded essentially identical kinetic energy distributions, with a maximum release of 0.4 eV (9.2 kcal/mol).

Alkene Elimination. The distributions associated with loss of C_2H_4 from $Co(1\text{-pentene})^+$, $Co(3\text{-methyl-1-butene})^+$ and $Co(\text{cyclopentane})^+$ are shown in Figure 5a. Loss of ethene from all acyclic cobalt pentene complexes occurs with only minor variations in the energy-release profile. A high-energy tail is observed from all the methylbutene complexes and is responsible for the higher average kinetic energy releases. A slightly broader kinetic energy distribution is found for the

Figure 2. a) Laboratory energy distribution for $\text{Co}(\text{C}_5\text{H}_{10})^+$ resulting from metastable fragmentation of $\text{Co}(\text{2-pentene})^+$.
b) Product kinetic energy distribution in the center-of-mass frame for the metastable loss of H_2 from $\text{Co}(\text{3-methyl-1-butene})^+$.
The maximum probability is set equal to unity.

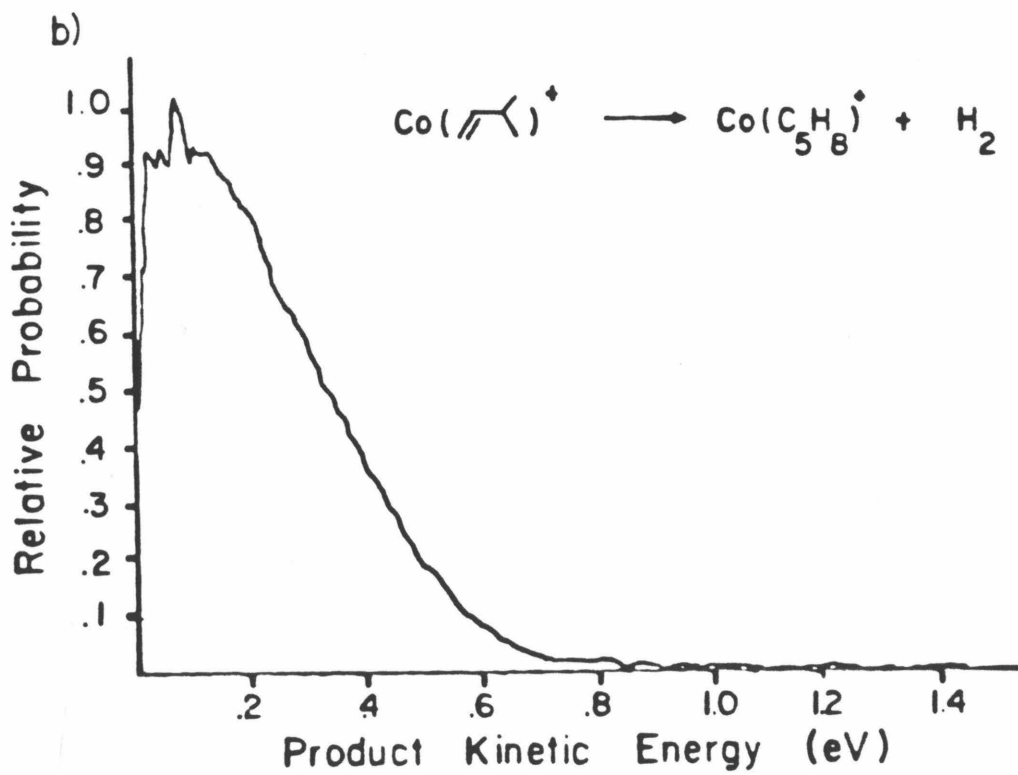
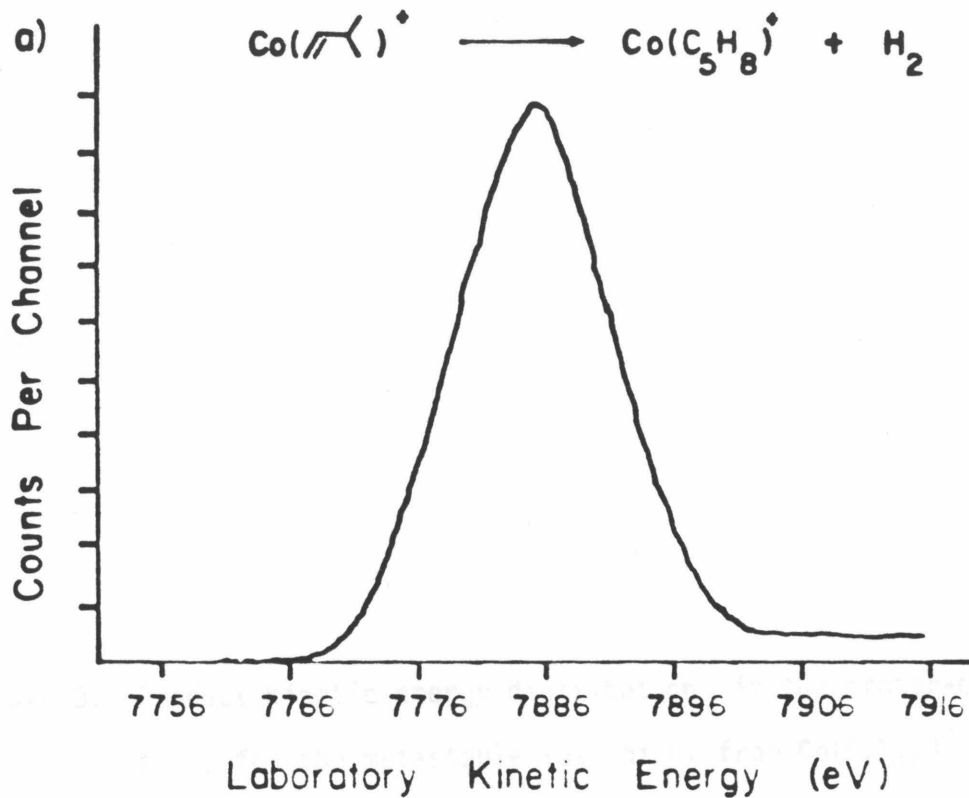


Figure 3. Product kinetic energy distribution in the center-of-mass frame for the metastable loss of H_2 from $Co(C_5H_{10})^+$ adducts formed from cyclopentane.

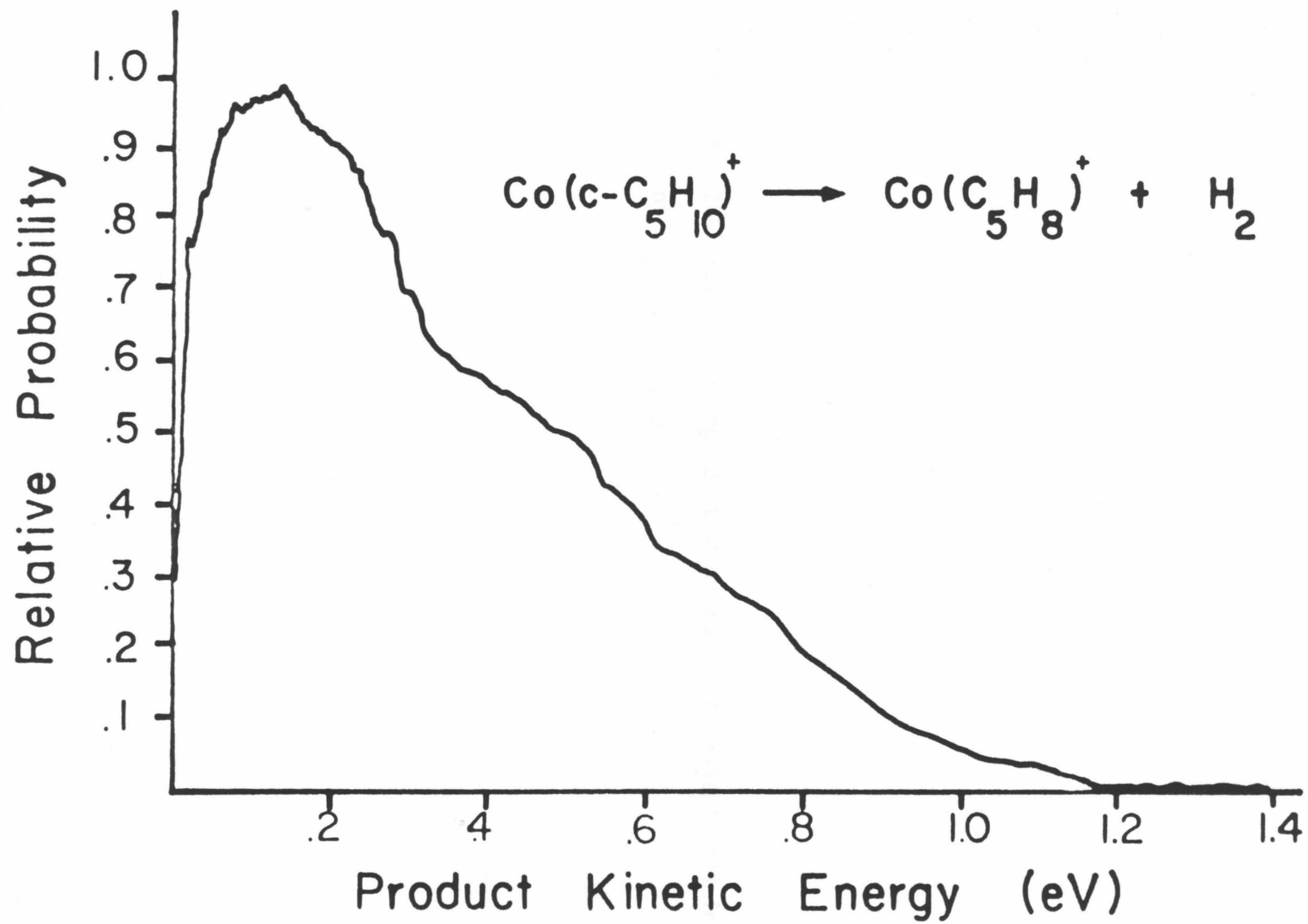


Figure 4. Translational energy distributions for metastable elimination of CH_4 from $\text{Co}(\text{2-pentene})^+$.

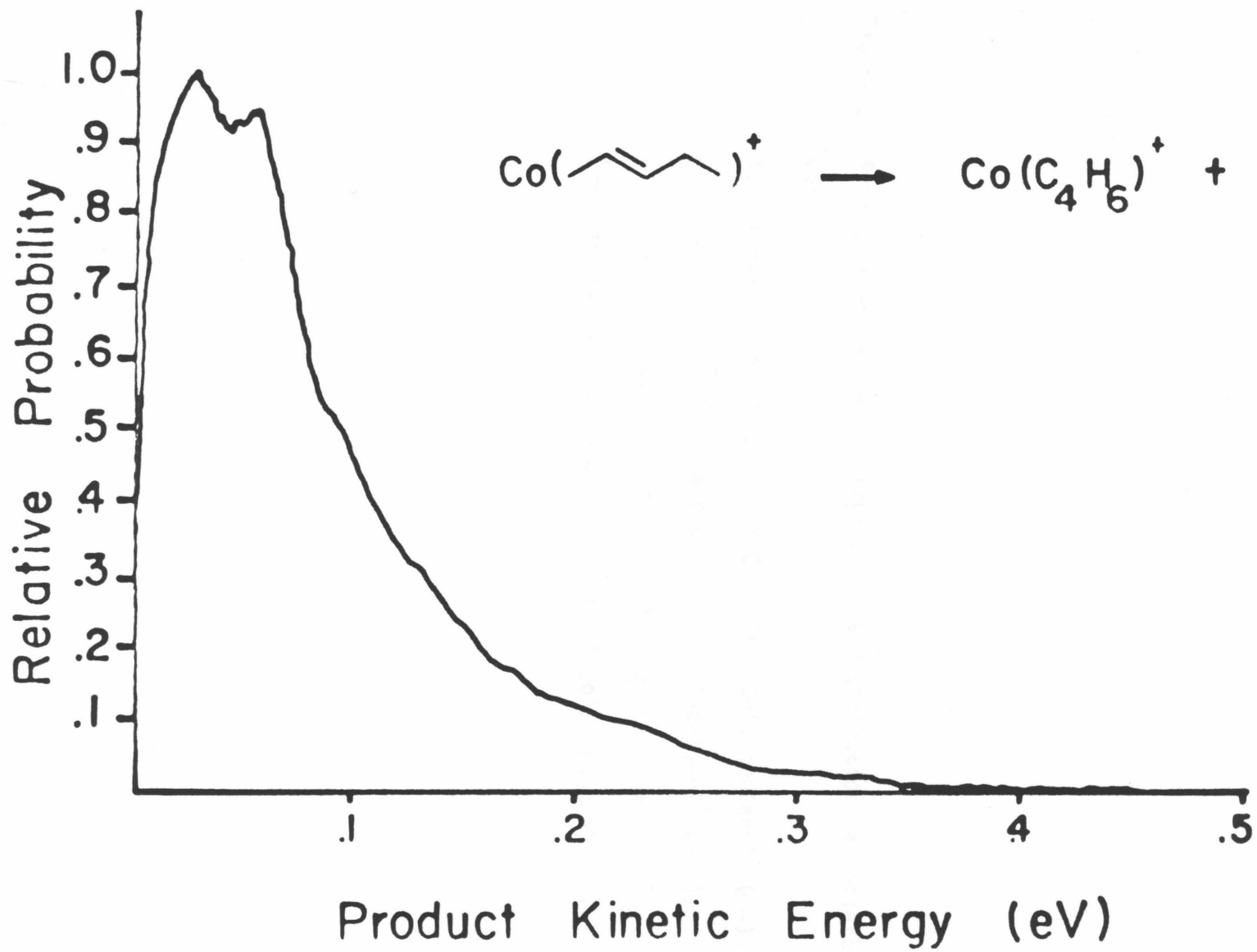
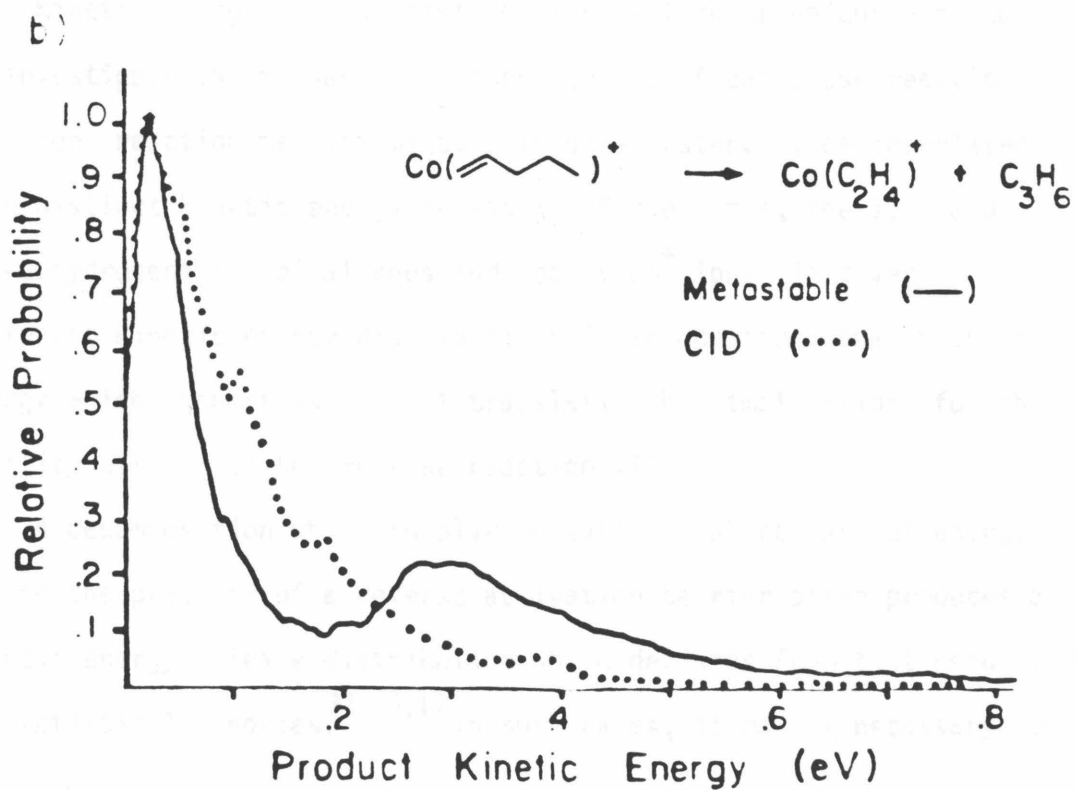
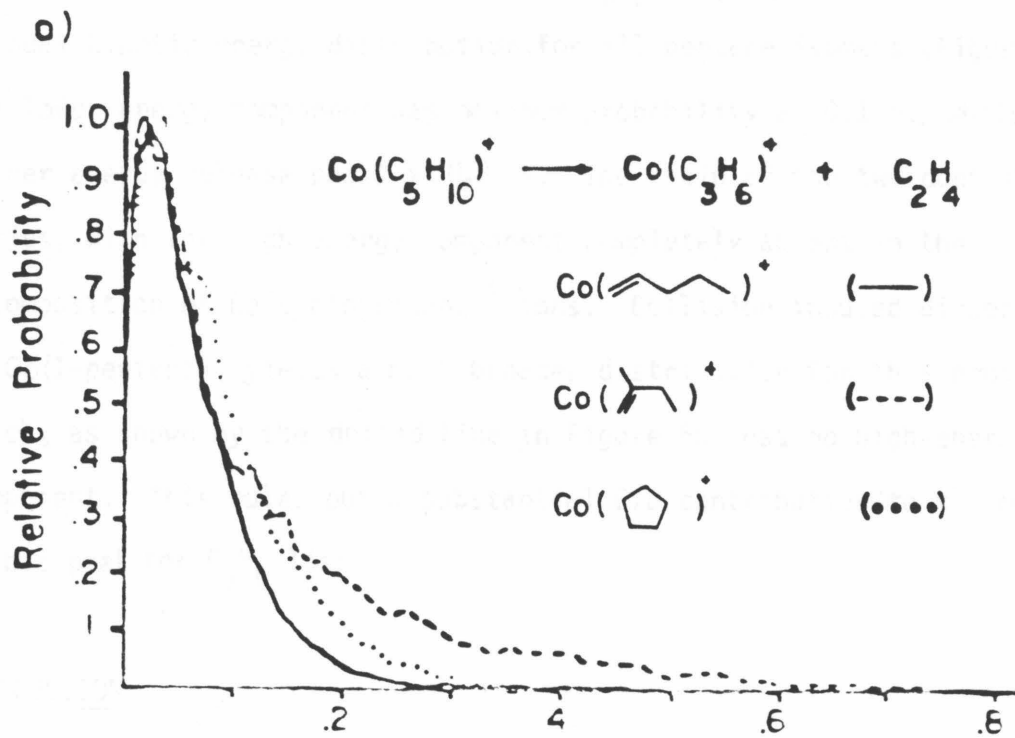


Figure 5. Product translational energy release distribution associated with:

- a) metastable elimination of C_2H_4 from $Co(1-pentene)^+$ (—), $Co(cyclopentane)^+$ (...) and $Co(2-methyl-1-butene)^+$ (---).
- b) C_3H_6 from metastable decomposition of $Co(1-pentene)^+$ (—) collision-induced dissociation of $Co(1-pentene)^+$ (...).



Co(cyclopentane)⁺ complex as illustrated by the dashed line in Figure 5a.

Although a minor channel, loss of C₃H₆ is characterized by a bimodal kinetic energy distribution for all pentene isomers (Figure 5b). The lower energy component has maximum probability at 0.1 eV, while the higher energy release peaks at 0.3 eV. The ratio of the two contributions varies, with the high-energy component completely absent in the decomposition of Co(cyclopentane)⁺ ions. Collision-induced dissociation of Co(1-pentene)⁺ yields a much broader distribution for this product which, as shown by the dotted line in Figure 5b, has no high-energy component. This rules out a substantial CID contribution to the metastable peak for C₃H₆ loss.

DISCUSSION

Kinetic energy-release distributions afford a unique opportunity to investigate the mechanisms and energetics of gas-phase reactions. Different reaction mechanisms can, in some instances, be correlated with distinct kinetic energy releases. For example, the 1,2- and 1,4-dehydrogenation of alkanes induced by Co⁺ ions yield very different kinetic energy distributions.⁷ In addition, the amount of energy which appears as product translation has implications for the facility with which the reverse reaction will occur.

A decomposition which involves a substantial release of energy due to the presence of a reverse activation barrier often produces a kinetic energy-release distribution which deviates from that predicted by statistical theories.^{11,16,17} In such cases, it may be necessary to

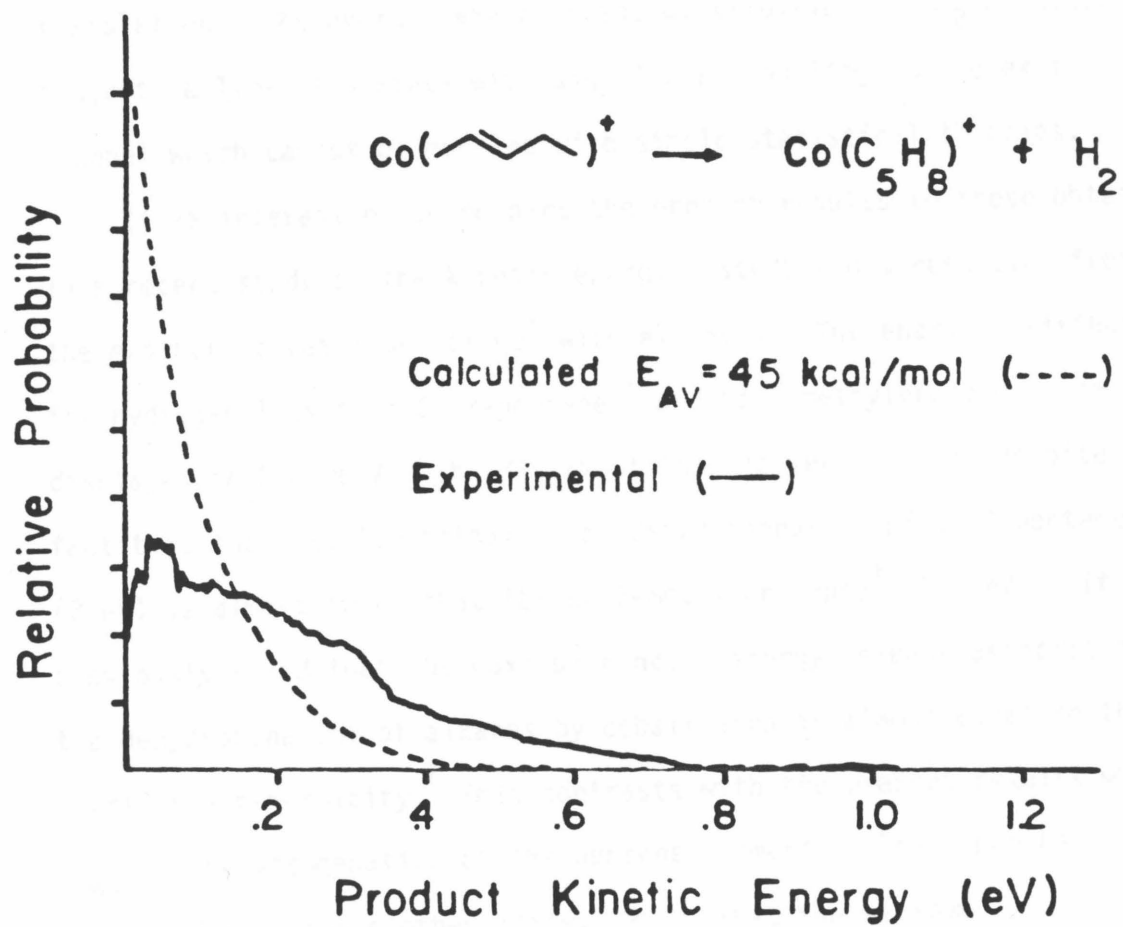
carry out more sophisticated trajectory calculations on model potential energy surfaces to reproduce the experimental kinetic energy releases. This has been feasible for only a limited number of systems.³² In this investigation, statistical RRKM theory¹¹ is used to model the experimental kinetic energy distributions. The calculations are described in more detail in Appendix I. The main purpose of the calculations is to determine whether a statistical model which assumes a Type I surface and equipartitioning of the excess energy is adequate to describe the experimental energy-release distribution. As discussed above, this can indicate the qualitative nature of the potential energy surface in the region of the exit channel.

The information obtained from CID and kinetic energy-release distributions is, in many cases, complementary. For example, similar CID spectra for different isomers suggest that isomerization occurs prior to dissociation. This, in turn, can help explain similarities in the kinetic energy-release distributions for the decomposition reactions of different isomers.

Kinetic Energy-Release Distributions

Dehydrogenation. Although loss of methane is estimated to have the greatest overall exothermicity (Table II), the largest kinetic energy releases are observed for the dehydrogenation reactions. The broad kinetic energy distributions in Figure 2 are representative of the releases accompanying dehydrogenation of all Co(pentene)⁺ adducts and suggest that a common structure is involved. The maximum energy release of 0.8 eV (18.4 kcal/mol) is far less than the estimated exothermicity of the reaction, 2.0 eV (45 kcal/mol). In Figure 6 the

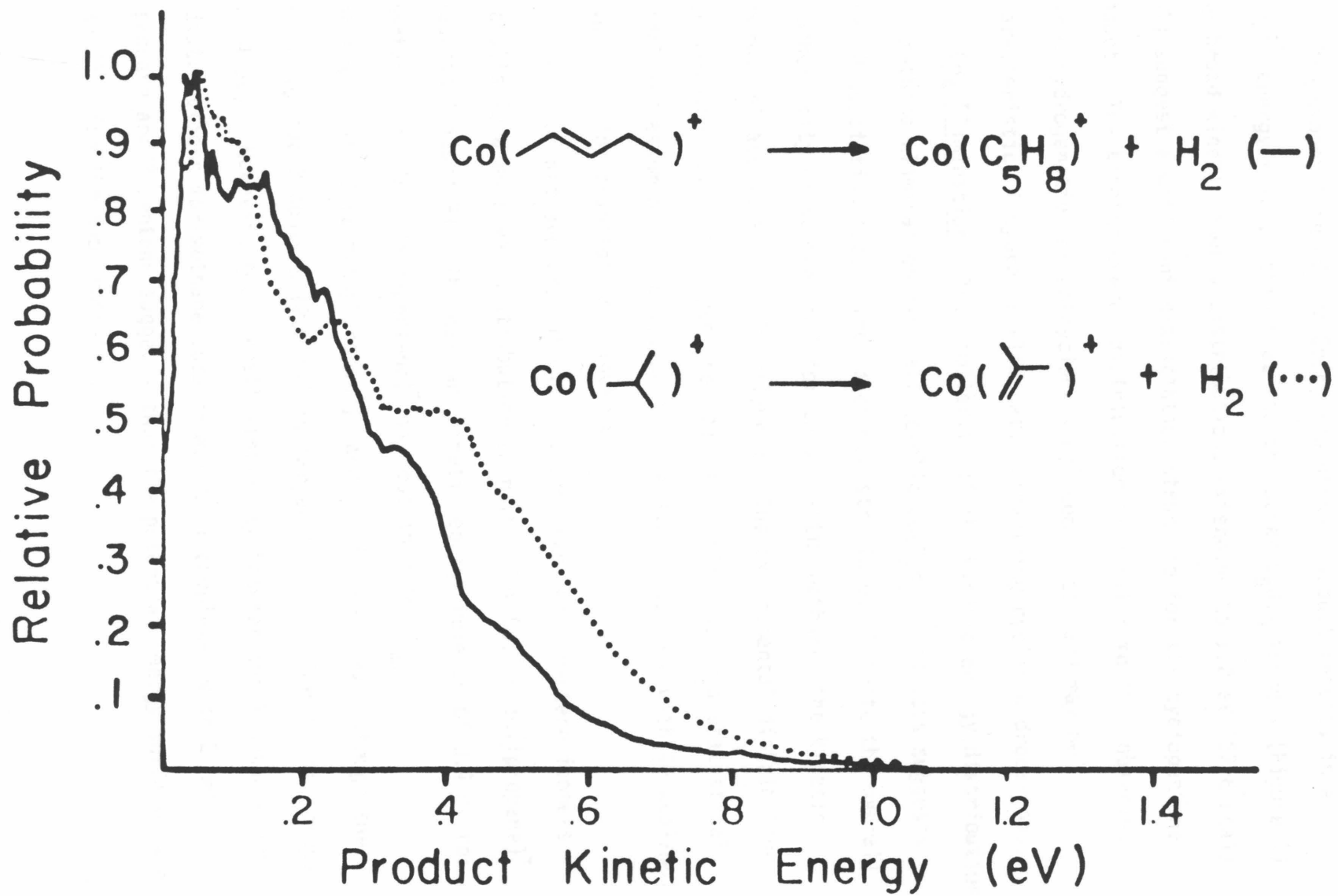
Figure 6. Experimental (—) and theoretical (---) product kinetic energy release distribution for loss of H_2 from $Co(2\text{-pentene})^+$. Theoretical distribution is calculated assuming no reverse activation barrier and 45 kcal/mol available for translation (E_{av}).



experimentally observed kinetic energy distribution for loss of H_2 from $Co(2\text{-pentene})^+$ is compared with the distribution predicted using a statistical model (described in Appendix I), assuming that 45 kcal/mol is available for translation. The theoretical distribution is area-normalized to the experimental distribution. As can be seen, the experimental distribution which peaks at 0.1 eV is broader than that expected for a Type I surface, even if the entire reaction enthalpy is available for translation. The overall shape of the distribution for H_2 elimination suggests a Type II surface with significant coupling in the exit channel which cannot be modeled with simple statistical theories.

It is interesting to compare the present results to those obtained in a recent study of the kinetic energy distributions resulting from the exothermic reactions of Co^+ with alkanes.⁷ The energy distributions for hydrogen loss from $Co(2\text{-pentene})^+$ and $Co(2\text{-methylpropane})^+$ are displayed in Figure 7. The distributions are very similar despite the fact that the reaction enthalpy for dehydrogenation of $Co(2\text{-pentene})^+$ (2 eV) is almost twice that for $Co(2\text{-methylpropane})^+$ (1.1 eV). It was previously noted that the maximum kinetic energy release associated with the dehydrogenation of alkanes by cobalt ions is almost equal to the reaction exothermicity.⁷ This contrasts with the present results where E_{max} for dehydrogenation of the pentene isomers is less than half the estimated reaction exothermicity. Note that the maximum kinetic energy release for dehydrogenation of the $Co(2\text{-pentene})^+$ complex is close to that for dehydrogenation of the $Co(2\text{-methylpropane})^+$ complex (1.1 eV). This suggests that there is very little effect of excess energy at the transition state and that the kinetic energy distributions primarily reflect the reverse activation barriers which

Figure 7. Kinetic energy distribution accompanying H_2 loss from $Co(2\text{-methylpropane})^+$ (\cdots) and $Co(2\text{-pentene})^+$ (—). Data for $Co(2\text{-methylpropane})^+$ taken from Reference 7.



appear to be similar.³³

Dehydrogenation of the $\text{Co}(\text{cyclopentene})^+$ adduct results in a larger energy release than that for the other C_5H_{10} isomers (Figure 3). The broad kinetic energy distributions extending to 1.2 eV (27.6 kcal/mol) suggest a different dissociation structure for the cyclopentane adduct. The kinetic energy distribution is similar to that observed for dehydrogenation of $\text{Co}(\text{cyclohexane})^+$ complexes⁷ and may be characteristic of hydrogen elimination involving cyclic hydrocarbons.

CH_4 Elimination. The similarity of the kinetic energy distributions for methane elimination from all acyclic $\text{Co}(\text{C}_5\text{H}_{10})^+$ adducts suggests that dissociation occurs from a common structure. Despite the overall exothermicity of 55 kcal/mol for this reaction pathway, the kinetic energy release is small (~9 kcal/mol). The experimental distribution for methane loss from 2-pentene can be fit using a statistical model and assuming dissociation along a Type I surface with 40 kcal/mol available for translation (Figure 8).

Loss of methane from the cobalt complexes with pentene isomers results in a narrower distribution than that for $\text{Co}(\text{2-methylpropane})^+$ adducts (Figure 9). The maximum kinetic energy release of 0.4 eV for methane loss from $\text{Co}(\text{2-pentene})^+$ is less than the E_{max} observed with $\text{Co}(\text{2-methylpropane})^+$ adducts (0.5 eV) even though the enthalpy for 2-pentene (2.3 eV) is larger than that for 2-methylpropane (1.4 eV). However, the overall similarity between the kinetic energy distributions for methane loss from cobalt complexes with 2-methylpropane and 2-pentene suggests that the potential energy surfaces are similar for the two processes.

Figure 8. Experimental (—) and theoretical (---) kinetic energy release distribution for loss of CH_4 from $\text{Co}(2\text{-pentene})^+$. The theoretical distribution assumes 40 kcal/mol is available for translation.

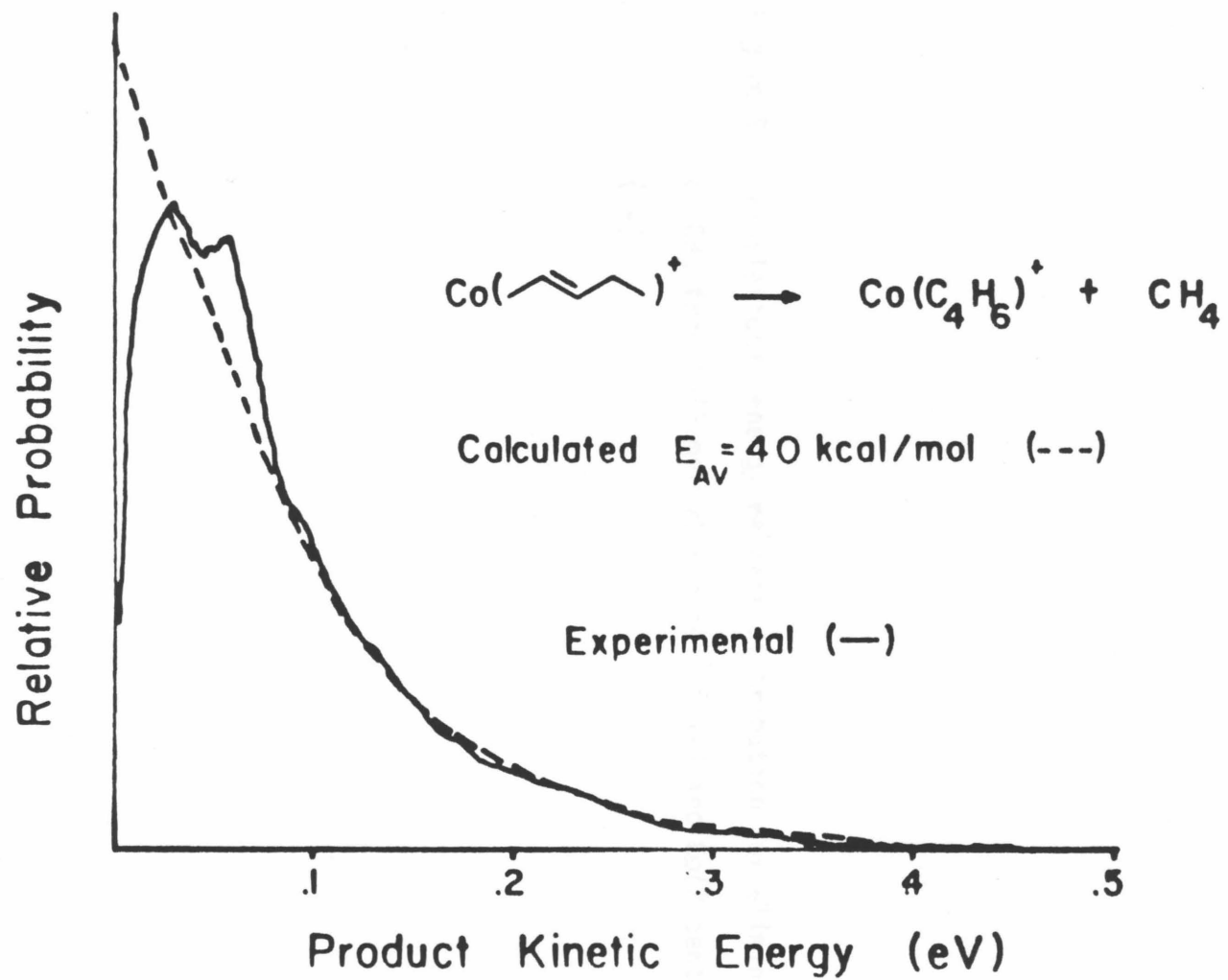
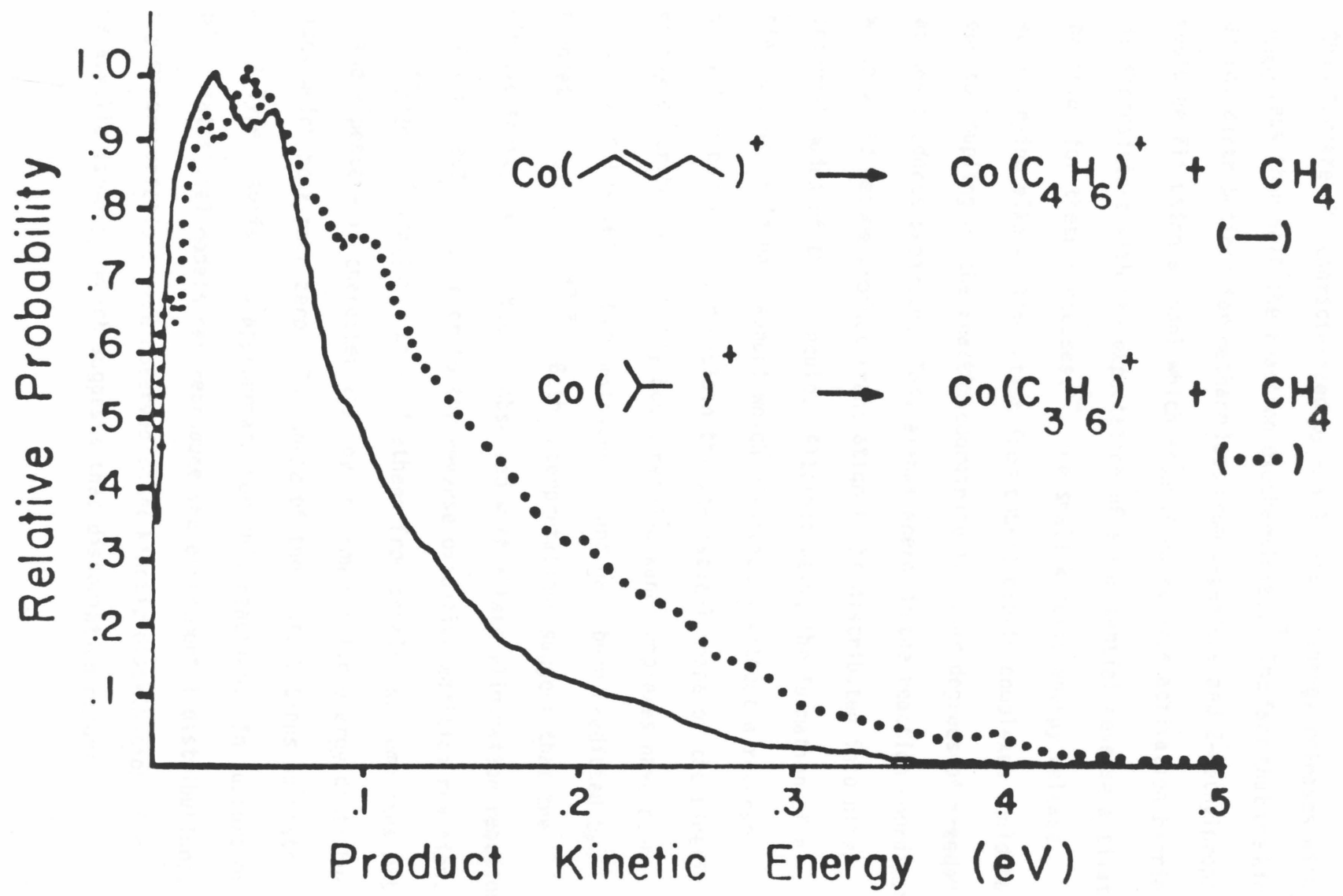


Figure 9. Translational energy release distribution for elimination of CH_4 from $\text{Co}(2\text{-methylpropane})^+$ (\cdots) and $\text{Co}(2\text{-pentane})^+$ (—).

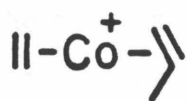


Alkane elimination reactions from cobalt complexes studied thus far are all characterized by small kinetic energy releases with E_{max} less than half the reaction exothermicity.⁷ The fact that the kinetic energy distributions for methane loss from 2-pentene and 2-methylpropane could be fit using a model which assumes no reverse activation barrier is inconsistent with the expectation of a substantial reverse activation barrier for these processes.³⁴ The small kinetic energy release accompanying alkane elimination from cobalt olefin complexes could be due to coupling of the reaction coordinate to other degrees of freedom as the products separate. This allows energy in the reaction coordinate which would become product translation to be distributed into other internal modes of the molecule. Alternatively, the formation of a stable Lewis acid-base adduct which dissociates without a reverse activation barrier could explain the statistical shape of the kinetic energy distribution. Weakly bound metal-alkane complexes have been observed in low-temperature matrices³⁵ and have been predicted by theoretical studies.^{34a,e} Both interpretations suggest that the kinetic energy distributions observed with alkane elimination reactions do not reflect the barrier to the reverse oxidative addition reaction.

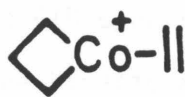
Alkene Elimination. Loss of ethene from cobalt ion complexes with 1- and 2-pentene is characterized by narrow kinetic energy distributions which peak near zero. The shape of the distributions suggests that a Type I surface is appropriate for this reaction. In support of this, statistical models can reproduce the experimental distributions. Only minor variations were observed in the kinetic distributions for the acyclic isomers, which suggests that dissociation occurs

predominantly from a single structure. The high-energy tail in the distribution for the $\text{Co}(2\text{-methyl-2-butene})^+$ ion (Figure 5a) may be due to a second channel with a larger energy release. The slightly broader kinetic energy distributions observed with the $\text{Co}(\text{cyclopentane})^+$ adduct could be due to dissociation via a channel not observed for the aliphatic pentene complexes or, alternatively, could be attributed to the effect of a larger amount of excess energy at the transition state.³⁶

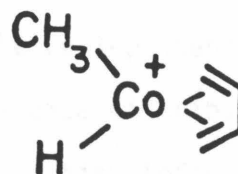
The bimodal release accompanying loss of C_3H_6 (Figure 5b) is observed for all acyclic C_5H_{10} isomers. The low-energy component with maximum probability near zero suggests a reaction which occurs along a Type I surface. In fact, it is very similar to the release associated with ethene elimination from $\text{Co}(1\text{-pentene})^+$ (Figure 5a). Loss of propene from the bis-olefin structure 1 is expected to occur without a reverse activation barrier and may be responsible for the low-energy release. The higher-energy component suggests that there is an additional process with an activation barrier to reverse reaction (Type II surface). A dissociation process which involves a barrier would be expected to be slow and may actually be enhanced in the metastable spectra relative to faster processes.⁹ Loss of cyclopropane from the cobalt cyclobutane intermediate 2 could be responsible for the higher energy release. Conversion to structure 1 would simply lead to the low-energy kinetic energy release component. The enthalpy for



1



2



3

the reaction of Co^+ and 1-pentene to yield cyclopropane and $\text{Co}(\text{ethene})^+$ is 0.66 eV, which is close to the maximum kinetic energy release associated with the high-energy component. It is interesting that this component is not present in the $\text{Co}(\text{cyclopentane})^+$ adduct distribution even though similar intermediates have been proposed to account for decomposition of this complex.^{6b} The kinetic energy distributions for C_3H_6 elimination from the acyclic isomers clearly indicate that more than one reaction pathway is involved.

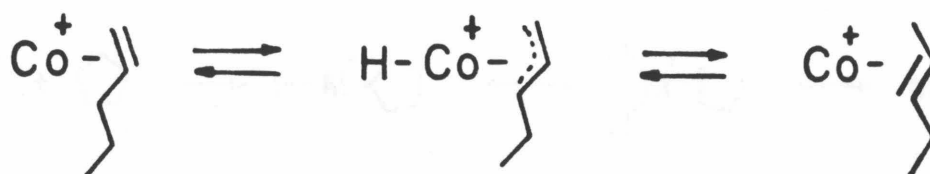
Collision-Induced Dissociation

2-Pentene and Methylbutenes. CID intensity patterns shown in Table I provide a further characterization of $\text{Co}(\text{C}_5\text{H}_{10})^+$ ion structures. The similarity of the product yields resulting from metastable decomposition and CID suggests that both processes are sampling the same surface. The dominance of methane and hydrogen elimination products in CID and metastable ion spectra for cobalt complexes with the methylbutenes and 2-pentene clearly distinguishes these complexes from 1-pentene and cyclopentene adducts. The nearly identical metastable and CID product yields for 2-pentene and methylbutene complexes suggest that isomerization to a common structure or structures occurs prior to dissociation.³⁷ This is further supported by the similarity of the kinetic energy distributions for the major fragmentation pathways.

1-Pentene. Products corresponding to loss of ethene are dominant in both the metastable-ion and CID spectrum of the $\text{Co}(\text{1-pentene})^+$ complex. These results and the kinetic energy release distribution for ethene loss are consistent with dissociation from a bis-olefin structure (1). The mechanism outlined in Scheme I (Pathway (i)) is proposed to

account for the formation of 1 and is consistent with the general finding that allylic carbon-carbon bond insertion is a facile process.³⁸ Interconversion between $\text{Co}(2\text{-pentene})^+$ and $\text{Co}(1\text{-pentene})^+$ may be achieved with a hydrogen shift as proposed in Scheme II. The respective kinetic

Scheme II



energy distributions for H_2 and CH_4 elimination for all $\text{Co}(\text{pentene})^+$ adducts are nearly identical and only minor variations are observed in the distributions for loss of C_2H_4 . This suggests that isomerization does occur. Loss of C_2H_4 from $\text{Co}(\text{methylbutene})^+$ and $\text{Co}(2\text{-pentene})^+$ complexes could be the result of isomerization to the bis-olefin complex (1).

Cyclopentane. Cobalt(cyclopentane)⁺ complexes yield distinct metastable and CID results. It is noteworthy that while C_2H_4 and H_2 losses are dominant in this system, H_2 elimination is not accompanied by a commensurate amount of CH_4 loss as was the case for the other isomers.³⁹ Elimination of H_2 and C_2H_4 results in kinetic energy distributions which are broader and have a larger maximum release compared to those for the acyclic isomers. The differences could be

due to fragmentation from structures different from the acyclic counterparts. One possibility for H₂ elimination, shown in Scheme III, involves an intact cyclopentane ring. There is

Scheme III



substantial evidence to support the mechanism proposed in Scheme III.^{40,41}

Loss of ethene, on the other hand, may involve ring cleavage. This isomerization may result in formation of a bis-olefin structure which contains a larger amount of internal energy than that formed from the acyclic isomers. This additional energy may then be responsible for the broader kinetic energy distribution observed with cyclopentane.³⁶

Alternatively, a unique structure could be involved. Apparently, isomerization to a structure such as 3 and subsequent loss of methane are not facile processes.

Implications for Reaction Energetics

A more complete description of the potential energy surfaces for the reactions of cobalt ions with C₅H₁₀ isomers can be inferred if the information obtained in the present study is integrated with that obtained in previous investigations. The qualitative potential energy diagrams for loss of H₂ and CH₄ from Co(2-pentene)⁺ and loss of C₂H₄ from Co(1-pentene)⁺ shown in Figures 10 and 11, respectively, represent

such composite pictures. While admittedly simple, they are consistent with the known features of the systems and useful for discussion of these reactions. For example, at thermal energies all reaction pathways in Scheme I are competitive. Infrared multiphoton activation has identified loss of methane from $\text{Co}(2\text{-pentene})^+$ and loss of ethene from $\text{Co}(1\text{-pentene})^+$ as the lowest energy decomposition pathways for these complexes.¹⁹ As can be seen from Table I, the ratio of products corresponding to H_2 and CH_4 elimination is similar in the metastable, CID, and low-energy ion beam experiments. This suggests that a common intermediate may be involved. The potential energy surfaces depicted in Figures 10 and 11 are consistent with these results. From the shape of the potential energy surfaces in the region of the exit channel, loss of H_2 and CH_4 from $\text{Co}(2\text{-pentene})^+$ complexes would be classified as Type II surfaces, while loss of C_2H_4 from $\text{Co}(1\text{-pentene})^+$ is depicted as a Type I surface.

To further characterize these reactions, ion cyclotron resonance spectrometry has been used to probe the reverse addition reactions using deuterium-labeled compounds.¹⁹ Since the elimination reactions are exothermic, the reverse reactions for ground-state products to reform reactants cannot occur. However, addition to the metal-olefin fragment can, in certain instances, be detected by deuterium exchange. In only one case, the addition of ethene- d_4 to $\text{Co}(\text{C}_3\text{H}_6)^+$, was deuterium exchange observed.⁴²⁻⁴⁴ This is consistent with the suggestion of a Type I potential surface for this reaction. While the failure to observe deuterium exchange for the other channels does not constitute proof of a barrier to the initial oxidative addition, it is consistent

Figure 10. Qualitative potential energy diagram for the reaction of $\text{Co}(\text{2-pentene})^+$ to yield $\text{Co}(\text{C}_5\text{H}_8)^+$ and $\text{Co}(\text{C}_4\text{H}_6)^+$.

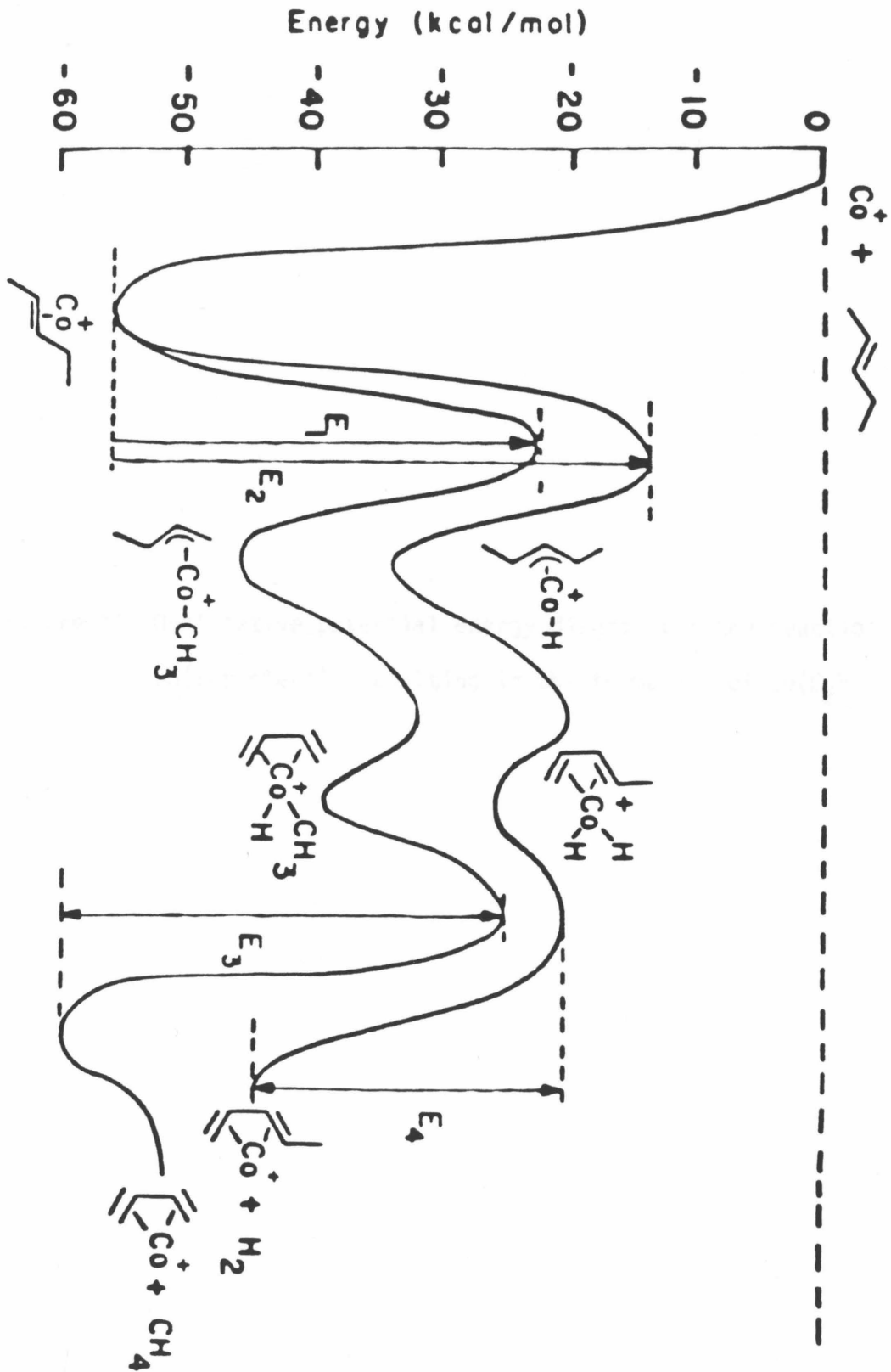


Figure 11. Qualitative potential energy diagram for the reaction of Co(1-pentene)^+ resulting in the formation of $\text{Co(C}_2\text{H}_4)^+$.

with the features of the potential energy surfaces shown in Figure 10. The failure to observe H_2 or hydrocarbon addition to a variety of ionic cobalt monolefin complexes suggests that such oxidative-addition reactions may, in general, have significant activation barriers.⁴²⁻⁴⁴

RELATED STUDIES

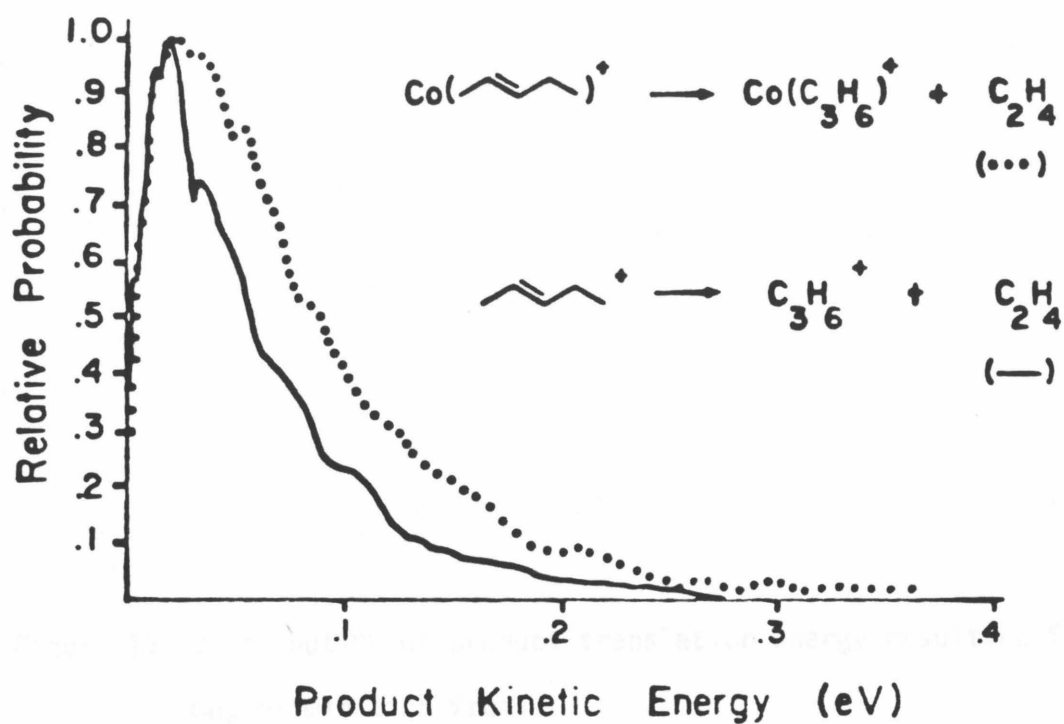
It is possible for the case of methane and ethene elimination from 1- and 2-pentene to compare the kinetic energy distributions for the organic radical cation produced from 150 eV electron impact with that of the corresponding organometallic adduct. These are shown in Figures 12 and 13. The metastable decomposition product intensities for the organometallic and organic cations are displayed in Table III. While the internal energy content of the pentene ions produced from direct electron impact ionization may be quite different from the $Co(pentene)^+$ ions produced via bimolecular association reactions, the kinetic energy distributions are not drastically different. In other instances where such a comparison was possible, the release associated with the organic ion was quite different from that of the related metal complex.⁷ The similarity between the kinetic energy distributions of the organic pentene ions and the ionic organometallic complexes, although initially surprising, may simply reflect potential energy surfaces with coincidentally similar energetics in the region of the exit channel. It is clear, however, from the metastable and CID yields for organic and metal-coordinated species that the metal ion does indeed exert strong influence on the observed reaction channels (Table III).

Figure 12. Product translational energy distribution for elimination of C_2H_4 from:

a) $Co(2\text{-pentene})^+$ (\cdots) and 2-pentene^+ ($—$)

b) $Co(1\text{-pentene})^+$ (\cdots) and 1-pentene^+ ($—$).

a)



b)

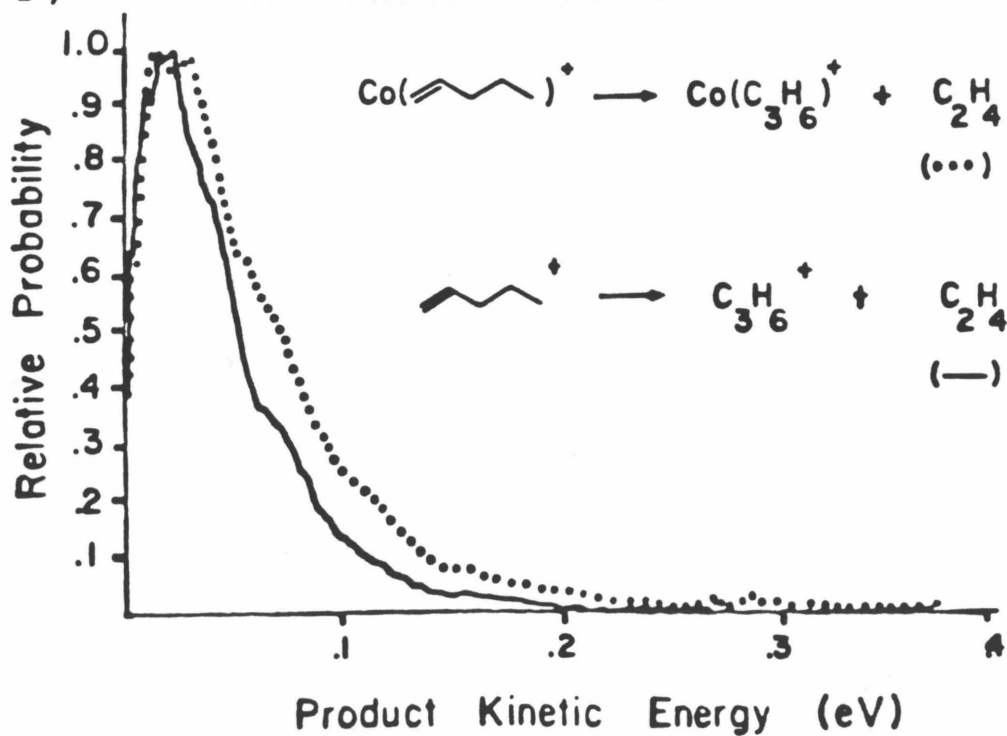


Figure 13. Distribution of product translation energy resulting from CH_4 elimination from:

a) $\text{Co}(2\text{-pentene})^+$ (\cdots) and 2-pentene^+ (---)

b) $\text{Co}(1\text{-pentene})^+$ (\cdots) and 1-pentene^+ (---).

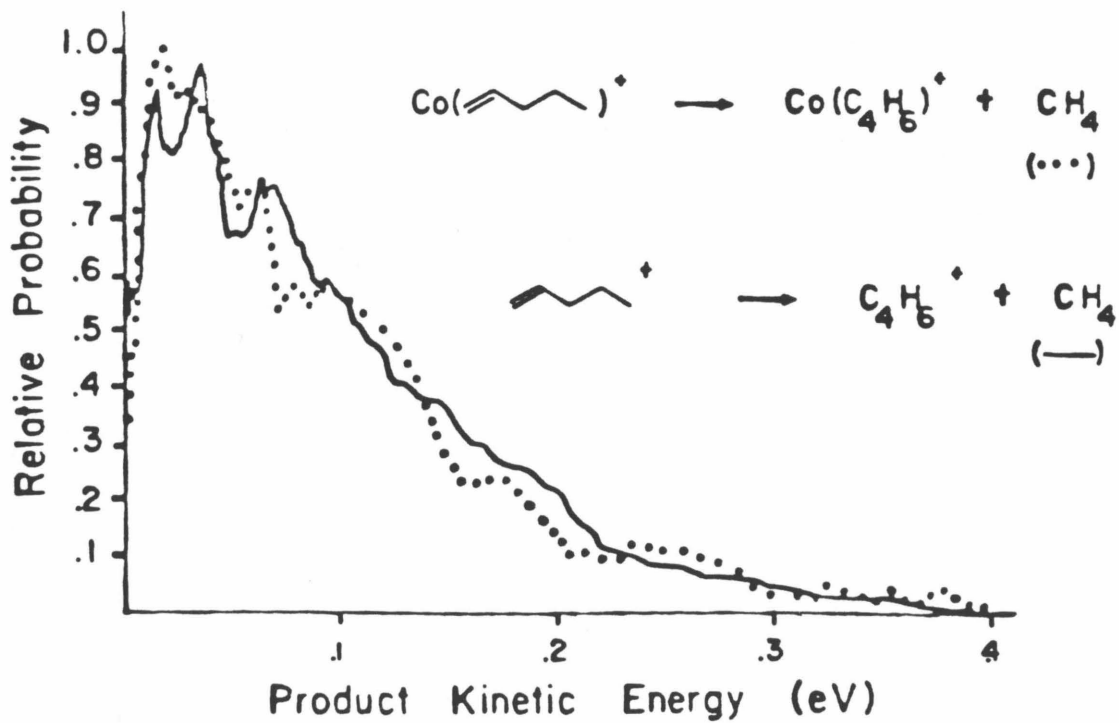
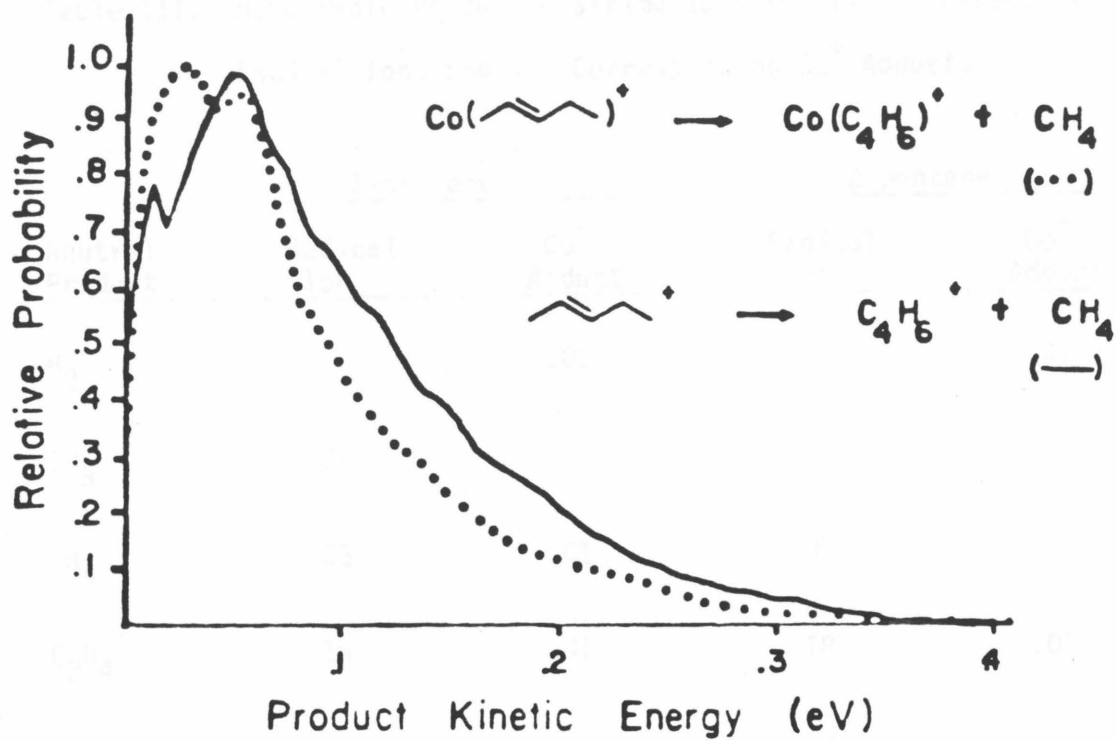


Table III. Metastable Product Distributions for 1- and 2-Pentene Radical Ions and the Corresponding Co^+ Adducts

Neutral Product	1-pentene		2-pentene	
	Radical Ion	Co^+ Adduct	Radical Ion	Co^+ Adduct
H_2		.02		.47
CH_3	.82		.78	
CH_4	.03	.01	.02	
C_2H_4	.14	.95	.18	.09
C_2H_5	.01		.02	
C_3H_6		.01		.01

CONCLUSIONS

The results of this study of the reactions of Co^+ with isomeric pentenes and cyclopentane complement the findings from previous investigations of these reactions and confirm many of the conclusions. The kinetic energy distributions and the CID product intensities suggest that interconversion occurs between isomeric $\text{Co}(\text{pentene})^+$ complexes formed at thermal energies. The present results also support the previous suggestions^{6b,40} of a unique structure for the $\text{Co}(\text{cyclopentane})^+$ adduct. The nearly constant ratio of H_2 and CH_4 loss observed with the pentene isomers in the metastable, ion beam, and ICR experiments suggests that the two processes have very similar activation barriers.

This study demonstrates that product kinetic energy release measurements can yield additional insight into the mechanisms and energetics for elimination reactions induced by transition metal ions. Comparison of the kinetic energy release distributions for hydrogen elimination from $\text{Co}(\text{pentene})^+$ and $\text{Co}(\text{2-methylpropane})^+$ complexes suggests that the two processes are very similar. This implies that the activation barriers for oxidative addition of H_2 to a $\text{Co}(\text{alkene})^+$ and $\text{Co}(\text{diene})^+$ complex are comparable. Interestingly, both processes appear to have smaller activation barriers than oxidative addition of H_2 to the $\text{Ni}(\text{bis-ethene})^+$ complex.⁷ Similarly, methane elimination from $\text{Co}(\text{alkene})^+$ and $\text{Co}(\text{alkane})^+$ complexes appears to involve a reverse activation barrier. Loss of ethene is the only reaction that occurs without a reverse activation barrier.

The results reported here are specific to cobalt ions. Whereas

H₂ to cobalt-alkene and -diene complexes involve a substantial activation barrier, the equivalent rhodium and niobium complexes are observed to add D₂ at thermal energies.⁴³ To understand the reasons for the variation in the behavior of the different metal systems will require a more detailed knowledge of the electronic structure correlations for reactants, intermediates and products. Such information will greatly enhance our understanding of many fundamental processes in organometallic chemistry.

ACKNOWLEDGMENTS

We gratefully acknowledge the support of the National Science Foundation under Grant CHE-8020464 (MTB) and CHE-8407857 (JLB). Graduate fellowship support by the Atlantic Richfield Foundation (MAH) is gratefully acknowledged.

REFERENCES

1. Byrd, G. D.; Freiser, B. S. J. Am. Chem. Soc. 1982, 104, 5944.
2. Allison, J.; Freas, R. B.; Ridge, D. P. J. Am. Chem. Soc. 1979, 101, 1332.
3. a) Burnier, R. C.; Byrd, G. D.; Fresier, B. S. J. Am. Chem. Soc. 1981, 103, 4360.
b) Burnier, R. C.; Byrd, G. D.; Fresier, B. S. J. Am. Chem. Soc. 1982, 104, 3565.
4. Tolbert, M. A.; Beauchamp, J. L. J. Am. Chem. Soc. 1984, 106, 8177.
5. a) Houriet, R.; Halle, L. F.; Beauchamp, J. L. Organometallics 1983, 2, 1818.
b) Halle, L. F.; Armentrout, P. B.; Beauchamp, J. L. Organometallics 1982, 1, 963.
6. a) Armentrout, P. B.; Halle, L. F.; Beauchamp, J. L. J. Am. Chem. Soc. 1981, 103, 6624.
b) Armentrout, P. B.; Beauchamp, J. L. J. Am. Chem. Soc. 1981, 103, 6628.
7. Hanratty, M. A.; Beauchamp, J. L.; Illies, A. J.; Bowers, M. T. J. Am. Chem. Soc., submitted.
8. Henschman, M. "Ion-Molecule Reactions"; Franklin, J. L., ed.; Plenum Press: New York, 1972, p. 101.
9. Cooks, R. G.; Beynon, J. H.; Caprioli, R. M.; Lester, G. R. "Metastable Ions"; Elsevier: New York, 1973.
10. Details on obtaining the kinetic energy distributions and average kinetic energy are in Jarrold, M. F.; Illies, A. J.; Kirchner, N. J.; Wagner-Redeker, W.; Bowers, M. T.; Mandich, M. L.;

- Beauchamp, J. L. J. Phys. Chem. 1983, 87, 2313.
11. A more complete discussion may be found in:
 - a) Waage, E. V.; Rabinovitch, B. S. Chem. Rev. 1970, 70, 377.
 - b) Forst, W. "Theory of Unimolecular Reactions"; Academic Press: New York, 1973.
 - c) Robinson, P. J.; Holbrook, K. A. "Unimolecular Reactions"; Wiley: New York, 1972.
 12. For a discussion see Su, Timothy; Bowers, M. T. in "Gas-Phase Ion Molecule Chemistry"; Bowers, M. T., ed.; Academic Press, New York, 1979.
 13. a) Pechukas, P.; Light, J. C.; Rankin, C. J. Chem. Phys. 1966, 44, 794.
b) Nikitin, E. Theor. Exp. Chem. (Engl. Trans.) 1965, 1, 285.
c) Chesnavich, W. J.; Bowers, M. T. J. Am. Chem. Soc. 1976, 98, 8301.
Chesnavich, W. J.; Bowers, M. T. J. Chem. Phys. 1978, 68, 901.
 14. Safron, S. A.; Weinstein, N. D.; Herschbach, D. R.; Tully, J. C. Chem. Phys. Lett. 1972, 12, 564.
 15. See, for example, Sudbø, S. Aa.; Schulz, P. A.; Grant, E. R.; Shen, Y. R.; Lee, Y. T. J. Chem. Phys. 1979, 70, 912.
 16. See, for example, Farrar, J. M.; Lee, Y. T. J. Chem. Phys. 1976, 56, 1414 and discussion of the results in Marcus, R. A. J. Chem. Phys. 1975, 62, 1372. Worry, G.; Marcus, R. A. J. Chem. Phys. 1977, 67, 1636.
 17. Sudbø, S. Aa.; Schulz, P. A.; Shen, Y. R.; Lee, Y. T. J. Chem. Phys. 1978, 63, 2312.
 18. Jacobson, D. B.; Freiser, B. S. J. Am. Chem. Soc. 1983, 105, 5197.
 19. Hanratty, M. A.; Paulsen, C. M.; Beauchamp, J. L. J. Am. Chem. Soc. submitted.

20. For a description of the experimental instrumentation and methodology, see:
- Illies, A. J.; Bowers, M. T. Chem. Phys. 1982, 65, 281.
 - Illies, A. J.; Bowers, M. T.; Jarrold, M. F.; Bass, L. M. J. Am. Chem. Soc. 1983, 105, 5575.
21. The uncertainty in the center-of-mass energy is given by the relationship
$$\Delta T = \left(\frac{M_1^2}{M_2 M_3 eV} \right)^{\frac{1}{2}} T^{\frac{1}{2}} \Delta E$$
 where M_1 and M_2 are the masses of the parent and fragment ion, respectively, M_3 is the mass of the neutral, eV is the acceleration voltage, and E is the laboratory energy (Reference 9).
22. Dissociation between the source and the magnet in the first field-free region is thought to be responsible for the majority of these peaks. See Ast, T.; Bozorgzaden, M. H.; Wiebers, J. L.; Beynon, J. H.; Brenton, A. G. Org. Mass Spec. 1979, 14, 313.
23. Cooks, R. G.; Hendricks, L.; Beynon, J. H. Org. Mass Spec. 1975, 10, 625.
24. Illies, A. J.; Bowers, M. T. Chem. Phys. 1982, 65, 281.
25. Cooks, R. G., ed.; "Collision Spectroscopy"; Plenum Press: New York, 1978.
26. Moore, C. E. "Atomic Energy Levels"; U.S. Government Printing Office: Washington, D. C., 1971, National Standard Reference Data Series, N.B.S. 35.
27. It was observed that CoCO^+ formed in an ion cyclotron resonance spectrometer from 40 eV electron impact on $\text{Co}(\text{CO})_3\text{NO}$ contributed ~10% to the product intensities for the reactions displayed in Scheme I (Reference 19).

28. The bond energy for CoCO^+ is not known but is estimated to be 46 kcal/mol. The binding energy of pentene to cobalt ions is estimated to be 55 kcal/mol. See Appendix II for further details.
29. In a low-energy ion beam CoCO^+ reacts with 1-pentene and 2-pentene to yield the same products as Co^+ but with different cross sections (Hanratty, M. A., and Beauchamp, J. L., unpublished work). In both this and the experiments reported in Reference 19, there was no indication of CO incorporation into products.
30. For an ion with m/e 123 this corresponds to a lifetime of ~15-20 microseconds.
31. Thermochemical data for hydrocarbons taken from Cox, J. D.; Pilcher, G.; "Thermochemistry of Organic and Organometallic Compounds"; Academic Press: New York, 1970. Values for bond energies for the organometallic ions are discussed in Appendix II.
32. See, for example:
 - a) Kato, S.; Morokuma, K. J. Chem. Phys. 1980, 73, 3900.
 - b) Santamaria, J; Benito, R. M. Chem. Phys. Lett. 1984, 109, 478.
33. This may be expected for a statistical partitioning of excess energy in a molecule as large as $\text{Co}(\text{C}_5\text{H}_{10})^+$.
34. See, for example:
 - a) Low, J. J.; Goddard, W. A. J. Am. Chem. Soc. 1984, 106, 8321.
 - b) Low, J. J.; Goddard, W. A. J. Am. Chem. Soc. 1984, 106, 6928.
 - c) Obara, S.; Kitaura, K.; Morokuma, K. J. Am. Chem. Soc. 1984, 106, 7482.
 - d) Siegbahn, P. E. M.; Blomberg, R. A.; Bauschlicher, C. W. J. Chem. Phys. 1984, 81, 1373.

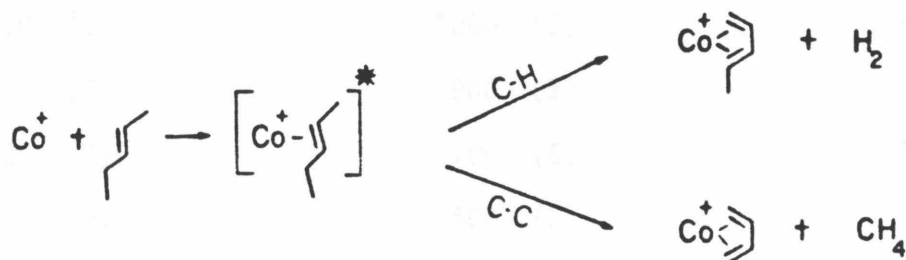
- e) Saillard, J. Y.; Hoffmann, R. J. Am. Chem. Soc. 1984, 106, 2006.
35. Turner, J. J.; Poliakoff, M. in "Inorganic Chemistry: Toward the 21st Century"; Chisholm, M. H., ed.; Am. Chem. Soc., 1983, p. 35. p. 35.
36. See Williams, Dudley H. Acc. Chem. Res. 1977, 10, 280.
37. The high-energy collision-induced dissociation spectra of $\text{Fe}(\eta^2\text{-pentene})^+$ and $\text{Fe}(\eta^3\text{-methylbutene})^+$ are also very similar (Reference 38).
38. Peake, D. A.; Gross, M. L.; Ridge, D. P. J. Am. Chem. Soc. 1984, 106, 4307.
39. Similar behavior was noted for $\text{Fe}(\eta^5\text{-cyclopentane})^+$ (Reference 38).
40. a) Jacobson, D. B.; Freiser, B. S. Organometallics 1984, 3, 513.
b) Jacobson, D. B.; Freiser, B. S. J. Am. Chem. Soc. 1983, 105, 492.
41. Cyclopentane adduct does not dissociate in the IR multiphoton activation experiments reported in Reference 19.
42. Jacobson, D. B.; Freiser, B. S. J. Am. Chem. Soc. 1985, 107, 72.
43. Kappes, M. M., Ph.D. Thesis, Massachusetts Institute of Technology, 1981.
44. We have been unsuccessful in our search for examples of alkane addition to $\text{Co}(\eta^2\text{-olefin})^+$ complexes.
45. The gas-phase IR spectrum of neutral pentene was used as a guide to frequency assignments for the association adduct. Additional vibrational frequencies were taken from: Ozin, G. A. Coord. Chem. Rev. 1979, 28, 117. Shimanouchi, T. "Tables of Molecular Vibrational Frequencies"; U. S. Government Printing Office: Washington D.C., 1972, National Standard Reference Data Series

N.B.S. 39.

46. Preexponential factors for three-centered reactions are expected to be in the range 10^{14} to 10^{13} sec^{-1} : Benson, S. W.; O'Neal, H. E. "Kinetic Data on Gas-Phase Unimolecular Reactions": U. S. Government Printing Office: Washington, D. C. 1970; National Standard Reference Data Series, N.B.S. 21.
47. See, for example, Bamford, C. H.: Tipper, C. F. H., ed.; "Comprehensive Chemical Kinetics"; Elsevier Scientific: New York, 1983, p. 149.
48. Armentrout, P.B.; Beauchamp, J.L. J. Am. Chem. Soc. 1981, 103, 784.

APPENDIX I

The experimentally observed metastable product ratios for H_2 and CH_4 loss were modeled using reaction rates predicted by RRKM theory. Dissociation rates as a function of energy were calculated using the Bunker-Hase RRKM program with harmonic approximation and semiclassical Whitten-Rabinovitch state counting.¹¹ External rotations were not treated. The calculations assume that both hydrogen and methane elimination occur from a common intermediate, namely the $Co(2\text{-pentene})^+$ association adduct, as shown in Scheme IV. For purposes of these



calculations, C-H or C-C bond insertion was assumed to be the rate-limiting step for hydrogen and methane elimination, respectively. The frequencies of the neutral pentene molecule with the appropriate lowering of the C-C double bond stretch and inclusion of a metal-carbon or metal-hydrogen stretch were used to assign frequencies for the $Co(pentene)^+$ adduct and transition states.⁴⁵ The C-H allylic stretch (2700 cm^{-1}) was chosen as the reaction coordinate for hydrogen elimination. The reaction coordinate for methane elimination was chosen to be the C-C stretch at 1150 cm^{-1} . The frequencies are listed in Table IA. There are, however, no A factors for similar reactions

Table IA. Vibrational Frequencies Used in RRKM Calculations for H₂ and CH₄ Elimination^a

Molecule	<u>H₂ Elimination</u> Complex	<u>CH₄ Elimination</u> Complex
3000 (3)	3000 (3)	3000 (3)
2950 (2)	2950 (2)	2950 (2)
2700 (5)	2700 (4)	2700 (2)
1450 (3)	1570 (1)	1500 (3)
1150 (11)	1450 (2)	1450 (1)
1000 (3)	1200 (5)	1150 (9)
900 (2)	1150 (5)	1000 (2)
700 (6)	1000 (3)	900 (5)
500 (2)	900 (3)	700 (4)
420 (2)	700 (6)	500 (2)
350 (2)	500 (2)	420 (2)
300 (1)	420 (2)	350 (3)

^aVibrational frequencies are in units of cm⁻¹; degeneracies are given in parentheses.

known to compare to the calculated A factors.

The intensity of each channel at a specific energy is given by Equation A-1 where $[A]_0$ is the intensity of the $\text{Co}(\text{pentene})^+$ adduct at

$$I_i = \frac{-K_i[A]_0}{K_1(E) + K_2(E)} \left[e^{-[K_1(E)+K_2(E)]t_f} - e^{-[K_1(E)+K_2(E)]t_i} \right] \quad (\text{A-1})$$

time $t = 0$, and t_i and t_f are the times the ion enters and leaves the second field-free region, respectively. To calculate the total ion yield, Equation A-2 should be integrated over the energy distribution.

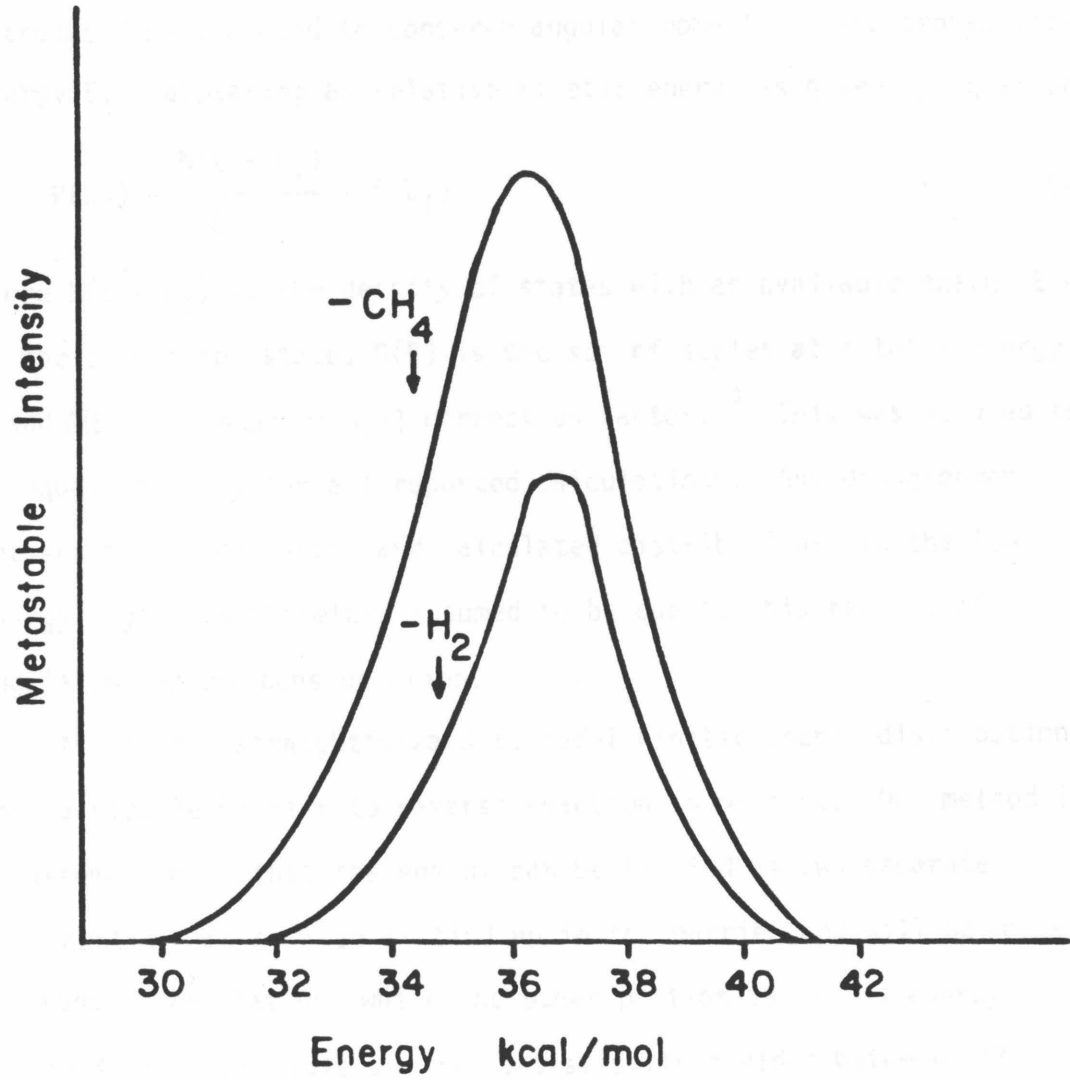
$$\text{Total } I_i = \int_0^{E_{\max}} I_i P(E) d(E) \quad (\text{A-2})$$

Since we lack any knowledge of $P(E)$, we will assume $P(E) = 1$ for $0 \leq E \leq E_{\max}$ and $P(E) = 0$ outside of this range. Plotting I_i vs. energy will result in a curve whose area is proportional to yield.

The best fit to the experimental product ratios for H_2 and CH_4 elimination is achieved using the frequencies listed in Table IA with values of 32 and 30 kcal/mol for the activation barriers to hydrogen and methane elimination, respectively. The reaction degeneracy for loss of hydrogen was chosen to be five, corresponding to the number of allylic hydrogens; while this is not strictly correct, it is expected that the 1,3-dimethyl allyl would not differ greatly from the 1-ethyl allyl complex. The calculated curves shown in Figure 1A reproduce the experimentally observed ratios with values of E^* in the range of 30 to 40 kcal/mol. This suggests that the ligand displacement Reaction 3 is responsible for the metastable ion population.⁴⁶

Modeling translational energy releases for reactions without a

Figure 1A. Yield of $\text{Co}(\text{C}_4\text{H}_6)^+$ and $\text{Co}(\text{C}_5\text{H}_{10})^+$ as a function of initial energy. The activation barriers for CH_4 and H_2 loss were assumed to be 30 and 32 kcal/mol, respectively.



barrier to reverse reaction is straightforward using statistical theories. The excess energy available at the transition state is assumed to be partitioned equally among all remaining degrees of freedom, and any energy in the reaction coordinate becomes translational energy of the separating fragments. Additional constraints may be introduced by the need to conserve angular momentum. The probability of energy E_t 's appearing as relative kinetic energy is given by Equation A-3

$$P(E_T) = \frac{N(E - E_T)}{G(E)} \cdot A(E_T) \quad (\text{A-3})$$

where $N(E - E_T)$ is the density of states with an available energy $E - E_T$ at the transition state, $G(E)$ is the sum of states at a total energy of E , and $A(E_T)$ is the centrifugal correction factor.¹⁴ This was assumed to be equal to unity for all reported calculations. Any disagreement between the experimental and calculated distributions in the low-energy region is therefore assumed to be due to this neglect of angular momentum consideration.

It is less straightforward to model kinetic energy distributions when a sizable barrier to reverse reaction is present. One method is to assume simply that the energy can be treated as two separate components: one portion is tied up in the barrier and will be released to product translation, while the other portion is excess energy at the transition state and is statistically divided between all remaining modes.⁴⁷ The kinetic energy release distribution can be calculated using Equation A-1, but the entire distribution will be shifted from zero by an amount equal to the reverse activation barrier.⁴⁷

There are several well-studied reactions for which the reaction

enthalpy and the reverse activation barrier are known. In these systems the partitioning of the internal energy is found to be contingent on the details of the transition state.^{15,17} Usually only a fraction of the reverse activation barrier appears as translational energy. For the organometallic systems investigated in the present study, there is a lack of pertinent thermochemical information, particularly regarding activation parameters. Therefore, a number of transition states and barrier heights were examined. The releases were modeled assuming a Type I surface where E_{excess} is statistically partitioned to all degrees of freedom. The calculated distributions were area-normalized to experimental distributions. For hydrogen and methane elimination, the frequencies listed in Table IIA corresponding to structures 4 and 5 were used. The values for $\log A$ of 13.21 and 13.82, respectively, for loss of CH_4 and H_2 are not unreasonable for three-centered transition states.⁴⁶ Ethene elimination was assumed to occur from the bis-olefin structure 6. Frequencies of the molecule and transition state for ethene dissociation are listed in Table IIIA.

Only the kinetic energy distributions for loss of C_2H_4 (and presumably the low-energy distribution for loss of C_3H_6) could be fit with this procedure. The experimental and theoretical distributions for ethene loss are shown in Figure 2A. A loose transition state, essentially structure 6 with an elongated metal-olefin bond, was used. For loss of ethene, the best fit was obtained assuming 10 kcal/mol is available for translation (E_{av}). Since simple bond cleavage is envisaged in this reaction, it is not surprising that the kinetic energy distributions can be modeled by statistical releases.

Table IIA. Vibrational Frequencies Used in Translational Energy Release Calculations^a

<u>CH₄ Elimination</u>		<u>H₂ Elimination</u>	
<u>Molecule</u>	<u>Complex</u>	<u>Molecule</u>	<u>Complex</u>
3037 (9)	3037 (9)	3037 (8)	3037 (8)
1650 (1)	1595 (3)	1650 (2)	
1595 (3)	1410 (2)	1595 (2)	1595 (2)
1410 (2)	1300 (3)	1410 (4)	1410 (3)
1300 (3)	1200 (2)	1300 (3)	1300 (3)
1200 (2)	1000 (4)	1200 (2)	1200 (4)
1000 (4)	900 (4)	1150 (1)	1000 (5)
900 (4)	770 (1)	1000 (4)	900 (5)
700 (3)	700 (2)	900 (5)	770 (1)
650 (2)	650 (2)	770 (2)	500 (4)
500 (3)	500 (3)	500 (4)	420 (1)
420 (2)	420 (2)	420 (1)	340 (4)
340 (3)	340 (3)	340 (3)	162 (1)
162 (1)	162 (1)	162 (1)	

^aVibrational frequencies are in units of cm^{-1} ; degeneracies are given in parentheses.

Table IIIA. Vibrational Frequencies Used in RRKM Calculations for Ethene Loss from $\text{Co}(1\text{-pentene})^+$ ^a

Molecule	Complex
3026 (6)	3026 (6)
2960 (6)	2960 (4)
1460 (5)	1620 (1)
1399 (1)	1460 (5)
1300 (2)	1399 (1)
1220 (2)	1300 (3)
1160 (1)	1220 (2)
1000 (6)	1000 (6)
940 (4)	940 (4)
500 (4)	500 (4)
810 (2)	810 (2)
340 (2)	340 (2)
177 (1)	177 (1)

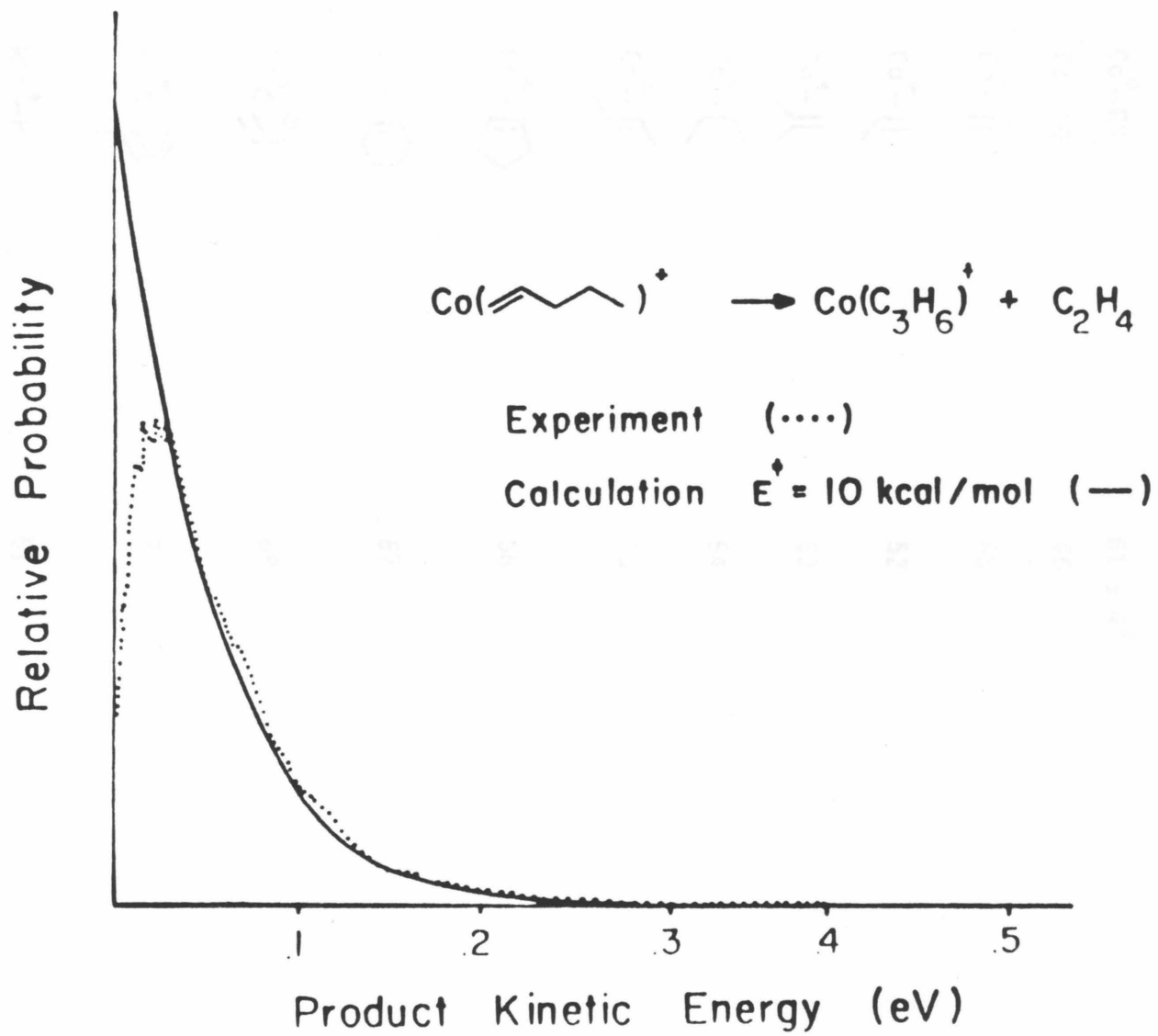
^aVibrational frequencies are in units of cm^{-1} ; degeneracies are given in parentheses.

For the loss of hydrogen, a purely statistical release cannot reproduce the experimental releases even if energy available for translation is equal to the reaction exothermicity. Figure 6 shows the predicted kinetic energy releases for H_2 loss from $Co(2\text{-pentene})^+$ assuming that there is no reverse activation barrier (solid line in Figure 6). Clearly the statistical model is unsatisfactory.

Statistical models could reproduce the experimental distributions for methane loss from $Co(\text{pentene})^+$ adducts. The experimental and theoretical distributions calculated, assuming 40 kcal/mol is available for translation, are shown in Figure 8. As discussed in the text, we feel that this may not be representative of the activation barrier for oxidative addition of an alkane to a cobalt-olefin complex.

Although these calculations are straightforward, they serve to highlight the fact that the releases for hydrogen loss are non-statistical and suggest the presence of a barrier to the reverse reaction. In contrast, ethene addition to a cobalt-olefin complex can be modeled adequately by assuming no activation barrier.

Figure 2A. Kinetic energy distribution corresponding to elimination of C_2H_4 from $Co(1-pentene)^+$. Solid line is the experimental. The dashed line was the best fit obtained using Equation 1 for $E_{av} = 10$ kcal/mol.



APPENDIX II

Table IVA. Thermochemical Estimates Used in Constructing Potential Energy Diagrams and Estimating Reaction Enthalpies.

<u>Bond</u>	<u>Binding Energy (kcal/mol)</u>
Co^+-H	52 ± 4^a
Co^+-CH_3	61 ± 4^a
Co^+-CO	46
$\text{Co}^+- $	48
$\text{Co}^+- $	52
$\text{Co}^+- $	53
$\text{Co}^+- $	54
$\text{Co}^+- $	55
$\text{Co}^+- $	56
$\text{Co}^+- $	57
$\text{Co}^+<=$	68
$\text{Co}^+<$	70
RCo^+-H	51
$\text{Co}^+-2(\text{CH}_3)$	110

<u>Bond</u>	<u>Binding Energy (kcal/mol)</u>
RCO^+-CH_3	50
HCO^+-R	57

^aDetermined in Reference 48.

CHAPTER V

FORMATION AND REACTIONS OF TRANSITION METAL CLUSTERS
IN THE GAS PHASE: A NOVEL SYNTHESIS
USING LASER-INDUCED DECARBONYLATION

Formation and Reactions of Transition Metal Clusters
in the Gas Phase: A Novel Synthesis
Using Laser-Induced Decarbonylation

Maureen A. Hanratty, C. A. Wight[‡],
and J. L. Beauchamp^{*}

Contribution No. 7166 from the Arthur Amos Noyes Laboratory
of Chemical Physics, California Institute of Technology,
Pasadena, California 91125

[‡]Present address: Chemistry Department, University of Utah,
Salt Lake City, Utah 84112

^{*}To whom reprint requests should be sent.

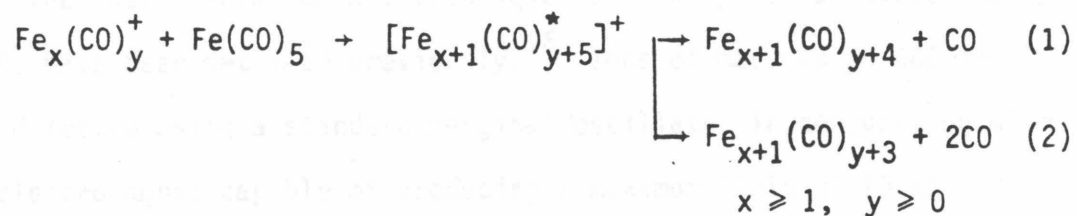
ABSTRACT

We describe a method for generation of polynuclear iron and nickel clusters in an ion cyclotron resonance spectrometer which takes advantage of ion-molecule condensation reactions and laser induced decarbonylation of metal carbonyl clusters. Ionized iron pentacarbonyl or nickel tetracarbonyl fragments will undergo successive condensation reactions with the neutral carbonyl to form polynuclear metal ions until clustering is terminated as a result of the ion's becoming coordinatively saturated. The clustering sequence can be re-initiated by laser induced decarbonylation of the unreactive polynuclear ions. Both visible and infrared laser radiation effects decarbonylation of iron clusters containing two to four metal atoms. Loss of two carbon monoxide ligands from $\text{Fe}(\text{CO})_5^+$ occurs only with 647 nm radiation, although dissociation of bimetallic or larger larger clusters exhibits no wavelength dependence. In contrast, polynuclear nickel clusters undergo photodissociation only when exposed to visible radiation, while $\text{Ni}(\text{CO})_4^+$ is not photoreactive with either IR or visible radiation. The reactivity of the ligated metal cluster species differs markedly with the behavior of the bare metal ions, with ligand displacement being the most prevalent reaction. By growing clusters in situ, it is possible to introduce unique and potentially reactive functional groups into the cluster. Although no reactions unique to the metal cluster species could be identified, infrared radiation is observed to induce CO loss in the substituted iron cluster, thus demonstrating the potential of this method for generation of highly specific unsaturated metal clusters.

INTRODUCTION

Innovative and diverse experimental techniques are now making possible the synthesis of a wide variety of metal-containing compounds that are intermediate between simple monometallic species and the bulk metal.¹⁻⁸ Enhanced and unique chemical reactivity of these compounds is anticipated due to the low coordination around the metal and the possibility of cooperative interactions between adjacent metal centers.^{1,2} The recent investigations of the chemical and physical properties of bare transition metal clusters in the gas phase have yielded results which suggest these expectations may be well founded.³⁻⁸ It is clearly of interest to compare the reactivity of these metal clusters with and without ligands which may significantly alter the chemical reactivity. We wish to describe a novel procedure for generating potentially reactive metal cluster species in situ in an ion cyclotron resonance spectrometer.

Formation of polynuclear iron and nickel clusters is initiated by electron impact ionization of volatile monometallic carbonyl compounds. Fragment ions rapidly condense with the neutral parent molecule to form higher nuclearity metal cluster compounds. Association of the fragment ion with the neutral metal carbonyl results in the formation of a chemically activated intermediate which can decompose by loss of a carbon monoxide ligand. Ionized iron carbonyl fragments, for instance, are observed to condense with neutral $\text{Fe}(\text{CO})_5$ and eliminate one or two CO ligands as exemplified by Reactions 1 and 2. Similar



reactions are observed for nickel carbonyl fragment ions. Condensation reactions accompanied by loss of one or more molecules of carbon monoxide are familiar in the gas-phase chemistry of cationic^{10,11}, anionic,¹² and neutral^{13,14} metal carbonyl complexes.

Metal carbonyl ions will continue to react via 1 and 2, producing polynuclear clusters until the condensation sequence is terminated, presumably as a result of the compound's becoming coordinately saturated. Decarbonylation of the unreactive species, however, reinitiates the clustering sequence and results in the formation of larger clusters with a higher metal-to-carbon monoxide ratio. We have explored the use of both chemical and photochemical methods to decarbonylate metal cluster compounds.

In view of the tremendous interest in synthesis gas chemistry,¹⁵ generation of clusters with bound CO and study of their reactivity is of particular relevance. We have investigated iron and nickel species containing up to four metal atoms with differing numbers of carbon monoxide ligands. Although larger clusters are formed, mass limitations of our instrument precluded investigation of these species. By growing the clusters in situ, it is possible in the early stages of cluster growth to introduce unique functional groups, e.g., a single potentially reactive metal-hydrogen bond or "promoters," such as halide or alkali ions, into the cluster.

EXPERIMENTAL

The instrumentation and techniques of ion cyclotron spectrometry (ICR) have been detailed previously.¹⁶ Ions of mass up to 600 amu are detected using a standard marginal oscillator in conjunction with an electromagnet capable of producing a maximum field of 23 kG. Reaction sequences were confirmed with double-resonance ejection techniques.¹⁶

Experimental modification necessary for photochemical investigations are described elsewhere.¹⁷ A typical experiment consists of a 10 to 20 msec electron pulse to generate the ions followed by a storage period of up to one second during which reactions occur. Electronically gating a mechanical shutter allows irradiation of the ions during any portion of the storage cycle. A line-tunable continuous wave CO₂ laser (Apollo 550A) is used for infrared studies. A krypton-ion laser (Coherent model Cr-2000) is employed for investigations in the visible region. Lithium attachment experiments were conducted using a thermionic lithium filament described elsewhere.¹⁸

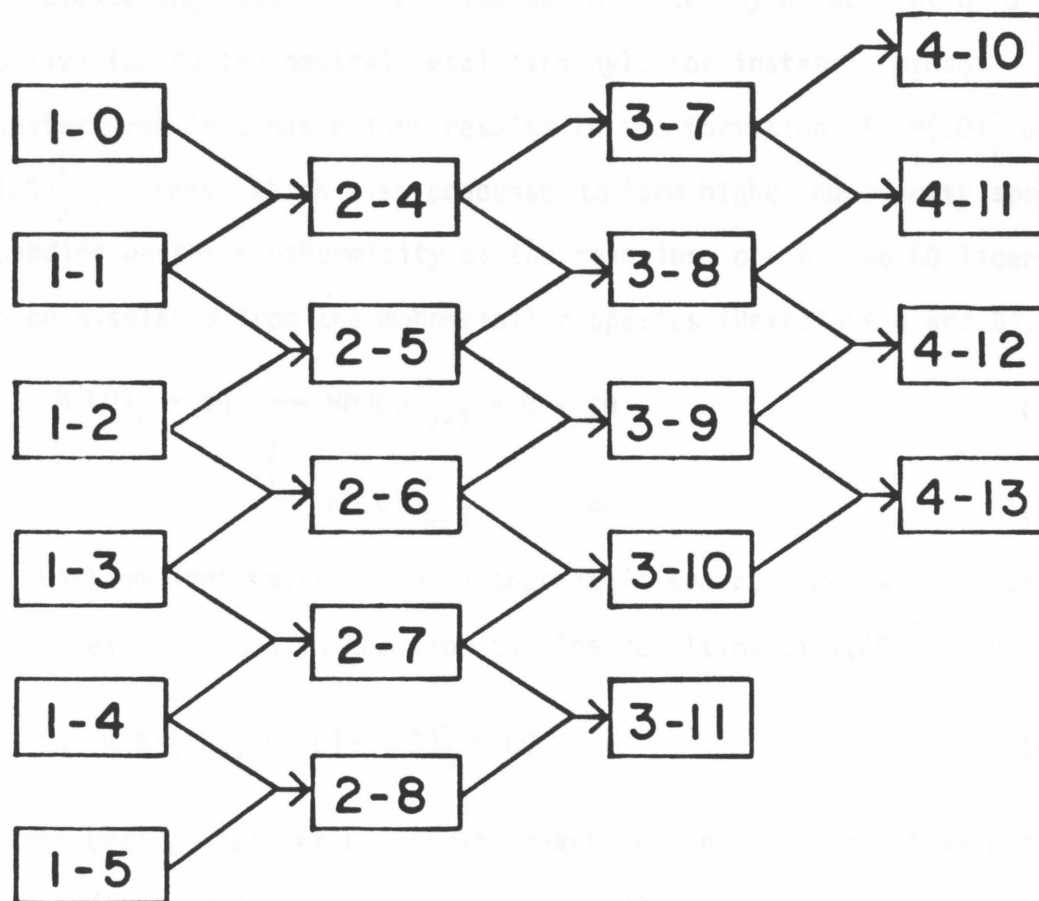
Pressures in the spectrometer were typically in the 10⁻⁶ to 10⁻⁷ torr range. The pressure of the metal carbonyl compound was generally below 1 x 10⁻⁶ torr. Pressure measurements were made using a Schulz-Phelps gauge calibrated at higher pressures against an MKS Instruments Baratron Model 90H1-E capacitance monometer. Iron pentacarbonyl (Alpha Inorganics) was filtered and stored over activated sieves. Nickel tetracarbonyl (Alpha Inorganics) and all other reagents were used as received. Successive freeze-pump-thaw cycles were performed to remove noncondensable gases. Samples of Fe(CO)₅ and Ni(CO)₄ were degassed at dry ice-acetone temperature.

RESULTSGrowth of Ionized Metal Clusters

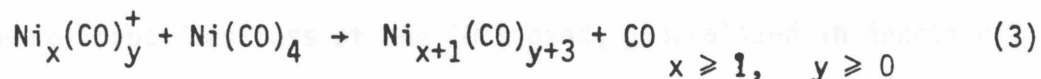
Polynuclear iron carbonyl clusters result from the stepwise condensation reactions of the ionized iron pentacarbonyl fragments with the parent molecule. Elimination of one or two molecules of carbon monoxide occurs at each step. This sequence of reactions resulting in formation of polynuclear clusters is illustrated in Scheme I. The notation x-y refers to ions of stoichiometry Fe_xCO_y^+ . The neutral reactant is understood to be $\text{Fe}(\text{CO})_5$. For instance, the reaction of $\text{Fe}(\text{CO})_2^+$ with neutral $\text{Fe}(\text{CO})_5$ leads to formation of the $\text{Fe}_2(\text{CO})_7^+$ collisional complex which immediately decomposes to give $\text{Fe}_2(\text{CO})_5^+$ (2,5) and $\text{Fe}_2(\text{CO})_6^+$ (2,6). These fragments in turn form $\text{Fe}_3(\text{CO})_8^+$, $\text{Fe}_3(\text{CO})_9^+$ and $\text{Fe}_3(\text{CO})_{10}^+$. Ejection of $\text{Fe}(\text{CO})_2^+$ from the reaction mixture would result in a decrease in the intensity of these ions. In this manner, reaction pathways can be deduced by double resonance techniques.

The reaction sequences shown in Scheme I are in agreement with the results of Foster and Beauchamp,⁹ which were determined at 70 eV. The present study was carried out with electron impact ionization energies below 20 eV, where the dominant fragment ions are $\text{Fe}(\text{CO})_5^+$, $\text{Fe}(\text{CO})_4^+$, and $\text{Fe}(\text{CO})_3^+$. At these lower electron energies, pathways involving loss of two carbon monoxide ligands, especially for the larger cluster, diminish in importance. The more unsaturated species are found to be more reactive. For instance, the rate of reaction of $\text{Fe}(\text{CO})_2^+$ is estimated to be $1.5 \times 10^{-10} \text{ cm}^3 \text{ molecule}^{-1} \text{ sec}^{-1}$ compared to $k < 10^{-11} \text{ cm}^3 \text{ molecule}^{-1} \text{ sec}^{-1}$ for $\text{Fe}(\text{CO})_5^+$.^{9,19}

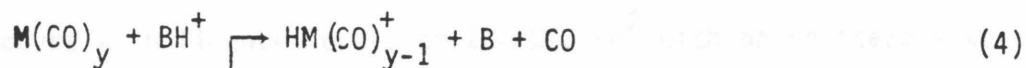
A clustering sequence similar to that shown in Scheme I for

Scheme I

iron carbonyl is observed with nickel carbonyl ions. In contrast to the iron system, condensation with loss of a single molecule of carbon monoxide (Reaction 3) is the dominant pathway.



Clustering reactions can also be initiated by attachment of a positive ion to the neutral metal carbonyl. For instance, proton transfer from less basic ions results in the formation of $\text{HM}(\text{CO})_y^+$ or $\text{HM}(\text{CO})_{y-1}^+$ ions which also condense to form higher nuclearity species. Depending on the exothermicity of the reaction, one or two CO ligands can be displaced from the monometallic species (Reactions 4 and 5).



Lithium ions emitted from a thermionic source react with neutral $\text{Ni}(\text{CO})_4$ as indicated in Reaction 6. The resulting $\text{LiNi}(\text{CO})_3^+$ complex

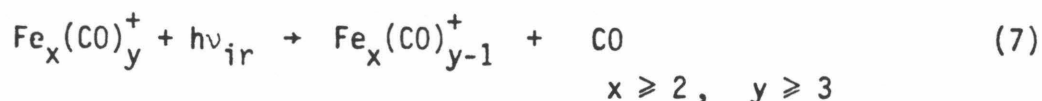


did not undergo further clustering reactions and was unreactive with N_2O . Infrared radiation (10.6 microns, 30 J/cm^2) did not decarbonylate this species or promote further condensation reactions. No reaction was observed between Li^+ and neutral $\text{Fe}(\text{CO})_5$.

Infrared Laser-Assisted Decarbonylation Reactions

Irradiation of the iron cluster ions with 9.2 -10.8 micron radiation using the unfocused output of a cw CO_2 laser (fluence of $\leq 70 \text{ J/cm}^2$) is observed to alter the relative ion intensities for complexes containing two to four iron atoms. The ions present 1 sec

after the ion formation pulse are the more saturated ions, $\text{Fe}_3(\text{CO})_{10}^+$, $\text{Fe}_3(\text{CO})_{11}^+$, and $\text{Fe}_3(\text{CO})_{12}^+$ (Figure 1a). Exposure to 10.6 micron radiation (70 J/cm^2) causes a dramatic decrease in the $\text{Fe}_3(\text{CO})_{10}^+$ and $\text{Fe}_3(\text{CO})_{11}^+$ intensities and an increase in the $\text{Fe}_4(\text{CO})_{12}^+$ signal (Figure 1b). Double resonance identifies loss of one CO ligand, generalized in Reaction 7, as



the primary photoactivated reaction. Product ions from photodissociation rapidly react to form higher mass clusters. The highly reactive nature of the photoproducts makes double resonance essential for identification of many of the photoreactions.

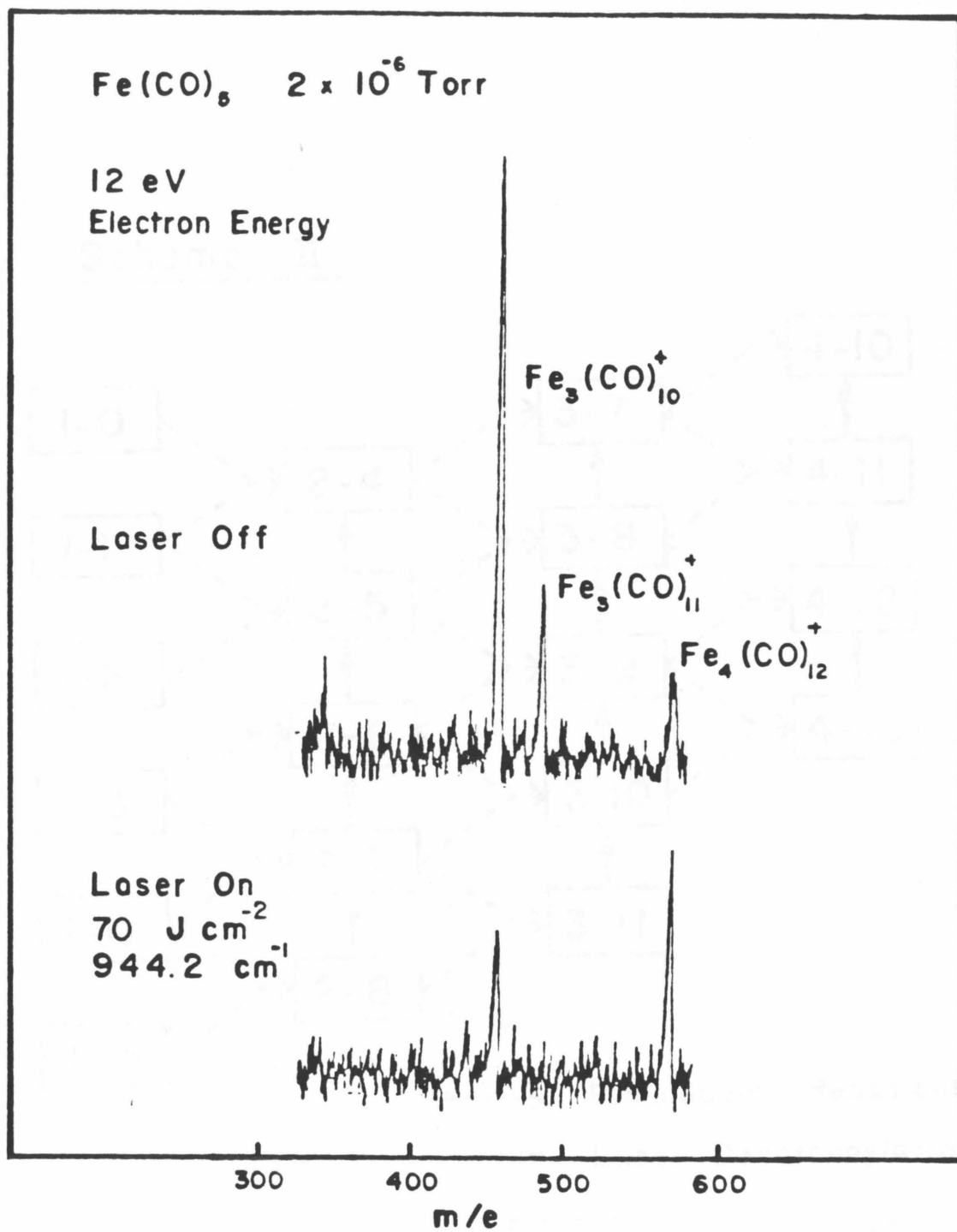
Photoinduced elimination of a single CO from polynuclear iron clusters occurs with fluence levels of $20\text{-}70 \text{ J/cm}^2$ with no noticeable wavelength dependence from 9.2 to 10.8 microns. The photoassisted decarbonylation reactions are indicated in Scheme II. In addition to the bimolecular reaction pathways discussed above (dashed lines), infrared-assisted pathways (solid lines) also become accessible. Monometallic $\text{Fe}(\text{CO})_x^+$ ions were not observed to photodissociate in the presence of infrared radiation.

In contrast to the results with the iron clusters, infrared radiation was not observed to induce decarbonylation of any $\text{Ni}_x(\text{CO})_y^+$ clusters for all wavelengths accessible to the CO_2 laser and with fluence levels up to 90 J/cm^2 .

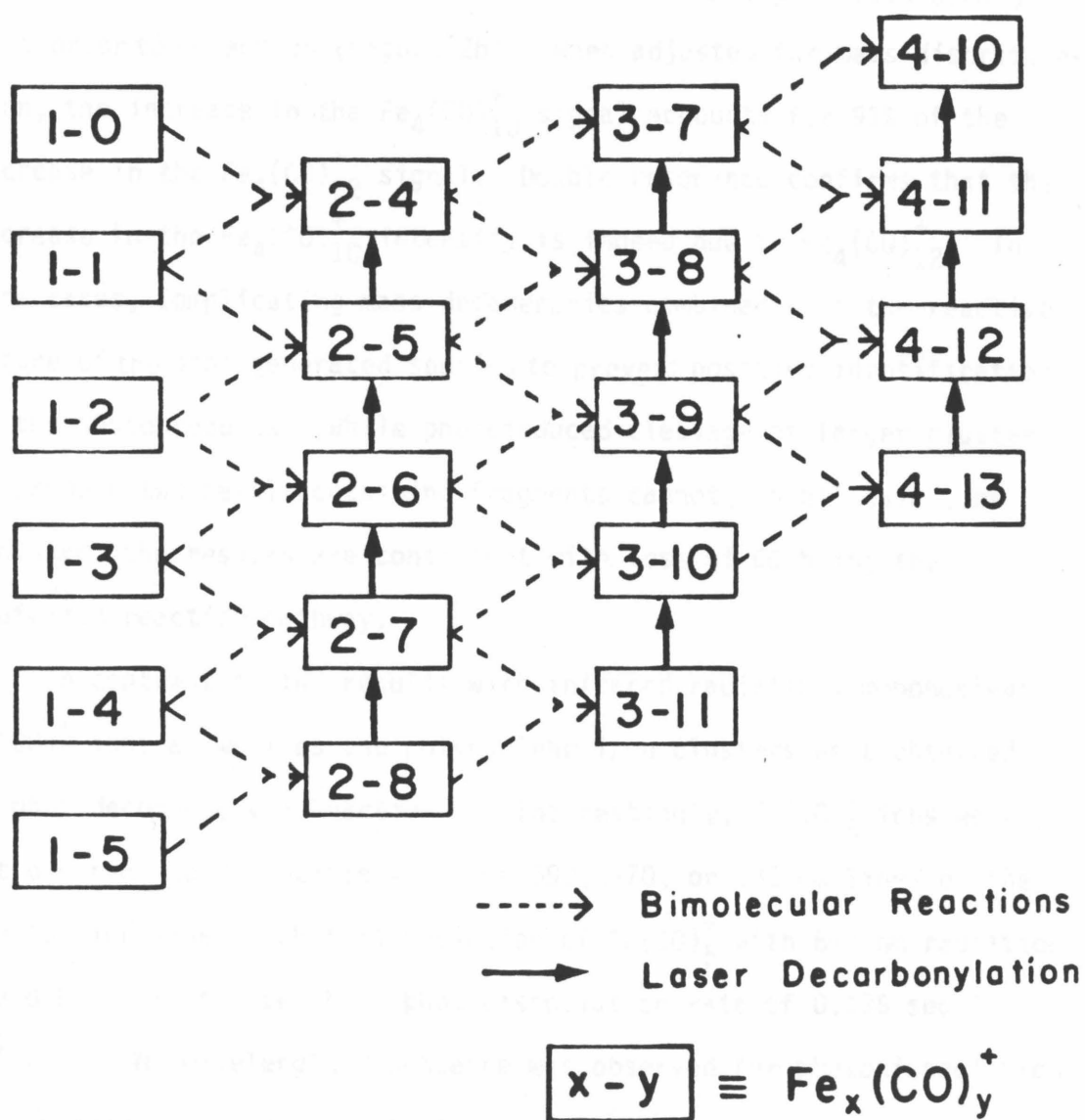
Visible Laser-Assisted Decarbonylation Reactions

More energetic photons (1.85 - 3.8 eV) are supplied by the output of a krypton-ion laser. Iron carbonyl clusters exposed to 647 nm radiation were observed to photodissociate with loss of two carbon monoxide

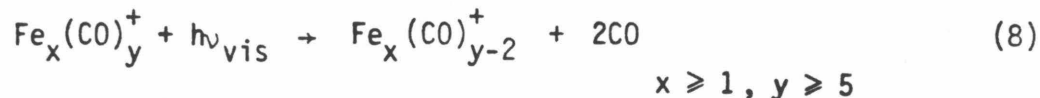
Figure 1. Mass spectra of iron cluster ions present 1 sec after the ion formation pulse: a) without, and b) with IR irradiation.



Scheme II



ligands (Reaction 8).

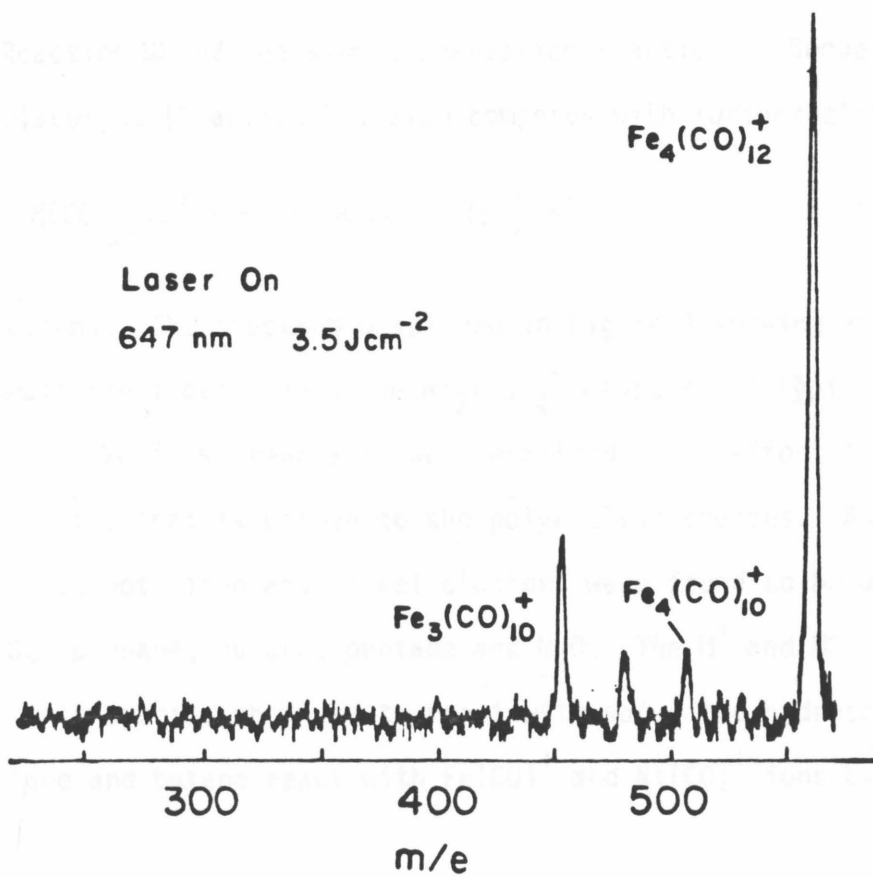
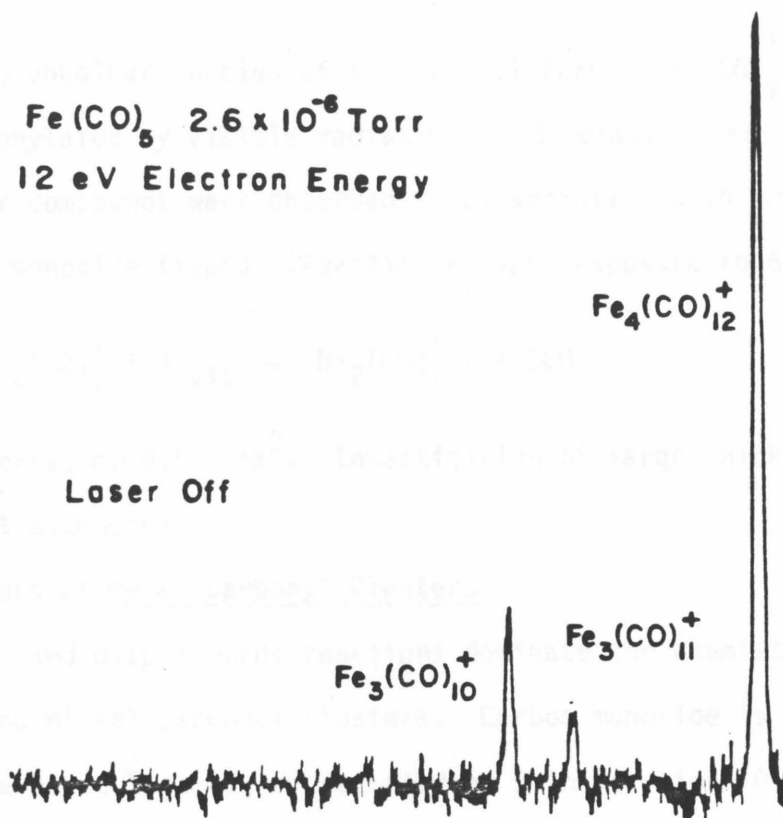


Photodissociation of the larger clusters with visible radiation is very rapid. As an example, the spectrum taken at 300 milliseconds' trapping time without laser radiation (Figure 2a) can be compared with that recorded after 50 msec exposure with 647 nm light (3.4 J/cm^2) just prior to detection (Figure 2b). When adjusted for mass discrimination, the increase in the $\text{Fe}_4(\text{CO})_{10}^+$ signal accounts for 91% of the decrease in the $\text{Fe}_4(\text{CO})_{12}^+$ signal. Double resonance confirms that the increase in the $\text{Fe}_4(\text{CO})_{10}^+$ intensity is indeed due to $\text{Fe}_4(\text{CO})_{12}^+$. In some cases, complicating mass degeneracies combined with the reactive nature of the photogenerated species to prevent positive identification of the photoproducts. While photoinduced cleavage of larger clusters to produce two metal-containing fragments cannot, in all cases, be excluded, the results are consistent with loss of CO being the preferred reaction pathway.

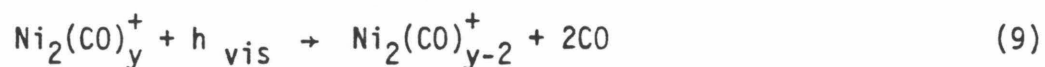
In contrast to the results with infrared radiation, mononuclear $\text{Fe}(\text{CO})_5^+$ ions as well as the polynuclear iron clusters were observed to photodecompose via Reaction 8. Interestingly, $\text{Fe}(\text{CO})_5^+$ ions were not observed to dissociate with the 590, 470, or 330 nm lines of the krypton-ion laser. Photodissociation of $\text{Fe}(\text{CO})_5^+$ with 647 nm radiation could be characterized by a photodissociation rate of $0.196 \text{ sec}^{-1} \text{ W}^{-1} \text{ cm}^2$. No wavelength dependence was observed for photodissociation of clusters containing two or more metal atoms.

Figure 2. Mass spectra of ions present at 300 msec trapping time:
a) without, and b) with visible laser exposure.

$\text{Fe}(\text{CO})_5$ 2.6×10^{-6} Torr
12 eV Electron Energy



Mononuclear species of the general form $\text{Ni}(\text{CO})_y^+$ were not decarbonylated by visible radiation. Bimetallic nickel cluster compounds were observed to dissociate with loss of two carbon monoxide ligands (Reaction 9) upon exposure to 647 nm radiation



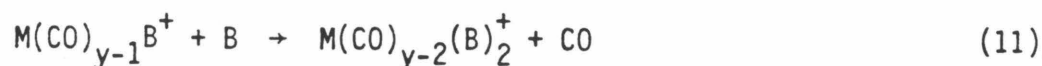
at fluences of 9.5 J/cm^2 . Investigation of larger nickel clusters was not attempted.

Reactions of Metal Carbonyl Clusters

Ligand displacement reactions dominate the chemistry of cationic iron and nickel carbonyl clusters. Carbon monoxide is readily replaced by more basic ligands, represented by B in Reaction 10. The products



of Reaction 10 undergo slow condensation reactions. Sequential ligand displacement (Reaction 11) also competes with further clustering



reactions. The spectrum displayed in Figure 3 showing incorporation of multiple ligands into the $\text{Ni}_2(\text{CO})_4^+$ clusters is typical.

Various reactants were examined in an effort to identify reactivity that is unique to the polynuclear species. As shown in Table I, both iron and nickel clusters were found to be unreactive to D_2 , propane, butane, pentane and N_2O . The M^+ and MCO^+ ions were the only species observed to react with saturated hydrocarbons. Pentane and butane react with $\text{Fe}(\text{CO})^+$ and $\text{Ni}(\text{CO})^+$ ions by ligand

Figure 3. Mass spectra of the binuclear nickel clusters present at 200 msec trapping time: a) with 6×10^{-7} Torr of $\text{Ni}(\text{CO})_4$, b) with additional 2×10^{-7} Torr of C_2H_2 . The nomenclature "2-Y" refers to ions of stoichiometry $\text{Ni}_2(\text{CO})_y^+$. The mass peaks corresponding to the number of C_2H_2 ligands which have displaced CO from the $^{58}\text{Ni}_2(\text{CO})_y^+$ ion are indicated.

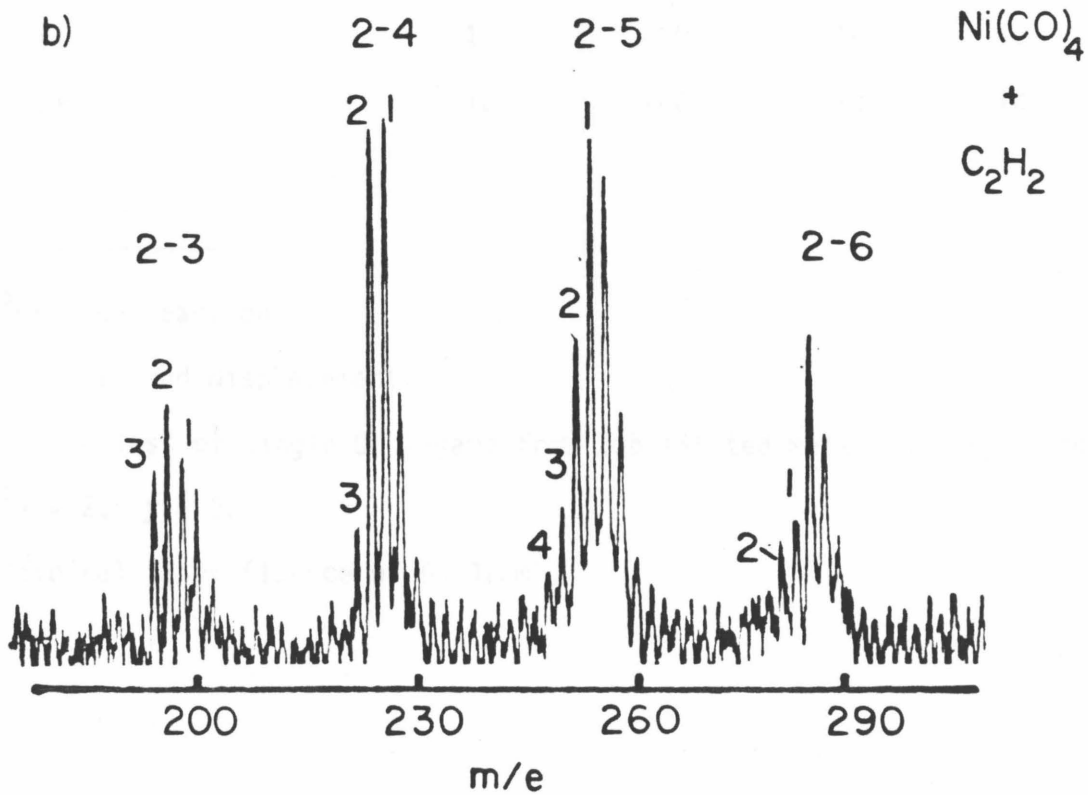
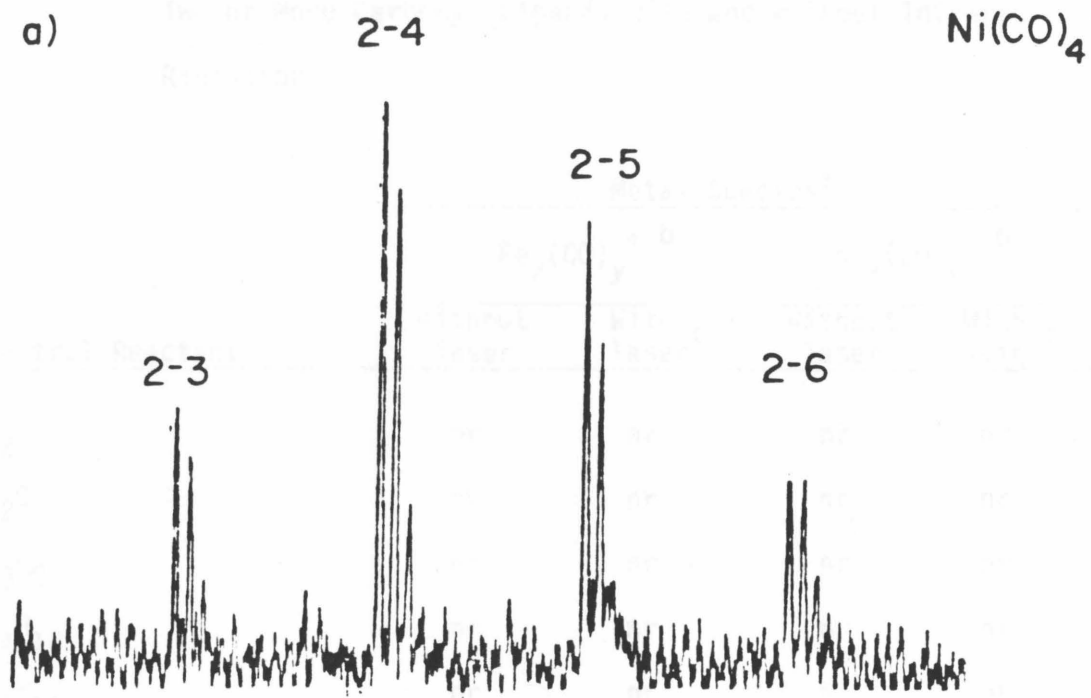


Table I. Observed Reactions for Iron and Nickel Compounds Containing Two or More Carbonyl Ligands with and without Infrared Radiation

Neutral Reactant	Metal Species ^a			
	$\text{Fe}_x(\text{CO})_y^{+b}$		$\text{Ni}_x(\text{CO})_y^{+b}$	
	Without laser	With laser ^c	Without laser	With laser ^c
D ₂	nr	nr	nr	nr
N ₂ O	nr	nr	nr	nr
C ₃ H ₈	nr	nr	nr	nr
C ₄ H ₁₀	nr	nr	nr	nr
C ₅ H ₁₀	nr	nr	nr	nr
C ₂ D ₄	ld	-CO	ld	ld
C ₂ H ₂	ld	-CO	ld	ld
CH ₃ OH	ld	-CO	ld	ld

^anr = no reaction.

ld = ligand displacement.

-CO = loss of single CO ligand from substituted metal carbonyl complex

^b $x \geq 2$; $y \geq 2$.

^cTypical laser fluence of 60 J/cm².

substitution; however, no larger clusters containing alkane ligands were observed. The alkanes examined did not react with the protonated metal species. Ligand displacement reactions were the only observed reactions with ethene, methanol and ethene.

The ligand displacement reactions were also examined in the presence of infrared radiation. The complex nature of the system and the mass limitations of the instrument precluded a thorough investigation of the reactive chemistry of larger mass clusters. Iron clusters with two to four iron atoms and containing C_2D_4 or methanol ligands were observed to eliminate CO when exposed to infrared radiation ($30 J/cm^{-2}$, 10.6 microns). No additional photo-initiated chemistry was observed.

DISCUSSION

Nucleation Reactions

Aggregation of transition-metal carbonyls to form larger complexes is commonly used for synthesis in solution-phase chemistry.^{1,14} Recently, the condensation reactions of Ni^+ ions produced by laser evaporation with a variety of neutral metal-carbonyl compounds have been demonstrated to be a convenient route to formation of mixed metal-carbonyl compounds in the gas phase.²⁰ In the present study, the condensation reactions of nickel-carbonyl ions are found to involve primarily loss of a single carbon monoxide molecule, whereas the reactions of iron ions proceed with loss of one or two carbon monoxide ligands. This could reflect differences in the M-CO bond strengths in the polynuclear compounds or differences in

exothermicity of the condensation reaction. For both nickel and iron complexes, it was noted that the more saturated species such as $\text{Fe}(\text{CO})_5^+$, $\text{Fe}_2(\text{CO})_8^+$, $\text{Fe}_3(\text{CO})_{10}^+$ and $\text{Fe}_4(\text{CO})_{12}^+$ were much less reactive toward clustering reactions. This is not surprising since a structure that is nearly coordinatively saturated can be drawn for each of these ions. Ridge and co-workers have suggested a general correlation between the electron deficiency of a metal-carbonyl cluster and the reactivity.^{7,10}

Photochemistry of Iron and Nickel Clusters

Metal-carbonyl compounds comprise a class of highly photoactive molecules. In condensed phase, visible or ultraviolet photons have frequently been used to create a highly reactive unsaturated metal species.¹⁴ In the present study, infrared radiation is found to promote decarbonylation of iron carbonyl clusters containing two to four iron atoms. $\text{Fe}(\text{CO})_5$ displays fairly weak absorption due primarily to C-Fe-C deformations in the region accessible to the CO_2 laser.²¹ It is likely that combination bands, especially in the polynuclear ionic species, are responsible for the absorption of infrared radiation. Although the bond strengths of carbon monoxide to the polynuclear ionic clusters are not known, the bond dissociation energies to the monometallic fragment ions have been measured using photoionization techniques.²² The removal of a CO ligand from $\text{Fe}(\text{CO})_5^+$ would require ~8 infrared photons (20 kcal/mol) and is not observed. In contrast, the larger clusters which are expected to have comparable metal-carbonyl bond strengths²³ undergo photo-assisted decarbonylation. Vibrational excitation may play a

significant role in both the bimolecular and photoassisted reactions. It was noted that the importance of the bimolecular pathways involving loss of two CO ligands from iron-carbonyl clusters diminishes as the electron energy is lowered. This suggests that the ions produced from electron-impact ionization of the neutral metal-carbonyl may be internally excited. In addition, internal excitation resulting from the exothermicity of the bimolecular condensation reaction may be retained in the newly formed cluster. The latter effect may, in part, be responsible for the facile photodissociation of the larger clusters.

Multiphoton infrared absorption by gas-phase ions can, in some instances, result in very selective dissociation reactions.^{24,25} At the fluence levels comparable to those employed in this investigation, decomposition has been observed to occur by the lowest energy pathway.^{25,26} The present study demonstrates that the additional energy necessary for dissociation of carbon monoxide from bimetallic and larger iron clusters can be conveniently supplied with infrared radiation. The preferential loss of CO suggests that the metal framework is less easily disrupted than the Fe-CO bond. The independence of the photodissociation yield over a wide frequency range is characteristic of photodissociation spectra of many gas-phase ions.²⁶

The salient difference between the nickel- and iron-carbonyl compounds is the lesser extent to which the nickel compounds can be photodissociated. $\text{Ni}(\text{CO})_y^+$ species are not decarbonylated with IR radiation which parallels the iron-carbonyl behavior. It is surprising, in view of the facile decarbonylation of the larger iron clusters with infrared radiation, that nickel compounds with up to three metal

atoms do not undergo photoinduced decarbonylation. This could reflect stronger M-CO bonds in the nickel clusters or a decrease in the exothermicity of the condensation reactions.

Visible Laser-Assisted Decarbonylation Reactions

Iron-carbonyl clusters are observed to lose two CO ligands upon exposure to visible radiation (647 nm). In contrast to the results obtained with infrared radiation, even the monometallic species $\text{Fe}(\text{CO})_5^+$ is observed to photodissociate. Interestingly, photodissociation of iron clusters containing two or more iron atoms is independent of excitation wavelength, while the $\text{Fe}(\text{CO})_5^+$ photodissociation occurs only with 647 nm radiation. The photoelectron spectrum of $\text{Fe}(\text{CO})_5^+$ has two broad bands centered at 9.85 eV (fwhm 0.95 eV) and 8.65 eV (fwhm 0.63 eV) which correspond to the ${}^2E''$ and ${}^2E'$ states of the ion, respectively.²⁷ Both 647 and 670 nm radiation can lead to population of the ${}^2E''$ ion state via the dipole-allowed transition ${}^2E'' \leftarrow {}^2E'$. No transitions at shorter wavelengths are apparent from the photoelectron spectrum, which explains the lack of photoreactivity of $\text{Fe}(\text{CO})_5^+$ in this wavelength region. Removal of two carbonyl ligands from $\text{Fe}(\text{CO})_5^+$ requires 1.89 eV, and one 647 nm photon (1.92 eV) provides sufficient energy for dissociation. Although the 670 nm laser line is also within the ${}^2E'' \leftarrow {}^2E'$ transition region and would provide sufficient energy for loss of one CO ligand, this process is not observed.

In comparison to the monometallic iron species, the larger iron clusters are found to be extremely photoreactive. For example, at a fluence of 7 J/cm^{-2} , less than 30% of the $\text{Fe}(\text{CO})_5^+$ ions dissociate while complete photolysis of $\text{Fe}_4(\text{CO})_{12}^+$ is achieved at this fluence. It is also interesting that cleavage of the metal-metal

bond in the larger clusters was not a significant photoreaction.

Ni(CO)_4^+ is not observed to lose CO upon exposure to visible radiation. The photoelectron spectrum of Ni(CO)_4 ²⁸ shows only one low-energy transition which is at 0.9 eV (1.4 microns), and this is not accessible with the Kr-ion laser lines. Interestingly, decarbonylation of bimetallic nickel clusters is observed with visible light. Although the larger nickel clusters were not investigated, it is probable that they would also undergo laser-induced decarbonylation reactions.

Chemical Reactivity

By far the dominant reaction observed with both nickel- and iron-carbonyl species is substitution of the carbonyl ligand by more basic groups. No unique reactivity could be associated with the larger metal-containing species. For instance, there were no reactions observed with alkanes other than those from M^+ and MCO^+ ions. Kappes and Staley observed similar behavior with mixed bimetallic carbonyl clusters.²⁰

Formation of a metal-hydrogen bond is easily achieved by proton transfer reactions. Numerous reactions may be envisaged for a cluster containing a hydride ligand. For example, alkane addition to the metal-hydride cluster and subsequent elimination of molecular hydrogen would represent a convenient route for gas-phase synthesis of a variety of metal-alkyl species. Although this reaction for iron-carbonyl species is estimated to be exothermic by ~ 19 kcal/mol, it is not observed.²⁹ This contrasts markedly with the reactivity of Fe-H^+

ions.³⁰ The reactivity of the ligated metal species is clearly different from the bare atomic ions. N_2O is observed to react with Fe^+ by oxygen transfer (Reaction 12). Further reaction of the FeO^+ product ion with CO results in the production of CO_2 (Reaction 13).³¹



Attempts to use N_2O to chemically remove CO from the iron- and nickel-cluster compounds were unsuccessful.

Although the chemical reactivity of metal clusters is likely to be the result of subtle electronic and geometric factors, recent experimental evidence suggests this may correlate with the number of metal atoms. D_2 addition is observed for neutral metal clusters containing nine or more iron atoms while very little reaction is observed with the smaller clusters.^{4c,5a} We also find no evidence for D_2 incorporation into iron or nickel clusters of up to four metal atoms.³² Interestingly, while neutral iron clusters of varying sizes up to Fe_{20} are unreactive with methane,^{4a} Sc_4^+ ions react with up to four methane molecules losing H_2 at each step.⁶ Clearly, it is of interest to compare the neutral and ionic clusters with and without ligands which may substantially modify the reactivity.

Alkali ions are frequently used as promoters for surface metal reactions.³³ Lithium ion attachment to a neutral metal carbonyl represents a convenient method of incorporating an alkali atom into the coordination sphere of a transition metal. It was hoped that the lithiated species would undergo further condensation and give rise to

larger metal clusters whose subsequent reactivity could be explored. Unfortunately, no clustering of the lithiated ions was observed. Observation of Reaction 6 implies that $D[\text{Li}^+-\text{Ni}(\text{CO})_3]$ $D[\text{Ni}(\text{CO})_3-\text{CO}] = 25 \text{ kcal/mol}$.³⁴ This is comparable to the binding energy of lithium ions to other oxygen-containing compounds.³⁵ No lithium adduct with iron carbonyl was observed. This may be due to the stronger $\text{Fe}(\text{CO})_4-\text{CO}$ bond of 41 kcal/mol ³⁶ which precludes ligand displacement as a means of stabilizing the lithium-iron complex. Although halide incorporation was not investigated in the present study, Foster and Beauchamp have demonstrated that F^- reaction with $\text{Fe}(\text{CO})_5$ can be used to generate anionic halide-containing metal-carbon compounds.⁹

SUMMARY AND PROGNOSIS

This investigation demonstrates that decarbonylating of iron clusters containing two to four iron atoms can be achieved with infrared radiation. Infrared wavelengths, however, are ineffective in promoting decarbonylation of nickel-carbonyl clusters containing up to four metal atoms. Visible radiation at 647 nm induces elimination of two carbon monoxide molecules from mononuclear and polynuclear iron complexes and from binuclear nickel compounds. Photochemical methods of carbon monoxide removal offer an alternative to chemical methods and are potentially more selective.

For reactions investigated in the presence of infrared radiation, only loss of carbon monoxide from the substituted metal-carbonyl clusters was observed. This demonstrates that IR activation can be

used to remove carbon monoxide ligands from substituted carbonyl clusters. Frequently, the rate-limiting step for hydrocarbon transformations involves formation of a vacant coordination site at the metal center.^{1,14,15} Although the results from this investigation are limited, they suggest the possibility of initiating chemical reactions by using infrared radiation to create sites of unsaturation.

The chemistry of carbonyl clusters observed in this study is clearly different from that of the atomic metal ions. Using ligand-exchange reactions, it is possible to create a number of stable species containing various functional groups in close proximity. This holds great promise as a method for synthesis of stable metal cluster compounds which could be activated with infrared or visible photons. In addition, photochemical activation may add insights into reaction energetics by identifying the lowest energy reaction pathway. The extended mass range and ion-selection capabilities of a Fourier-transform ICR instrument will undoubtedly allow the detailed chemistry of these larger metal clusters to become accessible. This promises to be a rich source of reaction chemistry.

ACKNOWLEDGMENTS

We gratefully acknowledge the support of the National Science Foundation under Grant CHE-8407857. Graduate fellowship support by the Atlantic Richfield Foundation (MAH) is gratefully acknowledged. We also thank Dr. Kenneth Janda for the gracious loan of the Kr-ion laser.

REFERENCES

1. Johnson, B. F. G. "Transition Metal Clusters"; Wiley: New York, 1980.
2. a) Muetterties, E. L.; Rhodin, T. N.; Band, E.; Brucker, C. F.; Pretzer, W. R. Chem. Rev. 1979, 79, 91.
b) Muetterties, E. L.; Wexler, R. M. Chem. Rev., submitted.
3. Geusic, M. E.; Morse, M. D.; Smalley, R. E. J. Chem. Phys. 1985, 82, 590.
4. a) Whetten, R. L.; Cox, D. M.; Trevor, D. J.; Kaldor, A. J. Phys. Chem. 1985, 89, 566.
b) Trevor, D. J.; Whetten, R. L.; Cox, D. M.; Kaldor, A. J. Am. Chem. Soc. 1985, 107, 518.
5. a) Riley, S. J.; Parks, E. K.; Mao, C. F.; Pobo, L. G.; Wexler, S. J. Phys. Chem. 1982, 86, 3911.
b) Riley, S. J.; Parks, E. K.; Nieman, G. C.; Pobo, L. G.; Wexler, S. J. Chem. Phys. 1984, 80, 1360.
c) Riley, S. J.; Parks, E. K.; Pobo, L. G.; Wexler, S. Ber. Bunsenges. Phys. Chem. 1984, 88, 287.
6. Wise, M. B.; Jacobson, D. B.; Freiser, B. S. J. Am. Chem. Soc. 1985, 107, in press.
7. Meckstroth, W. K.; Ridge, D. P.; Reents, W. D. J. Phys. Chem. 1985, 89, 612.
8. Allison, J.; Ridge, D. P. J. Am. Chem. Soc. 1979, 101, 4998.
9. Foster, M. S.; Beauchamp, J. L. J. Am. Chem. Soc. 1975, 94, 4804.
10. Wronka, J.; Ridge, D. P. J. Am. Chem. Soc. 1984, 106, 67.
11. Dunbar, R. C.; Ennever, J. F.; Fackler, J. P. Inorg. Chem. 1973, 12, 2734.

12. Jacobson, D. B.; Freiser, B. S. J. Am. Chem. Soc. 1984, 106, 5351.
13. a) Duncan, M. A.; Dietz, T. G.; Smalley, R. E. J. Am. Chem. Soc. 1981, 103, 5245.
b) Ouderkirk, A. J.; Weitz, E. J. Chem. Phys. 1983, 79, 1089.
c) Ouderkirk, A. J.; Werner, P.; Schultz, N. L.; Weitz, E. J. Am. Chem. Soc. 1983, 105, 3354.
14. a) Wrighton, M. S. Chem. Rev. 1974, 74, 401.
b) Geoffroy, G. L.; Wrighton, M. S. "Organometallic Photochemistry"; Academic Press: New York, 1979.
15. Parshall, G. "Homogeneous Catalysis"; Wiley-Interscience: New York, 1980.
16. Lehman, T. A.; Bursey, M. M. "Ion Cyclotron Resonance Spectrometry"; Wiley Interscience: New York, 1976. Beauchamp, J. L. Annu. Rev. Phys. Chem. 1971, 22, 527.
17. Bomse, D. S.; Woodin, R. L.; Beauchamp, J. L. J. Am. Chem. Soc. 1979, 101, 5503.
18. Hodges, R. V.; Beauchamp, J. L. Anal. Chem. 1976, 48, 825.
19. Similarly, for neutral $\text{Fe}(\text{CO})_5$, the less saturated fragment species are most reactive. See References 13b and 13c.
20. Kappes, M. M.; Staley, R. H. J. Phys. Chem. 1982, 86, 1332.
21. a) Sheline, R.; Pitzer, K. S. J. Am. Chem. Soc. 1950, 72, 1107.
b) Jones, L. H.; McDowell, R. S.; Goldblatt, M.; Swanson, B. L. J. Chem. Phys. 1972, 57, 2050.
22. Distefano, G. J. Res. Natl. Bur. Stand., Sect. A. 1970, 74A, 233.
23. M-CO bonds to iron and nickel surfaces are comparable to the mono-metallic M-CO bond strengths. See: Erley, W. J. Vac. Sci. Tech. 1981, 18, 472; Bertolini, J.C.; Tardy, B. Surf. Sci. 1981 102 131.

24. Bomse, D. S.; Berman, W. D.; Beauchamp, J. L. J. Am. Chem. Soc. 1981, 103, 3967.
25. a) Bomse, D. S.; Beauchamp, J. L. J. Am. Chem. Soc. 1981, 103, 3292.
 b) Hanratty, M. A.; Paulsen, C. M.; Beauchamp, J. L. J. Am. Chem. Soc., submitted.
26. a) For a review see: Woodin, R. L.; Bomse, D. S.; Beauchamp, J. L. in "Chemical and Biochemical Applications of Lasers" Vol. IV, Moore, C. B., ed.: Academic Press: New York, 1979.
 b) Schulz, P. A.; Sudbø, A. S.; Krajnovich, D. J.; Kwok, H. S.; Shen, Y. R.; Lee, Y. T. Ann. Rev. Phys. Chem. 1979, 30, 379.
27. Hubbard, J. L.; Lichtenberger, D. L. J. Chem. Phys. 1981, 75, 2560.
28. Cowley, A. H. Prog. in Inorg. Chem. 1979, 26, 45.
29. This assumes that $D[(CO)_x Fe^+ - H] = D[Fe^+ - H] = 58 \pm 5$ kcal/mol and $D[(CO)_x Fe^+ - R] = D[Fe^+ - CH_3] = 68 \pm 4$ kcal/mol, where R is an alkyl group. Armentrout, P. B.; Halle, L. F.; Beauchamp, J. L. J. Am. Chem. Soc. 1981, 103, 6501. A value of 95 kcal/mol is a typical C-H bond dissociation energy.
30. Carlin, T. J.; Sallans, S.; Cassady, C. J.; Jacobson, D. B.; Fresier, B. S. J. Am. Chem. Soc. 1983, 105, 6320.
31. Kappes, M. M.; Staley, R. H. J. Am. Chem. Soc. 1981, 103, 1286.
32. Addition of D_2 to $Fe(CO)_4$ isolated in a rare gas matrix has been reported to occur without an activation energy. Sweany, R. L. J. Am. Chem. Soc. 1981, 103, 2401.
33. a) Ertl, G.; Weiss, M.; Lee, B. S. Chem. Phys. Lett. 1979, 60, 391.
 b) Borden, G.; Gagner, G.; Bonzel, H. P. Surface Sci. 1979, 84, 295.

34. $D[(CO)_3Ni-CO] = 25 \pm 2$ kcal/mol. Stevens, A. E.; Feigerle, C. S.; Lineberger, W. C. J. Am. Chem. Soc. 1982, 104, 5026.
35. a) Weiting, R. D.; Staley, R. H.; Beauchamp, J. L. J. Am. Chem. Soc. 1975, 97, 924.
- b) Woodin, R. L.; Beauchamp, J. L. J. Am. Chem. Soc. 1978, 100, 501.
36. Lewis, K. E.; Golden, D. M.; Smith, G. P. J. Am. Chem. Soc. 1984, 106, 3905.